[American Journal of Science, Vol. 319, June, 2019, P. 431-472, DOI 10.2475/06.2019.01]

American Journal of Science

JUNE 2019

GROWTH AND STEADY STATE OF THE PATAGONIAN ANDES

DAVID AUERBACH COLWYN*†, MARK T. BRANDON*, MICHAEL T. HREN**, JEREMY HOURIGAN***, ASTRID PACINI*, MARTHA G. COSGROVE*, MAYA MIDZIK*, RENÉ D. GARREAUD§, and CHRISTINE METZGER§§

ABSTRACT. **Water isotopes are an important tool for reconstructing the amount of atmospheric lifting related to high topography in the geologic past. However, our capacity for meaningful interpretation requires understanding the climatic setting and isolating the influence of orography on water isotopes. Patagonia's simple, steady climatology and location within the Southern Westerlies makes it an ideal setting for successful application of water isotopes to measuring topography through time. Here we use hydrated volcanic glass to construct a new record of the size of the Patagonian Andes during the Cenozoic. We also utilize a novel method for identifying the contribution of orography in regional climate records. Our results show that variation in the observed record can largely be explained by variations in climate. Thus we conclude that the mountain range has maintained a size similar to modern since at least Paleocene. This result is in agreement with geologic data, which constrain the bulk of the surface uplift of the Andes to the Cretaceous. The reconstruction of the Patagonian Andes, which grew in the Cretaceous and remained high through the Cenozoic, is markedly different from the widely held view of Miocene formation of this mountain range. In particular, the topography appears to remain stable during the northward propagation and collision of offshore spreading centers.**

Key words: Patagonia, water isotopes, paleotopography, volcanic glass

INTRODUCTION

The western edge of South and North America is distinguished by a cordillera (literally *rope*, from Sp. *cuerda*) of orogenic topography, extending from Tierra del Fuego to the Russian Far East (fig. 1). This American Cordillera is often viewed as a distinctive orogenic setting, characterized by subduction of oceanic lithosphere, arc magmatism, and back-arc thrusting. DeCelles and others (2009) emphasize these features as defining attributes of a *cordilleran orogen.* An important aspect of this setting is the growth and maintenance of high topography for tens to hundreds of millions of years.

Herein, we focus on the topographic evolution of the Patagonian Andes, which extend from ~39°S to 56°S (Ramos and Ghiglione, 2008) along the active margin of South America (fig. 1). In this region, the Andes are characterized by high topography, a Late Jurassic–Cretaceous magmatic core called the Patagonian batholith (Hervé and others, 2007), and Late Cretaceous–Miocene back-arc thrust belt (Fosdick and others,

* Department of Geology and Geophysics, Yale University, New Haven, Connecticut, USA
** Center for Integrative Geosciences & Department of Chemistry, University of Connecticut, Storrs, Connecticut, USA
*** Department of Earth & Planetary Sciences, University of California-Santa Cruz, Santa Cruz, California, USA
§ Departamento de Geofísica and Center for Climate & Resilience Research, Universidad de Chile, Santiago, Chile
§§ California College of the Arts, San Francisco, California, USA
† Corresponding author: david.colwyn@colorado.edu. Now at University of Colorado-Boulder

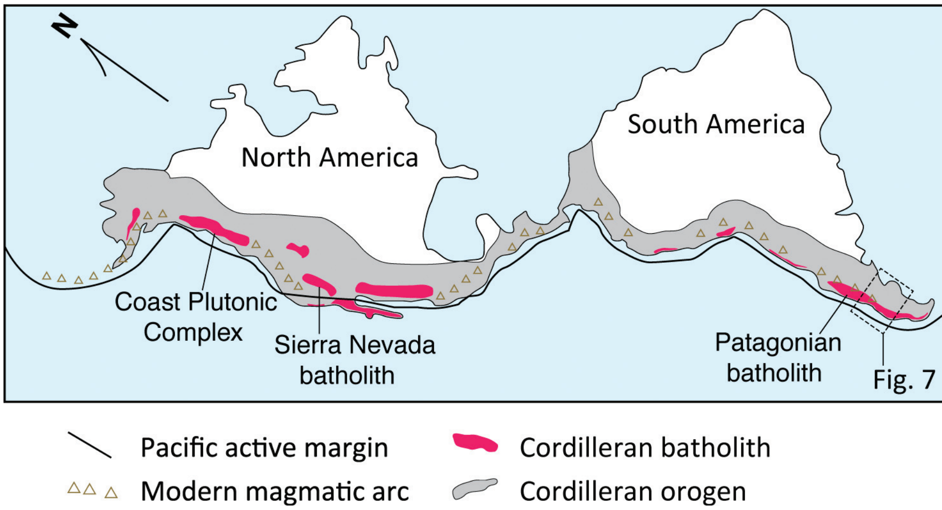

Fig. 1. Cordilleran orogens of North and South America. Cordilleran orogens are characterized by ocean-continent subduction, histories of arc magmatism that often include large-scale plutonism, and back-arc shortening. Dashed box indicates the area shown in figure 7. After Dickinson (2004) and DeCelles and others (2009).

2011). The Patagonian Andes share these characteristics with other well-known examples from the North American Cordillera, such as the Mesozoic Sierra Nevada of California (cored by the Sierra Nevada batholith), and the Late Cretaceous to Paleogene North Cascades/Coast Mountains of Washington and British Columbia (cored by the Coast Plutonic Complex). All of these orogens had high topography early in their evolution, as recorded by thick crust (based on thermobarometry), crustal shortening, and synorogenic sedimentary basins in the Sierra Nevada (Ague and Brimhall, 1988; Ducea, 2001; Cassel and others, 2009; Hren and others, 2010; McPhillips and Brandon, 2012) and the Coast Mountains/Cascades (Monger and others, 1982; Whitney and others, 1999; Miller and others, 2016).

Early workers estimated paleotopography using synorogenic sediments, thermochronology, and biogeography. Here we reconstruct ancient water isotopes (δD and δ^{18}O of precipitation), which are closely related to the size of topography through time (Garzione and others, 2000; Poage and Chamberlain, 2001; Mulch and Chamberlain, 2007; Rowley and Garzione, 2007). Lifting of moist air over high topography results in precipitation and fractionation of water isotopes—the so-called "altitude effect" (Dansgaard, 1964; Rozanski and others, 1993). Much of the isotopic work on paleotopography has made use of an empirical isotopic lapse rate. However, GCMs indicate that lapse rates may have varied in the geologic past (Poulsen and others, 2010).

Patagonia receives almost all of its atmospheric moisture from the Southern Hemisphere westerly winds impinging on the Andes (fig. 2, Garreaud and others, 2013). This circulation is known to be a fundamental and persistent feature of mid-latitude paleoclimatology (Parrish and others, 1982; Williams, 1988; Schneider, 2006). While Patagonia has moved westward during the Cenozoic, it has not rotated or changed latitude appreciably (Seton and others, 2012). We can therefore expect that the basic configuration of Patagonia—a north-south mountain range facing persistent Westerlies—has remained unchanged through the Cenozoic.

Water isotopes are recorded by a variety of geologic materials, including soil carbonate (Cerling and Quade, 1993), leaf waxes (Sachse and others, 2012), and

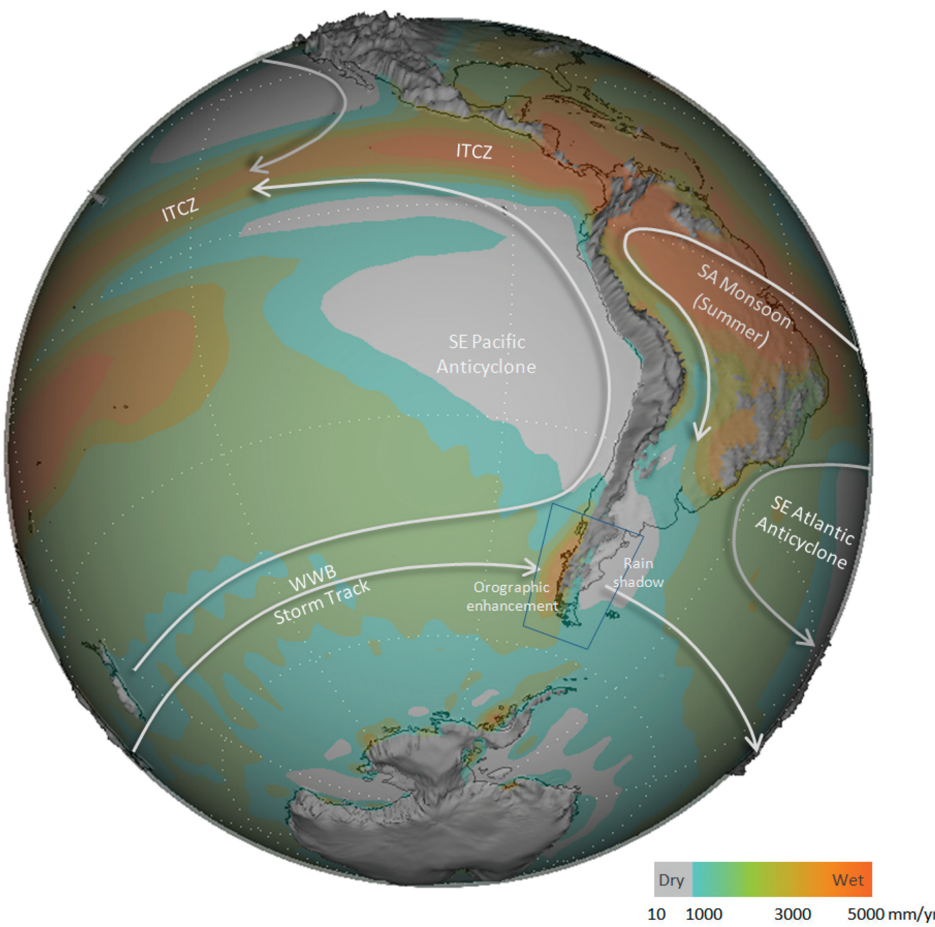

Fig. 2. Mean annual precipitation (from GPCP) and 700 hPa (about 3 km ASL) wind speed (from NCEP-NCAR reanalysis). The Southern Ocean is dominated by westerly flow, as indicated by the bold arrow, impinging directly on the Patagonian Andes. The study area (blue box) lies in the belt of mid-latitude westerly winds.

volcanic glass (Friedman and others, 1993b). Patagonia contains widespread, long-ranging terrestrial sedimentary sequences, which preserve all of these types of water isotope records. Here we (1) measure modern water isotopes in central Patagonia, (2) reconstruct paleo-water isotopes on the downwind side of the Patagonian Andes from volcanic glass, (3) model the effect of Cenozoic climate change on water isotopes under constant topography, and (4) compare our paleo-water isotope record to the modeled results to evaluate what part of the record is the result of changing topography as opposed to climate change.

GEOLOGIC CONTEXT

There are numerous tectonic interpretations for the formation of the Patagonian Andes. These include back-arc shortening (Ramos, 2005), ridge collision (Ramos and Kay, 1992; Gorring and others, 1997; Georgieva and others, 2016), geometry and rate of subduction (Blisniuk and others, 2005; Folguera and Ramos, 2011; Encinas and others, 2016), and migration of the Chile triple junction (Lagabrielle and others, 2004;

Breitsprecher and Thorkelson, 2009; Ghiglione and others, 2016). Many of these tectonic events are Miocene in age, which has led to the widely held view that the Patagonian Andes formed during the Miocene and the area was generally low prior to then. However, the existing geologic literature contains substantial evidence that high subaerial topography likely formed much earlier, during the Late Cretaceous. We follow here with a brief review of this literature.

The Patagonian Andes contain a record of arc magmatism back to at least the Early Jurassic. The arc had little or no subaerial topography at this time, as indicated by roof pendants of Early Jurassic volcanics and marine limestones preserved in the Patagonian batholith (Giacosa and Heredia, 2004) and spatially extensive submarine silicic volcanics of the Late Jurassic Tobifera Formation (Hanson and Wilson, 1991). The arc crust grew rapidly from ~155 to 115 Ma, as recorded by geochronology of the Patagonian batholith (figs. 3 and 4). This large composite plutonic complex of diorites, granodiorites, tonalites, and granites was intruded at an average depth of ~10 km (fig. 3) (Pankhurst and others, 1999; Seifert and others, 2005; Hervé and others, 2007). The batholith, extending ~1800 km along the length of the Patagonian Andes, defines the core of the range. Also present in this region are localized exposures of Miocene plutonic rocks (fig. 3), but given their distinctly younger age, we consider them genetically unrelated to the batholith.

The timing of subaerial emergence of the arc is recorded in the back-arc basin stratigraphy. Cretaceous paleogeographic reconstructions show the arc was separated from cratonic South America to the east by the Aysén-Magallanes back-arc basin (Pindell and Tabbutt, 1995; Maffione, 2016), which is now filled with >7 km of sediment (Fosdick and others, 2011). Paleocurrent directions (Dott and others, 1982), sandstone petrofacies (Fildani and others, 2003; Fildani and Hessler, 2005; Romans and others, 2011), and detrital zircon ages spanning the age of the arc (fig. 3B) indicate the arc was an emergent high by the Late Cretaceous. This time was also marked by rapid accumulation of ~4 km of marine deposits in the back-arc (Romans and others, 2011). Petrographic analysis of these sediments indicates that volcanic rocks of the arc became an increasingly important sediment source in the Late Cretaceous, while clast counts of conglomerates show no evidence of granitic cobbles (Crane, ms, 2004). Zircon fission-track ages in the Patagonian batholith (fig. 3C) show widespread cooling at this time, which we attribute to post-magmatic cooling and erosion of the arc.

The back-arc basin also became emergent in Cretaceous time, as indicated by terrestrial sediments in the northern part of the basin by ~125 Ma and in the southern part by ~70 Ma (Macellari and others, 1989; Suárez and others, 2000; Fosdick and others, 2011). Back-arc thrusting began at ~100 Ma (Fosdick and others, 2011) and continued until 9 Ma (Lagabrielle and others, 2004), with most of the convergence (27 km) occurring between ~88 and 74 Ma (Fosdick and others, 2011). Terrestrial back-arc basins continued to accumulate synorogenic sediment through at least the Miocene (Charrier and others, 2007), and these basins received frequent and widespread deposits of volcanic ash from the arc (Rapela and others, 1988; Bellosi, 2010a). Evidence exists for localized marine deposition during the Late Oligocene–Early Miocene (Flint and others, 1994; Bechis and others, 2014; Encinas and others, 2018), though terrestrial deposition continued elsewhere during this time (Blisniuk and others, 2005; Dunn and others, 2013; Metzger, ms, 2013). Such a setting may have resembled the eastern Aleutian Arc in modern Alaska, with mixed marine and terrestrial deposition occurring in a retro-arc basin adjacent to the mountainous topography of the arc. Sediment deposited in these basins continued to contain a large fraction of volcanic lithic material until ~14 Ma (Macellari and others, 1989; Matheos and Raigemborn, 2012), indicating the continued dominance of the volcanic arc as a

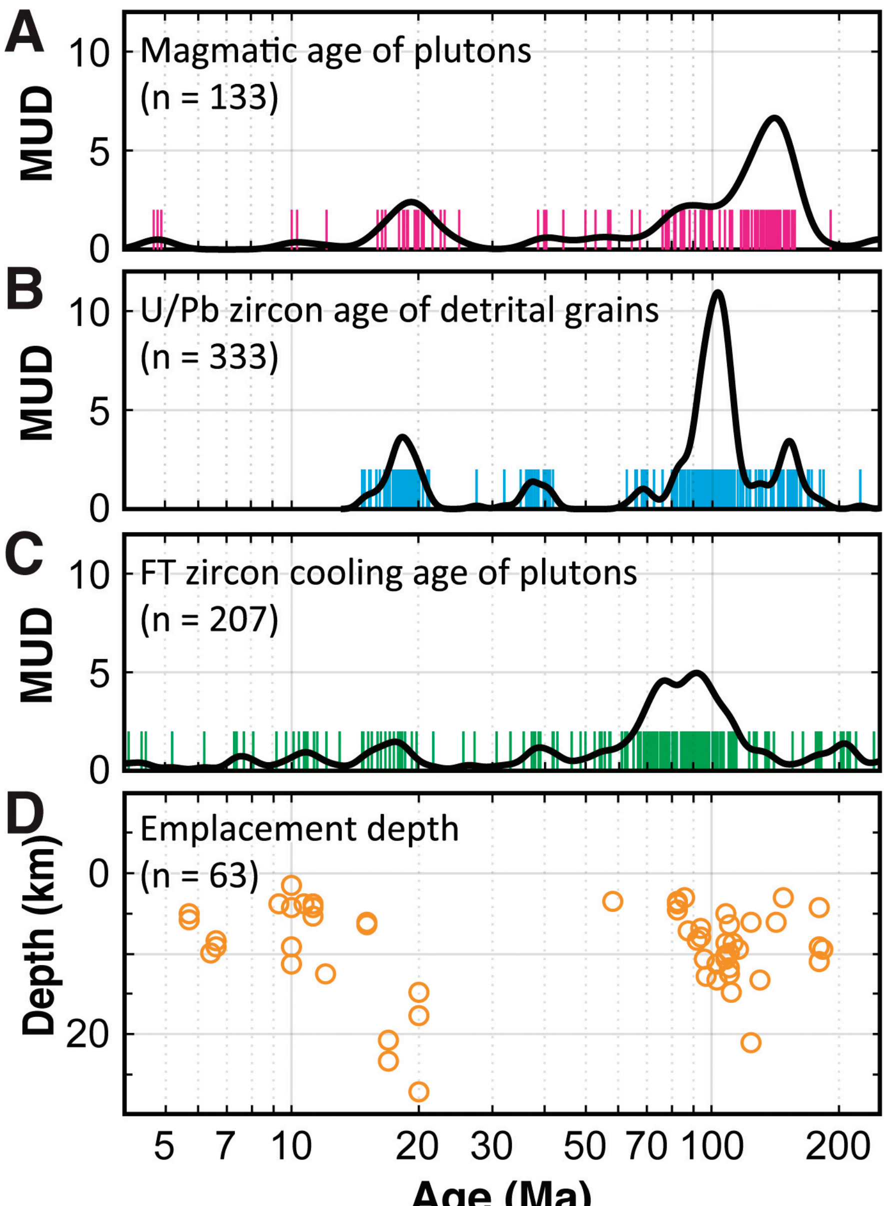

Fig. 3. Cooling history of the Patagonian batholith and derived material. (A) U/Pb and Rb/Sr ages of batholithic rocks, assumed to represent crystallization (Pankhurst and others, 1999; Hervé and others, 2007). (B) Detrital zircon U/Pb ages from the latest Cretaceous to Middle Miocene samples from the Magallanes back-arc basin (Fosdick and others, 2015). (C) Fission-track cooling ages of zircons from batholithic rocks (see compilation in Herman and Brandon, 2015). (D) Depth of emplacement of plutons as measured by Al-in-hornblende thermobarometry. For locations of geochronology samples, see figure 4. The primary event visible in these data is the large Late Cretaceous pulse of crystallization followed by erosion and cooling. Exhumation appears slow and steady since that time, despite the Miocene intrusive event. MUD = multiples of uniform density, an expression of deviation from the mean (values greater than 2 are significant).

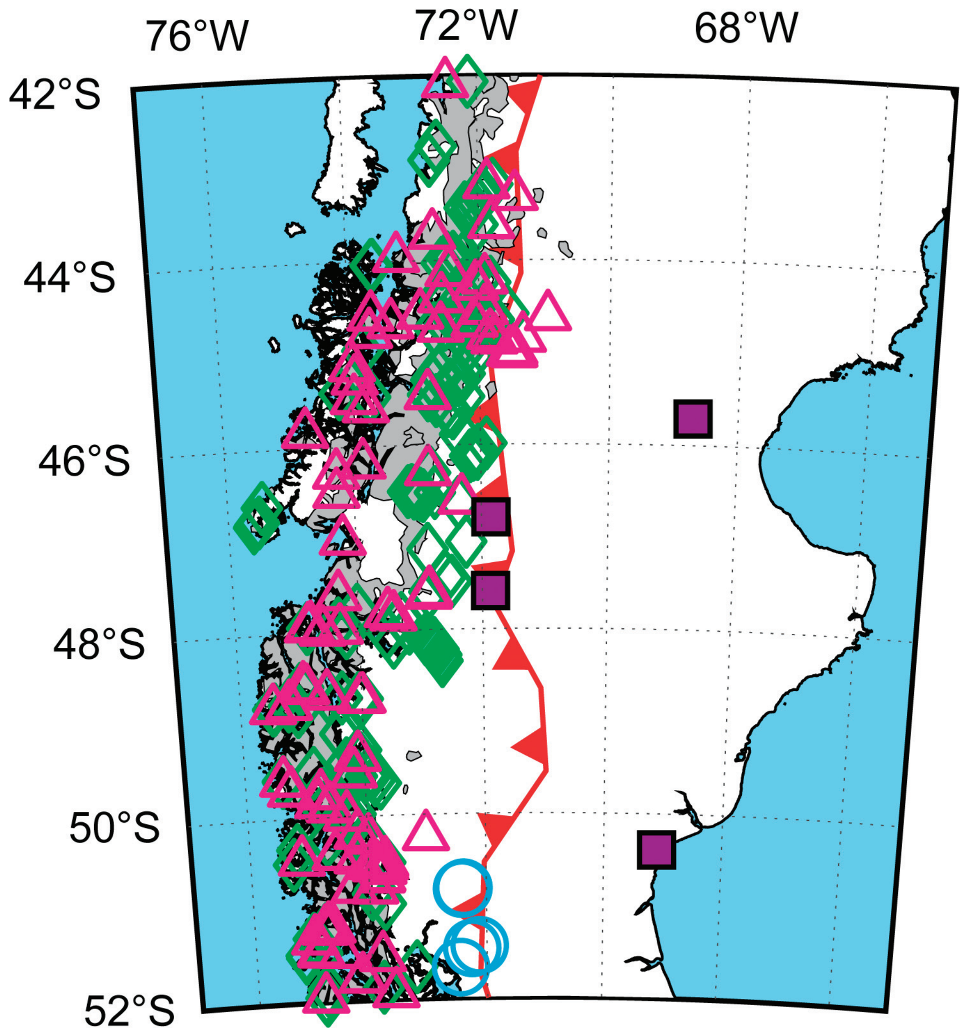

Fig. 4. Distribution of samples placing constraints on the crystallization and cooling history of the Patagonian batholith plotted in figure 3. Pink triangles are samples with magmatic ages, green diamonds are fission-track cooling ages of zircons, and blue circles are detrital zircon sampling locations. Purple squares indicate locations of sedimentary sections discussed in text.

sediment source while the batholith itself remained largely unexposed. Granitic cobbles are common in ~6 Ma glacial moraines (Wenzens, 2006; Christeleit and othes, 2017), which brackets the first widespread exposure of the batholith to ~14 to 6 Ma.

Today, the high topography of the Patagonian Andes extends to the bedrock peak of Monte San Valentin, ~4 km above sea level. The range is composed primarily of granitic rocks of the Patagonian batholith with screens of metamorphic rocks. In the San Valentin massif, a range of thermochronometers show old cooling ages (fission-track zircon = 100−72 Ma, fission-track apatite = 32−7 Ma, He apatite = 13−3 Ma), indicating slow erosion since the Late Cretaceous (Thomson and others, 2010). This pattern of relatively old cooling ages is common throughout the Patagonian Andes (Thomson and others, 2010; Herman and Brandon, 2015), suggesting slow erosion at a regional scale through the Cenozoic.

In summary, these observations indicate that the Patagonian arc evolved from a submarine arc in the Jurassic to a fully emergent subaerial arc in the Cretaceous. The detrital record shows erosion down through volcanic cover into the plutonic core of the arc. Sediments in the back-arc basin required a steep topographic gradient for sediment transport, indicating that the source area was mountainous (Wilson, 1991; Suárez and others, 2000; Gutiérrez and others, 2017). Genomic work indicates the presence and diversification of cold-adapted flora in what is today the Patagonian Andes prior to ~40 Ma (Mathiasen and Premoli, 2010), which requires high topography to account for a cold environment amidst a period of global warmth.

This interpretation conflicts with the currently widespread view of Miocene (~15 Ma) formation of the Patagonian Andes, which is explained by back-arc shortening or migration of the Chile triple junction (see references above). However, the geologic evidence does not support this view. Back-arc shortening is estimated at <13 km of convergence since ~74 Ma (Fosdick and others, 2011), which is insufficient to grow the topography of the Patagonian Andes. The northward migration of the Chile triple junction is important for tectonics south of its current position at ~47°S, but it cannot explain the high topography of the Patagonian Andes that continues north for an additional >1000 km. The Patagonian batholith is the only feature that is coincident with the entire length of the range, and it was emplaced at a time when sedimentological and provenance records indicate the emergence of high subaerial topography. Thus, we infer that the emplacement of the Patagonian batholith is a likely candidate for the formation of the topography of the Patagonian Andes.

CLIMATIC CONTEXT

Many mountain ranges are characterized by a wet windward side and an arid leeward side. In Patagonia, the mean annual precipitation (MAP) on the windward side of the Andes is >5 m yr^{-1}, while the leeward side is <0.3 m yr^{-1} (Smith and Evans, 2007; Garreaud and others, 2013). This orographic effect leads to decreasing water isotope values with increasing orographic lifting (Stern and Blisniuk, 2002; Smith and Evans, 2007; Garreaud and others, 2013). The resulting relationship between elevation and water isotopes forms a basis for reconstructions of past topography (Poage and Chamberlain, 2001; Rowley and Garzione, 2007). However, any water isotope record also includes the influence of climate, including changes in global temperature, atmospheric circulation, and mode of lifting (stable vs. convective) over time. Recent work indicates that these climatic effects might bias estimates of paleotopography (for example, Galewsky, 2009; Poulsen and others, 2010; Insel and others, 2012; Lechler and Galewsky, 2013; Rohrmann and others, 2014).

As a result, we have taken care to account for the role of climate in our study. First, we correct for the effect of global temperature on the isotopic record in the analysis of our data (see below). Second, we address here two important climatic assumptions: (1) the Southern Hemisphere (SH) Westerlies have dominated atmospheric flow across Patagonia during the Cenozoic, and (2) the distribution of water isotopes is primarily controlled by stable orographic lifting and fractionation of moist air from the Pacific Ocean.

We base the first assumption on the fact that the mid-latitude Westerlies, along with the Hadley cell at lower latitudes, (fig. 2) are a direct result of Earth's rotation (Held and Hou, 1980; Williams, 1988; Schneider, 2006) and should thus be a persistent feature of atmospheric circulation. This prediction is borne out by paleoclimate studies (Parrish and others, 1982). The SH Westerlies form a band currently centered at ~50°S, but are thought to shift several degrees of latitude in response to global cooling and warming (Lamy and others, 2001; Moy and others, 2008; Koffman and others, 2014). This effect, however, is small compared to the ~20°-wide latitudinal span of the SH Westerlies (fig. 2). For reference, plate reconstructions indicate the latitudinal position of Patagonia has been steady during the Cenozoic (Seton and others, 2012).

We consider the possibility that the South American Monsoon System (SAMS) (Vera and others, 2006) (fig. 2) might reach far enough south to contribute significant atmospheric flow to the eastern part of central Patagonia, particularly in a warmer world. However, the poleward extent of the SAMS is controlled not by temperature but by a ventilation mechanism that provides extratropical westerly flow (Chou and Neelin, 2001). Even in the current cool climate, the radiative and thermal forcing over eastern Patagonia is similar to the forcing at lower latitudes. The mid-level SH Westerlies bring air with low static energy (relatively low moisture/low temperature) from the Pacific that inhibits deep convection over the continental plains south of 35°S (Chou and Neelin, 2001), keeping the SAMS north and east of Patagonia. Thus, with respect to our first assumption, there is no physical basis for a change in the dominant wind direction of the SH Westerlies through the Cenozoic and it is reasonable to assume this is a longstanding atmospheric feature in Patagonia.

The second assumption rests on the fact that any flow of moist saturated air over topography will result in orographic precipitation and isotopic fractionation commensurate with the size of the topography. Storms moving across low continental areas also show isotopic fractionation, but these are small, on the order of $\delta D = -1.6$ ‰/100 km (Criss, 1999). Central Patagonia is ~600 km across, so in the absence of high topography, we would expect cross-continent fractionation of $\delta D < 10$‰. However, the modern Patagonian Andes are marked by a decrease in δD of ~80‰ across ~150 km (fig. 5).

Exceptions to this assumption – that incoming moist air will pass directly over topography – may occur for three reasons: (1) flow around mountain ranges with a low length:width ratio (for example, Galewsky, 2009; Lechler and Galewsky, 2013), (2) impedance by a combination of stable atmospheric conditions and slow wind speeds ("blocking") (for example, Smith, 1979; Galewsky, 2009), and (3) ascent of air masses due to deep convection (for example, Poulsen and others, 2010; Rohrmann and others, 2014). Mid-latitude Patagonia shows none of these conditions, having an extremely long (1000s of km), narrow mountain range standing in the path of relatively fast westerly winds (on the order of 10 m/s) with average atmospheric moist stability. The Patagonian Andes are analogous to the New Zealand Alps in size and climatology. Wheeler and Galewsky (2017) show that the simple notion of orographic lifting and isotopic fractionation works quite well there. Finally, convective rainfall is common along the west coast of South America but is rarely observed in the mid-latitudes (Garreaud and others, 2014). Considerable convection on the west coast of South America only occurs north of ~5°S, where sea surface temperature (SST) is 22°C. Despite warmer conditions in the past, coastal SSTs would still be well below that needed to excite convective activity over western Patagonia.

MODERN WATER ISOTOPES IN PATAGONIA

Modern water isotopes across Patagonia (figs. 5 and 6, table 1) illustrate their use for interpreting topography. These data are from samples of base-flow in small streams, which provide isotopic measurements average precipitation over the 1 to 3 year residence time of water typical of small catchments (McGuire and others, 2005). Base-flow waters also typically show minimal influence of evaporation. Figure 6 shows that most of our base-flow samples (blue) are unaffected by evaporation, while ~15 percent of samples (red) have a low deuterium excess, indicating evaporation. We highlight this because evaporation can be an issue for interpretation of ancient water isotope measurements (for example, Quade and others, 2007; Lechler and others, 2013; Cassel and Breecker, 2017). Because volcanic glasses largely sample groundwater, their isotopic record is generally insensitive to evaporation.

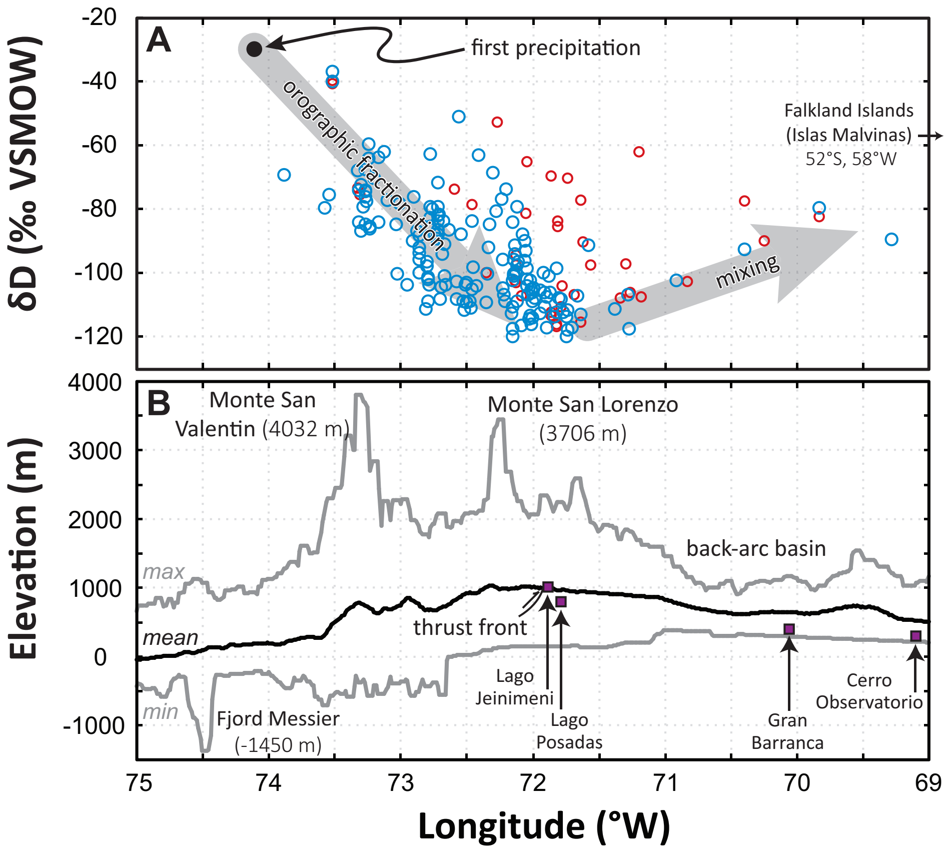

Fig. 5. Relationship between water isotopes (A) and topography (B) in central Patagonia between 44°S and 48°S. Blue symbols indicate stream water samples that have experienced little to no evaporation; red symbols indicate samples with low d-excess (see fig. 6). Swath topography in (B) is from a 2 km-wide moving window between 44°S and 48°S.

The modern water isotope distribution across Patagonia is dominated by orographic fractionation (fig. 5). The *first precipitation*—the precipitation that falls as an air mass begins to lift due to topography—reflects the composition of the incoming water vapor, and is approximately −30 permil in Patagonia (fig. 5, table 1). The primary water isotope values (blue) decrease from west to east, reaching a minimum of about −120 permil at 71°W, after which values rise to −80 permil. This rise is due to moisture from southeasterly Atlantic storms, which produce precipitation with δD as high as −30 permil in southern mid-latitude settings. Simple mixing of end-member values suggests that Atlantic precipitation could contribute up to ~30 percent of the water isotope composition in parts of eastern Patagonia. Case studies (Agosta and others, 2015; Tuthorn and others, 2015), climatological analysis (Garreaud and others, 2013), and HYSPLIT back-trajectories (Draxler and Rolph, 2013) give broadly similar results, indicating ≤20 percent Atlantic-sourced precipitation. Data from the Falkland Islands (fig. 5), which lie >500 km east of South America and ~1000 km from the Andes, still show a significant component of Andean-fractionated moisture.

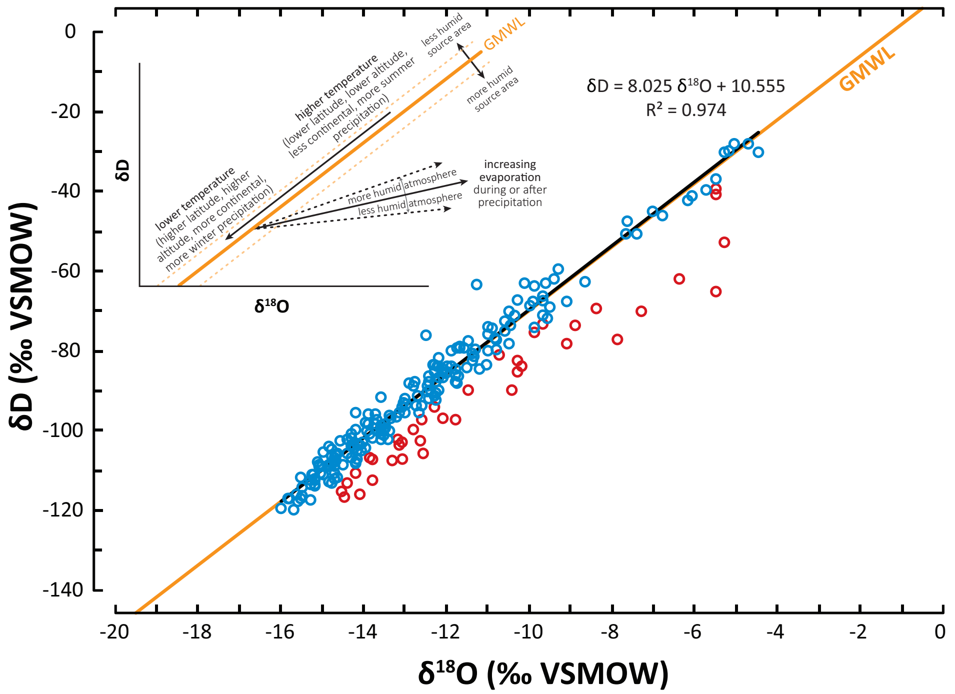

Fig. 6. Stable isotope composition of modern surface water samples in Patagonia. Samples in blue are unevaporated meteoric waters; samples in red have been influenced by evaporation (d-excess < 4.8‰). The linear fit through the unevaporated samples matches the global meteoric water line (GMWL) closely. Schematic inset after Coplen (1993), Gat (1996), and University of Arizona SAHRA.

SAMPLING LOCATIONS

We measured and sampled stratigraphic sections in three locations (fig. 7) on the leeward side of the Andes between 46°S and 51°S (fig. 8). The Paleocene-Eocene section at Mina Ligorio Márquez near Lago Jeinimeni is composed primarily of volcanic-rich mudstones and sandstones. It is underlain by Cretaceous rocks (Suárez and others, 2000), and is capped by a basalt flow assigned to the Basaltos Inferiores de la Meseta de Chile Chico Formation (Encinas and others, 2019). The Middle Eocene-Early Miocene sedimentology at Gran Barranca has been intensively studied for over a century (Ameghino, 1906; Simpson, 1930, 1933), and detailed information about the sedimentology of the numerous sections appears in Bellosi (2010a, 2010b). The geochronology is based on radiometric dates from Dunn and others (2013) and Ré and others (2010) and geochemical data (Colwyn and Hren, 2019). The sedimentology, geochronology, and detailed measured sedimentary section of the Early-Middle Miocene Santa Cruz Formation at Cerro Observatorio appear in Metzger (ms, 2013). We also discuss the data of Blisniuk and others (2005) from the Santa Cruz Formation at Lago Posadas (fig. 7).

Sections underlie a Miocene-to-Present aggradational surface (Martínez and Coronato, 2008), indicating that they have never been deeply buried. Cerro Observatorio and Gran Barranca have existing high-quality age constraints. The Lago Jeinimeni section has paleobotanical age constraints (Suárez and others, 2000), which are supplemented here with $^{40}Ar/^{39}Ar$ (Encinas and others, 2019) and new detrital zircon data.

Table 1

Stable isotope composition of modern stream waters

Sample	Latitude	Longitude	Elevation (m)	$\delta^{18}O$ (‰)	δD (‰)	d-excess	Source
15SW34	-47.118	-72.464	439	-9.1	-78	-5.5	1
15SW37	-47.065	-72.356	486	-12.8	-100	2.5	1
15SW16	-46.605	-71.690	338	-13.9	-107	4.2	1
15SW17	-46.546	-71.791	372	-14.2	-111	2.9	1
15SW01	-45.685	-72.057	360	-10.7	-81	4.7	1
15SW103	-48.156	-73.545	0	-10.6	-75	9.6	1
15SW101	-48.003	-73.581	7	-11.3	-80	10.9	1
15SW102	-47.919	-73.881	0	-9.5	-69	6.7	1
15SW100	-47.500	-72.955	85	-14.3	-104	10.4	1
15SW32	-47.153	-72.520	1060	-15.5	-112	12.6	1
15SW31	-47.152	-72.508	1156	-14.1	-104	9.3	1
15SW30	-47.149	-72.468	878	-15.3	-111	11.1	1
15SW33	-47.147	-72.528	773	-15.0	-109	11.3	1
15SW38	-47.128	-72.505	391	-14.9	-109	9.8	1
15SW28	-47.128	-72.705	176	-14.8	-108	10.0	1
15SW29	-47.127	-72.481	459	-14.8	-109	9.7	1
15SW27	-47.121	-72.776	192	-12.1	-85	11.5	1
15SW35	-47.121	-72.463	451	-14.1	-105	7.3	1
15SW26	-46.997	-72.797	393	-15.1	-109	12.0	1
15SW23	-46.839	-72.691	226	-12.7	-94	7.9	1
15SW13	-46.838	-72.011	847	-14.2	-105	8.4	1
15SW14	-46.838	-72.016	869	-15.6	-116	9.1	1
15SW07	-46.822	-72.665	214	-14.2	-104	9.9	1
15SW12	-46.819	-71.987	836	-14.7	-108	9.9	1
15SW11	-46.801	-71.945	791	-15.2	-113	9.1	1
15SW24	-46.793	-72.582	367	-14.6	-103	13.9	1
15SW25	-46.792	-72.579	385	-15.1	-108	13.1	1
15SW39	-46.792	-72.813	221	-15.2	-111	10.7	1
15SW10	-46.788	-71.911	723	-15.1	-111	9.9	1
15SW09	-46.727	-71.738	552	-14.6	-112	5.5	1
15SW40	-46.726	-72.803	261	-14.0	-98	13.7	1
15SW15	-46.707	-71.704	487	-15.5	-117	7.0	1
15SW22	-46.697	-72.433	300	-14.8	-104	14.7	1
15SW21	-46.625	-72.353	437	-14.7	-109	8.6	1
15SW20	-46.591	-72.226	247	-14.8	-105	13.3	1
15SW19	-46.562	-72.027	474	-15.5	-114	9.7	1
15SW18	-46.554	-71.893	408	-15.9	-117	9.6	1
15SW08	-46.546	-71.791	379	-14.2	-108	5.4	1
15SW46	-46.458	-72.722	208	-12.8	-88	14.2	1
15SW42	-46.458	-72.722	208	-12.3	-84	14.9	1
15SW44	-46.458	-72.722	208	-12.2	-82	15.7	1
15SW06	-46.427	-72.708	214	-11.3	-81	9.2	1
15SW43	-46.358	-72.765	234	-11.9	-80	15.3	1
15SW45	-46.172	-72.716	587	-11.6	-79	13.5	1
15SW05	-46.164	-72.637	527	-12.4	-87	13.0	1
15SW47	-46.159	-72.337	310	-13.0	-92	12.2	1
15SW48	-46.110	-72.117	501	-14.9	-109	10.3	1
15SW49	-46.060	-72.006	1030	-14.7	-106	11.5	1
15SW50	-45.988	-71.910	853	-14.6	-106	11.2	1
15SW04	-45.969	-71.869	930	-14.4	-106	9.5	1
15SW03	-45.807	-71.920	416	-13.5	-100	8.4	1
15SW02	-45.685	-72.057	360	-13.1	-93	11.4	1
15SW41	-45.535	-72.724	237	-12.8	-89	13.6	1
14LP80	-47.590	-71.825	1017	-14.5	-117	-1.0	1
14AR05	-47.075	-70.832	659	-12.6	-103	-1.3	1
14CL03	-47.128	-72.505	375	-14.0	-103	9.5	1

TABLE 1
(continued)

Sample	Latitude	Longitude	Elevation (m)	$\delta^{18}O$ (‰)	δD (‰)	d-excess	Source
14CL02	-47.121	-72.776	195	-11.4	-83	8.6	1
14CL01	-46.827	-72.001	839	-14.2	-105	9.4	1
14AR04	-46.583	-70.917	394	-13.4	-102	5.3	1
14AR06	-46.554	-71.640	232	-14.9	-113	6.0	1
14CL04	-46.192	-72.776	539	-11.7	-79	14.3	1
14AR03	-45.470	-69.834	411	-10.8	-80	6.9	1
Lago Potrok Aike	-51.950	-70.410		-12.6	-93	7.6	2
Río Gallegos met station	-51.620	-69.280		-11.6	-90	3.6	2
ArrPedegoso	-46.620	-71.267	247	-12.6	-106	-5.4	3
Las Chilcas	-46.612	-71.338	235	-13.3	-108	-1.2	3
GauchitaGil	-46.602	-71.179	274	-13.1	-107	-2.7	3
Los Antiguos	-46.555	-71.640	227	-14.6	-115	1.0	3
CerroPicoSur	-46.545	-71.783	354	-13.2	-104	1.4	3
RioMayo	-45.685	-70.251	420	-10.5	-90	-6.3	3
Rio Senguer	-45.470	-69.831	413	-10.3	-82	-0.1	3
Andrade2	-45.153	-73.519	22	-5.5	-41	3.3	3
Andrade1	-45.153	-73.519	22	-5.5	-39	4.5	3
Pte Catalan	-46.997	-72.796	393	-13.8	-102	8.4	3
Pt Bertrand	-46.944	-72.786	226	-14.3	-104	10.6	3
CerroCastillo	-46.933	-72.342	697	-13.9	-100	11.0	3
Pte Leonos	-46.737	-72.858	248	-13.0	-94	10.2	3
La Parra	-46.730	-72.793	242	-13.5	-101	7.1	3
PteSantaMarta	-46.726	-72.802	226	-13.2	-97	9.3	3
CerroJeinemeni	-46.720	-72.457	251	-13.7	-98	11.6	3
RioTrapial	-46.705	-72.696	312	-14.0	-105	7.2	3
PteBlas	-46.625	-72.673	218	-12.3	-91	7.5	3
PteChirito	-46.625	-72.673	219	-13.9	-101	10.2	3
Rio Aviles	-46.591	-72.225	254	-13.7	-96	13.9	3
Rio Jeinemeni	-46.581	-71.660	258	-14.2	-107	6.0	3
Rio Bana	-46.555	-71.894	423	-14.7	-107	10.0	3
RioEngano	-46.458	-72.723	222	-11.7	-86	7.3	3
PuertoMurta	-46.379	-72.746	250	-12.3	-88	10.3	3
Arr.Aserradeo	-46.171	-72.682	548	-12.3	-84	15.0	3
CerroSinNombre	-46.122	-72.543	353	-12.4	-88	11.5	3
Pte. Moro	-45.501	-72.154	135	-11.5	-84	8.1	3
RioSimpson	-45.479	-72.282	117	-11.4	-81	10.3	3
Las Pizarras	-45.470	-72.306	101	-10.0	-69	11.3	3
Pnte. El Salto	-45.447	-72.780	11	-8.7	-63	6.7	3
Pnte. Prieto	-45.432	-72.721	17	-9.6	-72	4.9	3
Pte. Rossel	-45.424	-72.416	73	-10.1	-63	17.9	3
Pnte Viviana	-45.351	-72.462	45	-11.1	-84	4.8	3
RioManihuales	-45.293	-72.326	96	-11.2	-85	4.9	3
Andrade3	-45.153	-73.519	22	-5.7	-40	6.1	3
Andrade4	-45.153	-73.519	22	-5.5	-37	7.1	3
PntePedregoso	-45.084	-72.118	257	-11.8	-79	14.9	3
Sta.Andres	-44.884	-72.204	349	-10.5	-74	10.2	3
RioCisnes	-44.694	-72.241	194	-10.8	-77	9.8	3
Waterfall Seno	-44.510	-72.558	3	-7.7	-51	10.4	3
MiradordelRio	-43.974	-72.466	37	-10.4	-71	11.6	3
PnteLoicas	-43.526	-72.342	165	-9.7	-66	11.1	3
Pnte Arauca	-43.307	-72.418	252	-9.9	-68	11.6	3
AldeaEscolar	-43.133	-71.556	350	-12.0	-86	10.4	3
Arr. Fontana	-42.990	-71.561	633	-12.2	-84	14.0	3
Arr. Raninto	-42.954	-71.592	599	-12.3	-86	12.8	3
Chaiten1	-42.890	-72.740	48	-6.8	-46	8.0	3
RioDeseguardero	-42.889	-71.609	518	-12.5	-89	11.1	3
Sta Barbara	-42.856	-72.794	16	-6.2	-42	7.3	3

TABLE 1
(continued)

Sample	Latitude	Longitude	Elevation (m)	$\delta^{18}O$ (‰)	δD (‰)	d-excess	Source
Cascada Tio Mindo	-42.839	-71.603	569	-12.5	-90	9.4	3
Arr.Montoso	-42.741	-71.098	982	-13.1	-95	9.7	3
Arr.Lepa	-42.615	-71.077	836	-12.7	-96	5.8	3
Leleque	-42.431	-71.103	726	-13.6	-99	10.1	3
RioButalcuva	-42.279	-73.709	62	-6.1	-41	7.6	3
PulchicanPnte	-41.962	-73.837	0	-5.2	-30	11.7	3
MechaicoPnte	-41.938	-73.830	6	-5.1	-28	12.3	3
Darwin	-41.882	-73.662	10	-5.3	-30	12.2	3
RioFoyal	-41.722	-71.456	672	-12.4	-92	7.4	3
MurrowPnte	-41.663	-73.317	26	-4.7	-28	9.5	3
Trapen Pnte	-41.523	-73.091	68	-4.5	-30	5.5	3
PuertoMontt	-41.470	-72.935	37	-7.0	-45	11.3	3
Guillermo	-41.439	-71.485	900	-13.1	-94	10.4	3
Escalera	-41.302	-71.492	799	-13.3	-97	9.7	3
Nahuelhuapi	-40.942	-71.369	822	-11.8	-88	5.9	3
RioPireco	-40.734	-71.832	804	-9.7	-68	10.0	3
PuertoArauca	-40.725	-71.687	794	-11.0	-80	8.1	3
RioPuychue	-40.725	-71.928	1154	-9.6	-63	13.9	3
PnteNique	-40.724	-72.433	203	-7.6	-47	13.6	3
Rio Totoral	-40.712	-71.790	779	-9.7	-71	6.3	3
Farm Pond	-40.605	-72.892	94	-7.4	-51	8.4	3
EastLake	-40.088	-71.184	782	-12.3	-92	5.7	3
PX1	-47.950	-72.134	918	-13.2	-102	3.2	4
PX6	-47.929	-72.045	890	-5.5	-65	-21.1	4
PASW99-5	-47.914	-73.326	80	-9.7	-73	4.2	4
PX5	-47.833	-72.126	866	-11.8	-98	-3.1	4
PX4	-47.833	-72.126	866	-13.1	-103	1.9	4
PASW22	-47.833	-71.296	849	-12.1	-97	-0.3	4
PASW27	-47.832	-72.127	866	-12.3	-94	4.2	4
PASW36	-47.803	-72.084	850	-13.8	-107	3.3	4
PASW99-9	-47.783	-73.307	125	-9.9	-76	3.7	4
PASW13	-47.743	-71.197	851	-6.4	-62	-10.8	4
PASW00-2	-47.588	-71.825	940	-14.1	-116	-3.4	4
PASW70	-47.578	-71.735	180	-7.3	-70	-11.9	4
PASW49	-47.575	-71.563	290	-12.6	-97	3.5	4
PASW51	-47.574	-71.620	190	-11.5	-90	1.9	4
PASW72	-47.570	-71.636	190	-7.9	-77	-14.0	4
PASW99-2	-47.555	-71.867	1105	-14.4	-113	1.8	4
PASW99-1	-47.553	-71.861	940	-13.8	-112	-2.0	4
PASW20	-47.459	-71.861	170	-8.4	-70	-2.4	4
PASW21	-47.455	-71.813	160	-10.2	-84	-2.2	4
PASW68	-47.455	-71.813	160	-10.3	-85	-2.9	4
PASW65	-47.312	-72.596	291	-8.9	-74	-2.4	4
PASW99-14	-47.056	-72.269	365	-5.3	-53	-10.4	4
PASW48	-47.991	-71.820	844	-13.5	-99	9.5	4
PASW44	-47.956	-72.111	890	-13.4	-96	10.8	4
PASW40	-47.954	-72.157	916	-13.6	-102	6.5	4
PX2	-47.953	-72.158	916	-14.7	-111	7.0	4
PX3	-47.952	-72.149	895	-13.4	-100	7.1	4
PASW41	-47.952	-72.148	895	-13.6	-101	7.9	4
PASW39	-47.951	-72.146	910	-13.0	-96	8.4	4
PASW43	-47.950	-72.121	892	-13.7	-97	12.3	4
PASW37	-47.949	-72.135	918	-12.7	-91	10.4	4
PASW42	-47.949	-72.134	898	-13.6	-100	9.0	4
PASW38	-47.949	-72.140	910	-12.6	-94	6.8	4
PASW45	-47.943	-72.083	890	-11.8	-88	6.6	4
PASW47	-47.943	-71.883	878	-14.3	-101	13.5	4

TABLE 1
(continued)

Sample	Latitude	Longitude	Elevation (m)	$\delta^{18}O$ (‰)	δD (‰)	d-excess	Source
PASW46	-47.938	-72.060	860	-12.2	-90	7.7	4
PASW99-4	-47.919	-73.330	60	-9.1	-68	5.0	4
PASW99-6	-47.895	-73.319	95	-9.9	-74	5.1	4
PASW99-7	-47.886	-73.318	245	-11.9	-84	11.1	4
PASW99-8	-47.852	-73.302	320	-12.2	-87	10.9	4
PASW26	-47.832	-72.127	866	-13.5	-100	8.4	4
PASW32	-47.817	-72.018	961	-14.8	-113	5.2	4
PASW31	-47.804	-72.008	933	-15.2	-114	7.6	4
PASW1	-47.778	-73.298	45	-10.6	-73	12.3	4
PASW52	-47.772	-73.288	45	-11.7	-79	14.3	4
PASW35	-47.768	-72.088	995	-15.5	-116	7.7	4
PASW33	-47.768	-72.221	961	-14.7	-107	10.7	4
PASW34	-47.768	-72.212	906	-15.1	-109	11.8	4
PASW2	-47.768	-73.273	45	-11.0	-76	12.0	4
PASW3	-47.767	-73.270	45	-10.9	-74	12.8	4
PASW99-10	-47.767	-73.265	48	-12.1	-85	12.2	4
PV2-01	-47.767	-73.264	7	-10.6			4
PASW4	-47.767	-73.265	48	-11.0	-74	13.9	4
P3-00-2	-47.766	-73.266	48	-10.3	-67	15.0	4
PASW53	-47.763	-73.257	45	-11.5	-78	14.4	4
PASW54	-47.757	-73.246	45	-9.9	-64	15.3	4
PASW55	-47.748	-73.240	38	-9.3	-60	14.8	4
PASW5	-47.736	-73.235	15	-12.0	-86	10.5	4
PASW6	-47.736	-73.235	3	-12.1			4
PASW99-11	-47.736	-73.236	5	-11.8	-86	8.3	4
PASW56	-47.723	-73.203	23	-10.5	-70	13.9	4
PASW57	-47.722	-73.173	7	-11.3	-64	26.8	4
PASW7	-47.722	-73.172	7	-12.2	-84	13.5	4
PASW28	-47.714	-72.153	895	-16.0	-120	8.3	4
PASW29	-47.714	-72.153	895	-15.8	-117	9.1	4
PASW30	-47.709	-72.167	973	-15.3	-113	9.7	4
PASW8	-47.703	-73.103	28	-10.8	-77	9.2	4
PASW58	-47.698	-73.125	40	-9.4	-62	13.1	4
PASW59	-47.697	-73.046	25	-12.0	-84	12.0	4
PASW60	-47.690	-73.035	43	-11.8	-85	9.6	4
P3-00-1	-47.682	-73.025	68	-13.6	-100	8.5	4
PASW61	-47.673	-73.015	35	-10.5	-78	5.7	4
PASW00-1	-47.672	-71.776	1800	-15.2	-112	9.4	4
PASW25	-47.648	-71.742	1520	-15.6	-118	7.0	4
PASW14	-47.634	-71.277	860	-15.3	-118	4.8	4
PASW24	-47.633	-71.745	1225	-15.7	-120	5.7	4
PASW99-13	-47.611	-72.914	120	-12.4	-90	9.3	4
PASW9	-47.610	-72.877	95	-12.1	-87	10.1	4
PASW62	-47.610	-72.905	138	-12.5	-76	23.9	4
PASW69	-47.590	-71.746	220	-15.2	-114	7.9	4
PASW71	-47.579	-71.284	624	-14.3	-107	7.5	4
PASW23	-47.576	-71.382	625	-15.0	-111	8.7	4
PASW50	-47.571	-71.584	245	-12.3	-91	7.1	4
PASW99-12	-47.567	-72.864	90	-14.2	-100	13.8	4
PASW10	-47.567	-72.864	90	-14.2	-96	17.9	4
G3-01	-47.567	-72.864	90	-13.6			4
PASW63	-47.547	-72.861	90	-12.9	-88	15.0	4
PASW67	-47.523	-71.803	160	-14.2	-108	5.7	4
PASW64	-47.514	-72.865	93	-13.6	-92	17.0	4
PASW15	-47.445	-72.064	475	-13.9	-96	15.1	4

Table 1
(continued)

Sample	Latitude	Longitude	Elevation (m)	$\delta^{18}O$ (‰)	δD (‰)	d-excess	Source
PASW16	-47.435	-72.036	490	-14.8	-107	11.8	4
PASW17	-47.434	-72.019	450	-14.4	-102	13.0	4
PASW18	-47.427	-72.002	410	-14.5	-109	7.3	4
PASW19	-47.420	-71.943	167	-15.0	-105	14.6	4
PASW99-3	-47.176	-71.822	630	-14.7	-112	5.3	4
PASW12	-47.161	-71.835	630	-15.3	-114	8.8	4
PASW99-15	-47.121	-72.047	556	-14.3	-104	10.5	4
PASW66	-47.121	-72.048	538	-13.9	-99	12.7	4
PASW11	-47.121	-72.048	590	-14.3	-102	12.6	4

Sources: [1]this work; [2]Mayr and others, 2007; [3]Smith and Evans, 2007; [4]Stern and Blisniuk, 2002.

age control

Four sandstones from the Lago Jeinimeni section were crushed and zircons were separated based on their high density and non-magnetic character. Crushed samples were hydraulically separated using a Gemeni shaking table, and the resulting high-density fraction was repeatedly passed through a Franz magnetic separator at increasing magnet strengths. The highest density fraction was isolated using methylene iodide heavy liquid ($\rho = 3.32$ g/cm^3). Zircons were analyzed at the University of California Santa Cruz LA-ICP-MS laboratory following the procedure described by Sharman and others (2013). Sri Lankan zircon (SL2) (563 Ma) was used as the primary standard and Plesovice (337 Ma) was used as a secondary standard. Results are reported in table 2.

The Lago Jeinimeni section has previously been considered to be of Paleocene–Eocene age based on the paleofloral assemblage at the site (Suárez and others, 2000). The lowest sandstone sampled in the section contains grains as young as Campanian (Late Cretaceous). The remaining three sandstones have, in ascending stratigraphic order, youngest zircon U/Pb ages of 57.3 ± 2.7 Ma, 53.7 ± 2.9 Ma, and 50.5 ± 2.5 Ma. We interpret these three samples as contemporaneous with deposition, given that arc magmatism was active during these times (figs. 3A and 3B). The age of the uppermost sandstone bed is statistically identical to the whole rock $^{40}Ar/^{39}Ar$ age of the basalt flow conformably overlying the sediments <3 m above it (Encinas and others, 2019). We also note that the ages become progressively younger with stratigraphic height and are consistent with the paleofloral age. The lowest sample is interpreted to be Paleocene as well, as it lies <6 m below the next dated sandstone and the lithologic character of the section appears continuous. The lack of young volcanic zircons is anomalous compared to the other samples.

hydrogen isotopes in hydrated glass

While modern water isotopes are easy to measure, reconstructing them in the past requires a material that records isotopic composition and then remains stable over long (>10 Myr) time scales. Soil carbonate nodules have been used in many paleoclimate and paleotopography studies (Quade and others, 2007). However, the evaporative origin of carbonate nodules and the seasonal and episodic nature of their formation (Breecker and others, 2009; Ringham and others, 2016) make them more difficult to interpret.

We employed hydrogen isotopes (δD) preserved in the hydration water of volcanic glass to reconstruct water isotopes through time. Knowledge of volcanic glass hydration has been utilized in obsidian hydration dating (for example, Friedman and

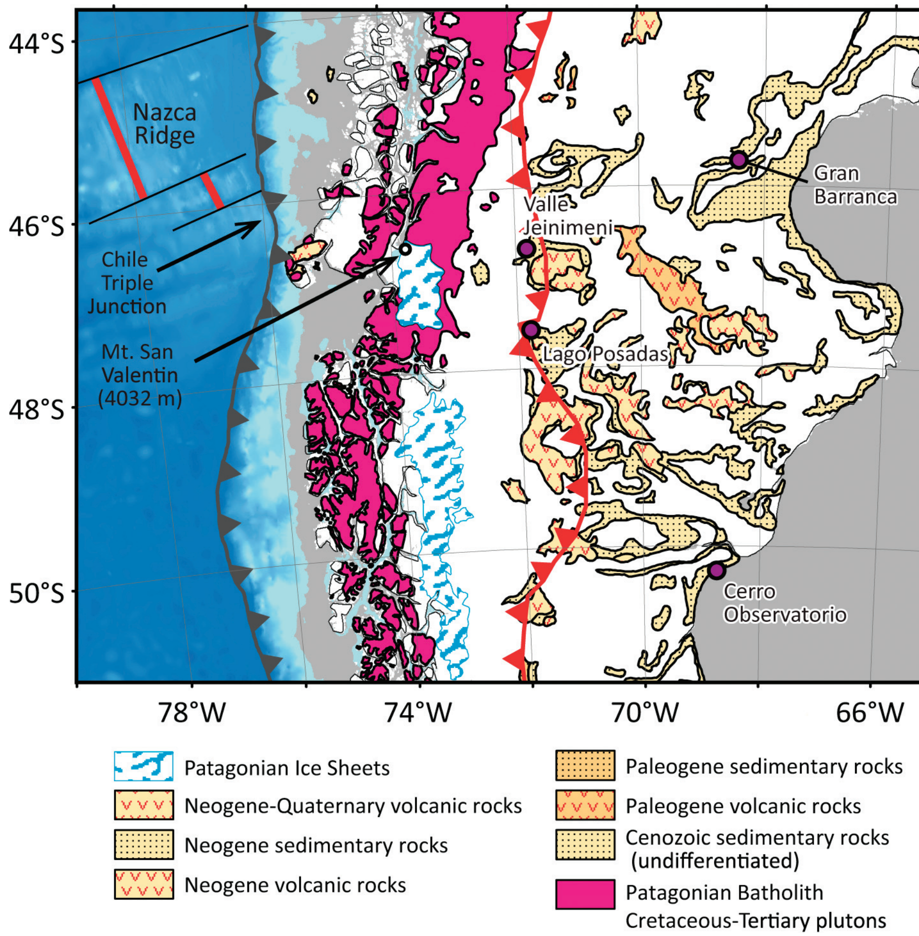

Fig. 7. Map of Patagonia showing selected tectonic features and geologic units. Sample sites and locations mentioned in the text are denoted by purple circles.

Smith, 1960) and assessing the stability of glasses used in nuclear waste storage (for example, Grambow, 2006), as well as isotopic reconstruction of ancient magmatic and environmental waters (Friedman and others, 1993b; Mulch and Chamberlain, 2007; Seligman and others, 2016). Following eruption, volcanic glass typically retains ≤0.3 weight percent magmatic water (Ross and Smith, 1955; Dingwell, 1996). This nominally dry glass is unstable in the surface environment, and as such will take up environmental water as it moves towards a more stable hydrated phase. Once bound, the hydration products are largely stable at earth surface conditions; Friedman and others (1993a) found that temperatures of >800 °C were required to liberate this hydrogen on laboratory time scales. Glass particles typically have thin walls and high surface area, which allows them to hydrate rapidly and completely (Nolan and Bindeman, 2013). The water donates H^+ ions that exchange with alkali cations (for example, Na^+, K^+) (Cerling and others, 1985). Anovitz and others (2009) show that fully hydrated glass is resistant to further change in hydrogen content. Complete hydration is observed to occur in the range of ~1 to 5 weight percent water, typically around ~3.5 weight percent (for example, Ross and Smith, 1955). Higher water contents may indicate the

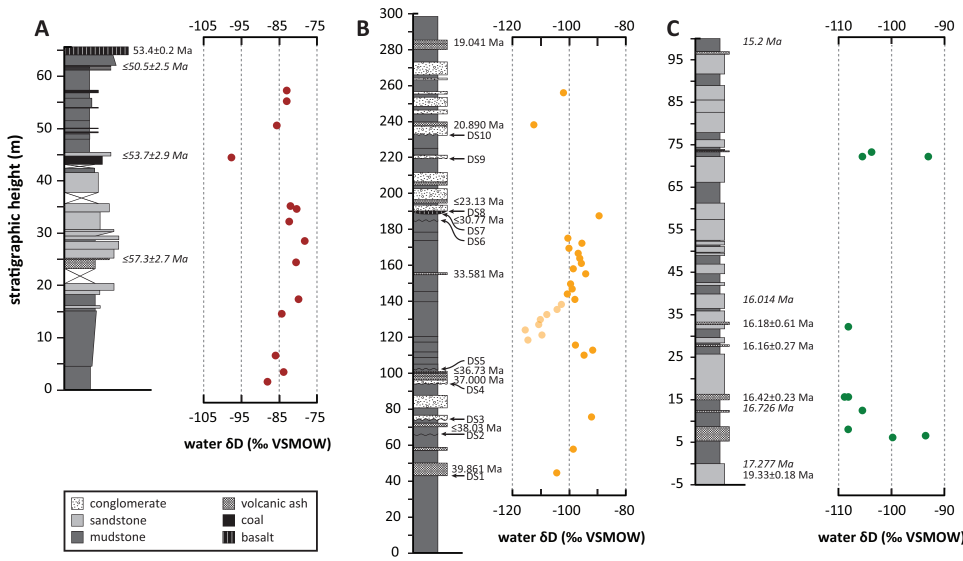

Fig. 8. Stratigraphic columns and reconstructed meteoric water δD for sections at (A) Lago Jeinimeni (Mina Ligorio Márquez), (B) Gran Barranca, and (C) Cerro Observatorio. Radiometric age measurements interpreted to be formation ages are indicated to the right of columns in roman type; indirect constraints from detrital zircons (Lago Jeinimeni and Gran Barranca) and paleomagnetism (Cerro Observatorio) are in italics. Detrital zircon ages are the minimum U/Pb age from the dated population of grains. Half-shaded δD points in Gran Barranca section are shown only for assessment of alteration (and thus not in fig. 10); their paleoclimate significance is discussed in Colwyn and Hren (2019).

added presence of clays or other hydrous phases. Sonication is widely used to remove these phases (for example, fig. 9). Full hydration typically occurs in 10^3 to 10^4 years (Friedman and Long, 1976; Cerling and others, 1985; Friedman and others, 1993b). This is advantageous because the hydration process tends to average out short-term isotopic variations due to climate.

The hydrogen isotopic composition of the hydrated glass can be related back to the ambient water composition via an effective fractionation factor (Friedman and Smith, 1958; Friedman and others, 1993b; Cassel and Breecker, 2017), and there is strong evidence for the long-term stability of the δD of the initial hydration water. First, studies of natural glasses show that after initial hydration, the δD is generally preserved, even in sediments that have been buried to depths of several kilometers. In particular, in a related study we have found that volcanic glass retains isotopic variability related to the Eocene-Oligocene climatic transition, which implies minimal to no resetting by younger water (Colwyn and Hren, 2019). Second, contemporaneous glasses record expected variations in δD between fluvial and lacustrine environments (Cassel and Breecker, 2017). Third, they preserve gradients in elevation (Jackson and others, 2017). These observations support the interpretation that hydrated glass has long-term stability and reflects the long-term (10^3–10^4 yr) average of the local precipitation during initial hydration (Friedman and others, 1993b; Dettinger and Quade, 2015; Seligman and others, 2016). Consequently, glass δD has been used to reconstruct Cenozoic paleoclimate and paleotopography (for example, Mulch and others, 2008; Cassel and others, 2009; Canavan and others, 2014; Fan and others, 2014; Pingel and others, 2014; Saylor and Horton, 2014).

In order to understand the mechanism(s) for the observed stability of the isotopic composition of glass hydration water, some studies have explored the behavior of glass

TABLE 2

Detrital zircon U-Pb geochronologic analyses by LA-ICP-MS analysis

Sample	Isotopic data: $^{207}Pb/^{235}U$	±2SE	$^{206}Pb/^{238}U$	±2SE	Error correlation	$^{238}U/^{206}Pb$	±2SE	$^{207}Pb/^{206}Pb$	±2SE	Error correlation	Calculated ages (Ma): $^{207}Pb/^{235}U$ age	±2SE	$^{206}Pb/^{238}U$ age	±2SE	$^{207}Pb/^{206}Pb$ age	±2SE	% discordant	Best age	±2SE
15LJ55	0.0862	0.009	0.01223	0.00067	0.078	81.76615	4.479421	0.0508	0.0045	0.25866	83.4	8.4	78.3	4.3	220	170	-6.51	78.3	4.3
15LJ55	0.0788	0.0085	0.01232	0.00065	0.075	81.16883	4.282446	0.046	0.0041	0.26269	76.6	8	78.9	4.1	40	160	2.92	78.9	4.1
15LJ55	0.0834	0.0097	0.01238	0.00064	0.150	80.77544	4.17579	0.0497	0.0049	0.22261	81.5	8.8	79.3	4.1	160	170	-2.77	79.3	4.1
15LJ55	0.091	0.012	0.01241	0.0007	0.025	80.58018	4.545215	0.0533	0.0067	0.29408	87	11	79.5	4.5	290	230	-9.43	79.5	4.5
15LJ55	0.111	0.013	0.01634	0.00086	0.096	61.19951	3.221027	0.0489	0.0048	0.30052	105	12	104.4	5.4	140	180	-0.57	104.4	5.4
15LJ55	0.113	0.01	0.01661	0.00082	0.354	60.2047	2.972176	0.0492	0.003	0.15294	108.3	9.1	106.2	5.2	170	120	-1.98	106.2	5.2
15LJ55	0.1202	0.0095	0.01672	0.00079	0.384	59.80861	2.825885	0.0519	0.0024	0.17137	115.1	8.6	106.9	5	280	100	-7.67	106.9	5
15LJ55	0.124	0.011	0.01692	0.00081	0.170	59.10165	2.829335	0.0533	0.0036	0.21338	118	10	108.2	5.1	330	140	-9.06	108.2	5.1
15LJ55	0.121	0.011	0.01702	0.00084	0.186	58.75441	2.899747	0.0518	0.0035	0.24537	115.1	9.9	108.8	5.3	250	130	-5.79	108.8	5.3
15LJ55	0.1204	0.0099	0.01719	0.0008	0.167	58.17336	2.707312	0.0513	0.0029	0.29396	115.7	9.1	109.8	5	250	110	-5.37	109.8	5
15LJ55	0.11	0.01	0.01724	0.00081	0.068	58.00464	2.725276	0.0465	0.0032	0.24389	105.7	9.3	110.2	5.1	60	130	4.08	110.2	5.1
15LJ55	0.112	0.011	0.01725	0.00083	0.167	57.97101	2.78933	0.0469	0.0032	0.14948	107.3	9.6	110.2	5.2	70	130	2.63	110.2	5.2
15LJ55	0.1163	0.0089	0.01734	0.00079	0.185	57.67013	2.627416	0.0486	0.0023	0.33971	112	8	110.8	5	147	99	-1.08	110.8	5
15LJ55	0.1135	0.0088	0.01736	0.00082	0.330	57.60369	2.720911	0.0474	0.0022	0.27036	109	8	110.9	5.2	80	93	1.71	110.9	5.2
15LJ55	0.125	0.011	0.01732	0.00083	0.162	57.73672	2.766829	0.0527	0.0035	0.074456	119	10	110.9	5.3	240	120	-7.30	110.9	5.3
15LJ55	0.1192	0.0093	0.01744	0.00082	0.485	57.33945	2.696006	0.0494	0.0023	0.26157	114.2	8.5	111.4	5.2	163	94	-2.51	111.4	5.2
15LJ55	0.125	0.013	0.0174	0.00088	0.108	57.47126	2.906593	0.0519	0.0045	0.25723	122	12	111.5	5.7	300	170	-9.42	111.5	5.7
15LJ55	0.1148	0.0095	0.01746	0.00079	0.206	57.27377	2.591425	0.0481	0.0027	0.17306	110.6	8.8	111.6	5	110	110	0.90	111.6	5
15LJ55	0.119	0.01	0.01746	0.00084	0.197	57.27377	2.755439	0.0506	0.0029	0.32171	114.3	9.3	111.6	5.3	210	110	-2.42	111.6	5.3
15LJ55	0.116	0.012	0.01746	0.00092	0.171	57.27377	3.017862	0.0484	0.0039	0.20016	112	11	111.6	5.8	120	140	-0.36	111.6	5.8
15LJ55	0.12	0.011	0.01751	0.00085	0.037	57.11022	2.772341	0.0495	0.0034	0.22667	115	9.8	111.9	5.4	190	130	-2.77	111.9	5.4
15LJ55	0.1194	0.0095	0.01754	0.00081	0.242	57.01254	2.632848	0.0495	0.0024	0.3002	114.3	8.6	112.1	5.2	190	100	-1.96	112.1	5.2
15LJ55	0.1218	0.0098	0.01758	0.00081	0.336	56.88282	2.620881	0.05	0.0025	0.10816	116.5	8.9	112.3	5.1	190	100	-3.74	112.3	5.1
15LJ55	0.127	0.012	0.0176	0.00088	0.322	56.81818	2.840909	0.0507	0.0034	0.11796	121	11	112.4	5.6	230	130	-7.65	112.4	5.6
15LJ55	0.119	0.011	0.01763	0.00087	0.310	56.7215	2.799076	0.0488	0.0033	0.19433	114	10	112.6	5.5	140	130	-1.24	112.6	5.5
15LJ55	0.1131	0.0096	0.01765	0.00084	0.485	56.65722	2.696434	0.0466	0.0025	0.037422	109	8.8	112.8	5.3	60	100	3.37	112.8	5.3
15LJ55	0.1193	0.0097	0.01765	0.00083	0.259	56.65722	2.664334	0.0495	0.0026	0.15099	114.2	8.8	112.8	5.3	170	110	-1.24	112.8	5.3
15LJ55	0.121	0.011	0.01767	0.00086	0.225	56.5931	2.754389	0.049	0.003	0.25587	115.9	9.6	112.9	5.5	170	120	-2.66	112.9	5.5
15LJ55	0.1172	0.0098	0.01768	0.00084	0.341	56.56109	2.687291	0.0487	0.0027	0.027739	113.3	8.9	113	5.3	130	110	-0.27	113	5.3
15LJ55	0.1188	0.009	0.01773	0.00081	0.535	56.40158	2.576722	0.0489	0.0021	0.19277	113.9	8.1	113.3	5.1	135	91	-0.53	113.3	5.1
15LJ55	0.1172	0.0089	0.01774	0.0008	0.465	56.36979	2.542042	0.0482	0.002	0.13772	112.7	8	113.4	5.1	119	91	0.62	113.4	5.1
15LJ55	0.1202	0.0094	0.01776	0.00081	0.512	56.30631	2.568024	0.0501	0.0022	-0.0078247	115.1	8.6	113.5	5.1	191	94	-1.41	113.5	5.1
15LJ55	0.131	0.01	0.01789	0.00085	0.423	55.89715	2.655818	0.0526	0.0024	0.29961	124.5	9.2	114.3	5.4	300	100	-8.92	114.3	5.4
15LJ55	0.1182	0.0095	0.0179	0.00084	0.259	55.86592	2.621641	0.0485	0.0025	0.2671	113.6	8.5	114.4	5.3	120	100	0.70	114.4	5.3
15LJ55	0.123	0.011	0.01792	0.00087	0.113	55.80357	2.709214	0.0498	0.0033	0.24768	118	10	114.5	5.5	210	130	-3.06	114.5	5.5
15LJ55	0.131	0.011	0.0179	0.00085	0.361	55.86592	2.652851	0.0529	0.0027	0.1787	124.4	9.6	114.6	5.3	330	110	-8.55	114.6	5.3
15LJ55	0.1299	0.0099	0.01804	0.00084	0.212	55.43237	2.581108	0.0524	0.0024	0.4392	123.9	8.9	115.5	5.4	300	100	-7.27	115.5	5.4
15LJ55	0.123	0.01	0.01816	0.00084	0.231	55.06608	2.547109	0.0495	0.0027	0.049305	117.3	9.2	116	5.3	160	110	-1.12	116	5.3
15LJ55	0.124	0.011	0.01816	0.00089	0.000	55.06608	2.698723	0.0498	0.0028	0.34676	117.9	9.5	116	5.6	180	110	-1.64	116	5.6

TABLE 2

(continued)

Sample	Isotopic data: $\frac{^{207}Pb}{^{235}U}$	±2SE	$\frac{^{206}Pb}{^{238}U}$	±2SE	Error correlation	$\frac{^{238}U}{^{206}Pb}$	±2SE	$\frac{^{207}Pb}{^{206}Pb}$	±2SE	Error correlation	Calculated ages (Ma): $\frac{^{207}Pb}{^{235}U}$ age	±2SE	$\frac{^{206}Pb}{^{238}U}$ age	±2SE	$\frac{^{207}Pb}{^{206}Pb}$ age	±2SE	% discordant	Best age	±2SE
15LJ55	0.1242	0.0093	0.01819	0.00084	0.657	54.97526	2.538715	0.0494	0.002	0.20855	119	8.3	116.2	5.3	168	90	-2.41	116.2	5.3
15LJ55	0.129	0.011	0.01822	0.00086	0.289	54.88474	2.590608	0.0518	0.003	0.18776	124.3	9.8	116.4	5.5	270	120	-6.79	116.4	5.5
15LJ55	0.126	0.01	0.01843	0.00088	0.285	54.25936	2.590789	0.0495	0.0027	0.19932	119.8	9.4	117.7	5.6	170	110	-1.78	117.7	5.6
15LJ55	0.1256	0.0097	0.01844	0.00085	0.359	54.22993	2.499753	0.0493	0.0022	0.28773	120	8.8	117.8	5.4	166	95	-1.87	117.8	5.4
15LJ55	0.125	0.011	0.01859	0.0009	0.168	53.79236	2.604256	0.0487	0.0031	0.27044	119	10	118.7	5.7	130	120	-0.25	118.7	5.7
15LJ55	0.12	0.01	0.01868	0.00088	0.049	53.53319	2.521906	0.0475	0.0028	0.39757	115.4	8.9	119.3	5.6	90	110	3.27	119.3	5.6
15LJ55	0.12	0.012	0.01871	0.00093	0.218	53.44735	2.656656	0.0481	0.0038	0.20019	116	11	119.5	5.9	100	140	2.93	119.5	5.9
15LJ55	0.121	0.01	0.01881	0.0009	0.132	53.16321	2.543694	0.0458	0.0027	0.29057	115.8	9.3	120.1	5.7	30	110	3.58	120.1	5.7
15LJ55	0.127	0.01	0.01902	0.00088	0.378	52.57624	2.432549	0.0489	0.0023	0.076984	121.7	8.9	121.4	5.6	160	100	-0.25	121.4	5.6
15LJ55	0.13	0.011	0.01901	0.0009	0.269	52.60389	2.490453	0.0502	0.0026	0.21063	124.8	9.4	121.4	5.7	190	100	-2.80	121.4	5.7
15LJ55	0.127	0.011	0.01933	0.00092	0.189	51.73306	2.462204	0.0478	0.0028	0.21221	121.2	9.8	123.4	5.8	110	120	1.78	123.4	5.8
15LJ55	0.13	0.01	0.01963	0.00088	0.319	50.94244	2.283716	0.0483	0.0022	0.18607	123.8	9.1	125.3	5.6	119	94	1.20	125.3	5.6
15LJ55	0.141	0.011	0.02059	0.00095	0.516	48.56727	2.24084	0.0499	0.0022	0.07557	133.9	9.8	131.4	6	182	97	-1.90	131.4	6
15LJ55	0.145	0.013	0.021	0.001	0.294	47.61905	2.267574	0.0506	0.003	0.17406	139	11	133.9	6.3	200	120	-3.81	133.9	6.3
15LJ55	0.146	0.012	0.02121	0.00097	0.279	47.14757	2.156207	0.0503	0.0026	0.16363	138	10	135.3	6.1	200	110	-2.00	135.3	6.1
15LJ55	0.153	0.014	0.0216	0.001	0.254	46.2963	2.143347	0.0522	0.0032	0.12839	145	12	137.7	6.5	280	120	-5.30	137.7	6.5
15LJ55	0.149	0.011	0.0221	0.001	0.598	45.24887	2.04746	0.0491	0.0021	0.10341	141	10	140.8	6.5	150	93	-0.14	140.8	6.5
15LJ55	0.17	0.013	0.0238	0.0011	0.471	42.01681	1.941953	0.0521	0.0023	0.099394	159	11	151.9	6.8	280	96	-4.67	151.9	6.8
15LJ55	0.167	0.014	0.0245	0.0012	0.397	40.81633	1.999167	0.0505	0.0029	0.15151	156	12	156	7.4	200	110	0.00	156	7.4
15LJ55	0.169	0.013	0.0252	0.0012	0.322	39.68254	1.889645	0.0494	0.0023	0.22555	158	11	160.6	7.3	169	98	1.62	160.6	7.3
15LJ55	0.192	0.019	0.0265	0.0013	0.087	37.73585	1.851193	0.053	0.0042	0.24586	177	16	168.5	8.4	330	150	-5.04	168.5	8.4
15LJ55	0.196	0.021	0.0267	0.0014	0.151	37.45318	1.963837	0.0532	0.0047	0.26439	181	17	169.6	9	320	170	-6.72	169.6	9
15LJ55	0.181	0.017	0.0269	0.0013	0.095	37.17472	1.796548	0.0493	0.0035	0.33215	171	15	170.8	8.2	170	130	-0.12	170.8	8.2
15LJ55	0.186	0.019	0.0272	0.0014	0.182	36.76471	1.892301	0.0515	0.0043	0.23076	174	17	173.1	8.5	230	160	-0.52	173.1	8.5
15LJ55	0.183	0.015	0.0273	0.0013	0.333	36.63004	1.744287	0.0482	0.0024	0.19254	170	13	173.9	8.1	111	98	2.24	173.9	8.1
15LJ55	0.21	0.017	0.0277	0.0013	0.125	36.10108	1.694275	0.0558	0.0032	0.22903	193	14	175.8	8.2	390	110	-9.78	175.8	8.2
15LJ55	0.193	0.016	0.0278	0.0013	0.091	35.97122	1.682108	0.0503	0.0029	0.29953	179	14	176.5	8.1	230	120	-1.42	176.5	8.1
15LJ55	0.212	0.019	0.0278	0.0014	0.283	35.97122	1.8115	0.0547	0.0033	0.1872	194	16	176.9	8.8	370	120	-9.67	176.9	8.8
15LJ55	0.202	0.017	0.0283	0.0013	0.270	35.33569	1.623194	0.0519	0.0031	-0.052297	186	14	180.1	8.2	240	110	-3.28	180.1	8.2
15LJ55	0.201	0.017	0.0285	0.0013	0.233	35.08772	1.600492	0.0517	0.003	0.24747	187	15	180.8	8.3	260	120	-3.43	180.8	8.3
15LJ55	0.453	0.078	0.0584	0.0029	0.385	17.12329	0.8503002	0.0564	0.0054	-0.04543	378	31	366	17	440	110	-3.28	366	17
15LJ59	0.0598	0.0057	0.00893	0.00043	0.178	111.9821	5.392194	0.0488	0.0036	0.13412	58.8	5.5	57.3	2.7	150	140	-2.62	57.3	2.7
15LJ59	0.0734	0.0057	0.0113	0.00053	0.645	88.49558	4.150677	0.0471	0.0021	-0.021547	71.8	5.4	72.4	3.4	76	91	0.83	72.4	3.4
15LJ59	0.077	0.011	0.01178	0.00067	0.236	84.88964	4.828189	0.0479	0.0057	0.090495	75	10	75.5	4.3	40	200	0.66	75.5	4.3
15LJ59	0.0827	0.0077	0.01204	0.00061	0.000	83.05648	4.208011	0.0494	0.0037	0.41451	80.4	7.2	77.1	3.9	180	140	-4.28	77.1	3.9
15LJ59	0.0784	0.0085	0.01252	0.00062	0.000	79.8722	3.955333	0.0466	0.0043	0.42004	76.2	7.9	80.2	4	50	160	4.99	80.2	4
15LJ59	0.0824	0.0083	0.01254	0.00063	0.107	79.74482	4.006319	0.0489	0.0041	0.31335	80	7.8	80.3	4	150	150	0.37	80.3	4
15LJ59	0.1154	0.0093	0.01696	0.00078	0.136	58.96226	2.711708	0.0489	0.0026	0.37763	111.1	8.3	108.4	5	140	100	-2.49	108.4	5

TABLE 2
(continued)

Sample	Isotopic data $\frac{^{207}Pb}{^{235}U}$	±2SE	$\frac{^{206}Pb}{^{238}U}$	±2SE	Error correlation	$\frac{^{238}U}{^{206}Pb}$	±2SE	$\frac{^{207}Pb}{^{206}Pb}$	±2SE	Error correlation	Calculated ages (Ma) $\frac{^{207}Pb}{^{235}U}$ age	±2SE	$\frac{^{206}Pb}{^{238}U}$ age	±2SE	$\frac{^{207}Pb}{^{206}Pb}$ age	±2SE	% discordant	Best age	±2SE
15LJ59	0.122	0.01	0.01711	0.00079	0.250	58.44535	2.698529	0.0518	0.0029	0.18856	116.8	9.4	109.4	5	270	110	-6.76	109.4	5
15LJ59	0.119	0.012	0.01732	0.00086	0.169	57.73672	2.866835	0.0487	0.0039	0.1403	114	11	110.7	5.5	140	150	-2.98	110.7	5.5
15LJ59	0.1132	0.0095	0.01733	0.00084	0.159	57.7034	2.796934	0.0487	0.0029	0.40978	108.6	8.7	110.8	5.3	140	120	1.99	110.8	5.3
15LJ59	0.12	0.01	0.01735	0.00079	0.211	57.63689	2.624389	0.0497	0.0028	0.17581	115.4	9	110.9	5	180	110	-4.06	110.9	5
15LJ59	0.122	0.012	0.01742	0.0009	0.178	57.40528	2.96583	0.0512	0.004	0.20276	117	11	111.3	5.7	230	150	-5.12	111.3	5.7
15LJ59	0.1118	0.0095	0.01747	0.0008	0.094	57.24098	2.621224	0.0479	0.0029	0.25831	107.3	8.7	111.7	5.1	110	120	3.94	111.7	5.1
15LJ59	0.1229	0.0098	0.0175	0.0008	0.358	57.14286	2.612245	0.0513	0.0025	0.065306	117.9	9	111.8	5.1	240	100	-5.46	111.8	5.1
15LJ59	0.1193	0.0098	0.01758	0.00081	0.373	56.88282	2.620881	0.049	0.0025	0.075203	114.2	8.9	112.4	5.1	140	100	-1.60	112.4	5.1
15LJ59	0.1186	0.0091	0.01766	0.00082	0.524	56.62514	2.629253	0.049	0.0021	0.18669	113.7	8.2	112.8	5.2	160	93	-0.80	112.8	5.2
15LJ59	0.1166	0.0089	0.01768	0.00083	0.521	56.56109	2.6553	0.0486	0.0021	0.26398	111.9	8.1	113	5.3	127	95	0.97	113	5.3
15LJ59	0.13	0.012	0.01775	0.00083	0.297	56.33803	2.634398	0.0517	0.0034	-0.027121	123	11	113.4	5.3	250	130	-8.47	113.4	5.3
15LJ59	0.1222	0.0094	0.01783	0.00081	0.451	56.08525	2.5479	0.0499	0.0022	0.080257	117.3	8.4	113.9	5.1	183	93	-2.99	113.9	5.1
15LJ59	0.121	0.01	0.01787	0.00086	0.000	55.95971	2.693081	0.0495	0.0028	0.38791	116.2	9	114.2	5.5	170	110	-1.75	114.2	5.5
15LJ59	0.124	0.01	0.01793	0.00083	0.401	55.77245	2.58177	0.0507	0.0025	0.098304	118.9	9	114.5	5.3	220	100	-3.84	114.5	5.3
15LJ59	0.1212	0.0095	0.01792	0.00083	0.250	55.80357	2.584652	0.0503	0.0024	0.27835	116.1	8.6	114.5	5.3	200	100	-1.40	114.5	5.3
15LJ59	0.123	0.0099	0.01792	0.00084	0.145	55.80357	2.615792	0.0515	0.0028	0.3654	117.6	9	114.5	5.3	250	110	-2.71	114.5	5.3
15LJ59	0.12	0.01	0.01804	0.00085	0.207	55.43237	2.611836	0.0486	0.0027	0.22021	114.9	9.1	115.3	5.4	140	110	0.35	115.3	5.4
15LJ59	0.1191	0.0092	0.01807	0.00083	0.390	55.34034	2.541919	0.0478	0.0021	0.22972	114.5	8.5	115.4	5.3	97	90	0.78	115.4	5.3
15LJ59	0.125	0.01	0.01825	0.00083	0.676	54.79452	2.492025	0.0491	0.0022	0.35602	119.6	8.9	116.6	5.2	146	88	-2.57	116.6	5.2
15LJ59	0.128	0.011	0.01832	0.00085	0.099	54.58515	2.532608	0.0505	0.0028	0.30768	122.6	9.4	117	5.4	210	110	-4.79	117	5.4
15LJ59	0.124	0.01	0.01832	0.00087	0.194	54.58515	2.592199	0.0496	0.0028	0.24966	119.5	9.4	117	5.5	170	110	-2.14	117	5.5
15LJ59	0.115	0.011	0.01834	0.00094	0.170	54.52563	2.794661	0.0466	0.0032	0.37761	111.7	9.2	117.1	5.9	60	120	4.61	117.1	5.9
15LJ59	0.126	0.01	0.01833	0.00084	0.259	54.55537	2.500083	0.0512	0.0027	0.1523	120.7	9.2	117.1	5.3	230	110	-3.07	117.1	5.3
15LJ59	0.121	0.0097	0.01838	0.00086	0.090	54.40696	2.545701	0.0478	0.0027	0.3269	115.8	8.8	117.4	5.4	100	110	1.36	117.4	5.4
15LJ59	0.132	0.011	0.01838	0.00086	0.149	54.40696	2.545701	0.0524	0.0028	0.15906	126	10	117.4	5.5	310	100	-7.33	117.4	5.5
15LJ59	0.127	0.011	0.01837	0.00086	0.221	54.43658	2.548474	0.0506	0.0027	0.20569	121.3	9.5	117.4	5.5	230	110	-3.32	117.4	5.5
15LJ59	0.127	0.01	0.01838	0.00083	0.234	54.40696	2.456898	0.0508	0.0025	0.23147	121.6	9.1	117.4	5.3	220	100	-3.58	117.4	5.3
15LJ59	0.123	0.011	0.0184	0.00089	0.214	54.34783	2.628781	0.0482	0.0028	0.23547	117.7	9.5	117.5	5.6	140	120	-0.17	117.5	5.6
15LJ59	0.129	0.011	0.01843	0.00086	0.217	54.25936	2.531907	0.052	0.003	0.15882	123.2	9.8	117.7	5.5	260	120	-4.67	117.7	5.5
15LJ59	0.122	0.01	0.01842	0.00086	0.333	54.28882	2.534657	0.0487	0.0027	0.033538	117	9.3	117.7	5.4	130	110	0.59	117.7	5.4
15LJ59	0.125	0.011	0.01849	0.00089	0.176	54.08329	2.603252	0.0511	0.0033	0.23608	119.5	9.9	118.1	5.6	230	130	-1.19	118.1	5.6
15LJ59	0.125	0.011	0.01854	0.00089	0.216	53.93743	2.58923	0.0501	0.003	0.24074	118.8	9.7	118.4	5.6	190	120	-0.34	118.4	5.6
15LJ59	0.134	0.013	0.01855	0.00089	0.063	53.90836	2.586439	0.0548	0.0043	0.2976	128	12	118.5	5.6	350	160	-8.02	118.5	5.6
15LJ59	0.135	0.013	0.0186	0.00091	0.000	53.76344	2.630362	0.0525	0.0039	0.37528	128	11	118.8	5.7	300	140	-7.74	118.8	5.7
15LJ59	0.124	0.01	0.0186	0.00086	0.206	53.76344	2.485837	0.0478	0.0026	0.20027	118.1	9.1	118.8	5.4	110	110	0.59	118.8	5.4
15LJ59	0.128	0.01	0.01867	0.00086	0.367	53.56186	2.467231	0.0498	0.0024	0.054419	122.5	9.2	119.2	5.4	180	100	-2.77	119.2	5.4
15LJ59	0.128	0.011	0.0187	0.00087	0.212	53.47594	2.487918	0.049	0.0027	0.19788	122.3	9.7	119.4	5.5	160	110	-2.43	119.4	5.5
15LJ59	0.127	0.011	0.01878	0.0009	0.272	53.24814	2.551828	0.0492	0.0028	0.21708	121.2	9.6	119.9	5.7	170	110	-1.08	119.9	5.7
15LJ59	0.127	0.011	0.01881	0.00089	0.247	53.16321	2.515431	0.0499	0.0029	0.15024	120.7	9.7	120.1	5.6	200	110	-0.50	120.1	5.6

TABLE 2
(continued)

Sample	Isotopic data: $^{207}Pb/^{235}U$	±2SE	$^{206}Pb/^{238}U$	±2SE	Error correlation	$^{238}U/^{206}Pb$	±2SE	$^{207}Pb/^{206}Pb$	±2SE	Error correlation	Calculated ages (Ma): $^{207}Pb/^{235}U$ age	±2SE	$^{206}Pb/^{238}U$ age	±2SE	$^{207}Pb/^{206}Pb$ age	±2SE	% discordant	Best age	±2SE
15LJ59	0.132	0.011	0.0189	0.00087	0.287	52.91005	2.435542	0.0499	0.0028	0.10082	127	10	120.7	5.5	190	110	-5.22	120.7	5.5
15LJ59	0.134	0.012	0.01904	0.00089	0.117	52.52101	2.455026	0.0505	0.0032	0.21973	127	11	121.6	5.6	200	130	-4.44	121.6	5.6
15LJ59	0.127	0.013	0.01999	0.00098	0.119	50.02501	2.452452	0.0471	0.0037	0.23517	122	11	127.6	6.2	70	140	4.39	127.6	6.2
15LJ59	0.143	0.011	0.02128	0.00097	0.524	46.99248	2.142044	0.0488	0.0021	0.13912	135.4	9.7	135.8	6.1	143	91	0.29	135.8	6.1
15LJ59	0.15	0.012	0.0215	0.001	0.271	46.51163	2.163332	0.0506	0.0026	0.25821	143	10	137.3	6.3	230	110	-4.15	137.3	6.3
15LJ59	0.16	0.013	0.0216	0.001	0.449	46.2963	2.143347	0.0531	0.0025	0.11151	150	11	137.6	6.4	350	110	-9.01	137.6	6.4
15LJ59	0.163	0.014	0.0226	0.001	0.496	44.24779	1.957867	0.0536	0.0028	-0.092383	153	12	144	6.6	330	110	-6.25	144	6.6
15LJ59	0.157	0.012	0.023	0.0011	0.315	43.47826	2.079395	0.051	0.0024	0.20494	147	11	146.7	6.6	230	100	-0.20	146.7	6.6
15LJ59	0.189	0.017	0.0272	0.0013	0.121	36.76471	1.757137	0.05	0.0034	0.20092	175	15	173.1	8.2	190	130	-1.10	173.1	8.2
15LJ59	0.189	0.017	0.0272	0.0013	0.073	36.76471	1.757137	0.0527	0.0038	0.37391	174	15	173.1	8.3	290	140	-0.52	173.1	8.3
15LJ59	0.191	0.017	0.0278	0.0013	0.147	35.97122	1.682108	0.0502	0.0032	0.24703	178	14	176.6	8.1	210	130	-0.79	176.6	8.1
15LJ59	0.195	0.017	0.0279	0.0013	0.185	35.84229	1.670071	0.0515	0.0032	0.11127	180	15	177.8	8.3	240	120	-1.24	177.8	8.3
15LJ59	0.189	0.016	0.0283	0.0013	0.070	35.33569	1.623194	0.0491	0.0029	0.33546	175	14	179.9	8.4	150	120	2.72	179.9	8.4
15LJ59	0.195	0.016	0.0285	0.0013	0.328	35.08772	1.600492	0.0506	0.0025	0.16807	181	14	181.4	8.2	210	100	0.22	181.4	8.2
15LJ59	0.199	0.018	0.0286	0.0014	0.280	34.96503	1.711575	0.0503	0.003	0.1787	184	15	181.9	8.7	220	120	-1.15	181.9	8.7
15LJ59	0.284	0.022	0.0395	0.0018	0.460	25.31646	1.153661	0.0524	0.0023	0.29341	253	17	250	11	287	94	-1.20	250	11
15LJ59	0.308	0.024	0.0398	0.0018	0.278	25.12563	1.136335	0.0565	0.0026	0.2945	272	18	251	11	440	100	-8.37	251	11
15LJ59	0.303	0.023	0.0412	0.0018	0.326	24.27184	1.06042	0.0537	0.0023	0.2391	268	18	260	11	345	97	-3.08	260	11
15LJ59	0.51	0.039	0.0671	0.0032	0.638	14.90313	0.7107305	0.0557	0.0023	0.14459	419	26	419	19	447	92	0.00	419	19
15LJ59	1.84	0.14	0.1731	0.0081	0.610	5.777008	0.2703279	0.077	0.0031	0.31764	1058	49	1029	44	1127	79	-2.82	1127	79
15LJ02	0.0518	0.0065	0.00836	0.00046	0.000	119.6172	6.581809	0.0472	0.0055	0.31276	50.9	6.3	53.7	2.9	40	200	5.21	53.7	2.9
15LJ02	0.0543	0.0056	0.00884	0.00047	0.086	113.1222	6.014414	0.0447	0.0038	0.26717	53.5	5.4	56.9	3	-10	150	5.98	56.9	3
15LJ02	0.0866	0.0073	0.01218	0.00058	0.252	82.10181	3.90961	0.0512	0.0029	0.23894	84.1	6.8	78	3.7	270	110	-7.82	78	3.7
15LJ02	0.0812	0.0067	0.01233	0.00057	0.124	81.103	3.749287	0.0488	0.0027	0.26991	79.2	6.3	79	3.6	140	110	-0.25	79	3.6
15LJ02	0.086	0.011	0.01244	0.00069	0.055	80.38585	4.458701	0.0514	0.0059	0.34901	84	10	79.7	4.4	230	200	-5.40	79.7	4.4
15LJ02	0.0823	0.0081	0.01266	0.00064	0.111	78.98894	3.993122	0.0486	0.0039	0.26835	79.9	7.6	81.1	4.1	130	150	1.48	81.1	4.1
15LJ02	0.0897	0.0094	0.01328	0.00066	0.156	75.3012	3.742379	0.0476	0.004	0.16524	86.7	8.7	85.1	4.2	90	150	-1.88	85.1	4.2
15LJ02	0.1132	0.0099	0.01621	0.00076	0.275	61.69031	2.892328	0.0491	0.0029	0.11729	108.5	9	103.6	4.8	160	120	-4.73	103.6	4.8
15LJ02	0.12	0.0091	0.01689	0.00078	0.603	59.20663	2.734232	0.0518	0.0021	0.26494	115	8.2	107.9	4.9	276	94	-6.58	107.9	4.9
15LJ02	0.1088	0.009	0.01689	0.00077	0.318	59.20663	2.699177	0.0469	0.0025	0.10168	104.6	8.2	108	4.9	80	100	3.15	108	4.9
15LJ02	0.1215	0.0091	0.01698	0.00077	0.628	58.89282	2.67064	0.0521	0.0021	0.21185	116.6	8.1	108.5	4.9	283	92	-7.47	108.5	4.9
15LJ02	0.1138	0.0095	0.01719	0.00081	0.038	58.17336	2.741153	0.0475	0.0028	0.43386	109.6	8.8	109.9	5.1	90	110	0.27	109.9	5.1
15LJ02	0.12	0.01	0.01726	0.00084	0.353	57.93743	2.819666	0.0504	0.0028	0.18871	115.6	9	110.3	5.3	230	120	-4.81	110.3	5.3
15LJ02	0.1088	0.0089	0.01731	0.00079	0.368	57.77008	2.636531	0.0458	0.0023	0.065293	104.7	8.1	110.7	5	17	96	5.42	110.7	5
15LJ02	0.1179	0.009	0.01735	0.00079	0.372	57.63689	2.624389	0.0499	0.0022	0.20179	113.4	8.3	110.9	5	189	95	-2.25	110.9	5
15LJ02	0.121	0.01	0.01733	0.00081	0.000	57.7034	2.697043	0.0516	0.0034	0.47117	116.7	9.5	111	5.2	250	130	-5.14	111	5.2
15LJ02	0.1175	0.0099	0.01738	0.00083	0.229	57.5374	2.747758	0.0485	0.0028	0.23183	113	8.8	111.1	5.2	150	110	-1.71	111.1	5.2
15LJ02	0.1125	0.0088	0.0174	0.0008	0.251	57.47126	2.642357	0.0481	0.0024	0.31239	108.1	8.1	111.2	5.1	120	100	2.79	111.2	5.1

TABLE 2

(continued)

Sample	Isotopic data $\frac{^{207}Pb}{^{235}U}$	±2SE	$\frac{^{206}Pb}{^{238}U}$	±2SE	Error correlation	$\frac{^{238}U}{^{206}Pb}$	±2SE	$\frac{^{207}Pb}{^{206}Pb}$	±2SE	Error correlation	Calculated ages (Ma) $\frac{^{207}Pb}{^{235}U}$ age	±2SE	$\frac{^{206}Pb}{^{238}U}$ age	±2SE	$\frac{^{207}Pb}{^{206}Pb}$ age	±2SE	% discordant	Best age	±2SE
15LJ02	0.12	0.011	0.01746	0.00088	0.156	57.27377	2.88665	0.0501	0.0034	0.24198	115.3	9.8	111.5	5.6	200	130	-3.41	111.5	5.6
15LJ02	0.1169	0.0096	0.01748	0.0008	0.265	57.20824	2.618226	0.0483	0.0025	0.15068	112.5	8.9	111.7	5.1	130	100	-0.72	111.7	5.1
15LJ02	0.111	0.0093	0.01752	0.00083	0.443	57.07763	2.70402	0.0457	0.0024	-0.0071057	106.6	8.5	112	5.3	17	99	4.82	112	5.3
15LJ02	0.1183	0.0097	0.01759	0.0008	0.165	56.85048	2.585582	0.0495	0.0027	0.17415	113.3	8.8	112.4	5.1	170	110	-0.80	112.4	5.1
15LJ02	0.1189	0.0094	0.01763	0.00081	0.481	56.7215	2.606036	0.0484	0.0023	0.033672	113.9	8.5	112.6	5.1	114	96	-1.15	112.6	5.1
15LJ02	0.1227	0.0094	0.01764	0.00082	0.604	56.68934	2.635219	0.0506	0.0021	0.16335	117.7	8.4	112.7	5.2	216	90	-4.44	112.7	5.2
15LJ02	0.1202	0.0096	0.01766	0.00081	0.476	56.62514	2.597189	0.0496	0.0024	0.099107	115.5	8.8	112.8	5.1	170	100	-2.39	112.8	5.1
15LJ02	0.116	0.011	0.01768	0.0009	0.232	56.56109	2.879241	0.0473	0.0037	0.19067	110	10	113	5.7	70	140	2.65	113	5.7
15LJ02	0.1159	0.0094	0.01773	0.00082	0.399	56.40158	2.608533	0.0474	0.0024	0.12913	111.6	8.4	113.3	5.2	88	99	1.50	113.3	5.2
15LJ02	0.1208	0.0093	0.01774	0.00082	0.325	56.36979	2.605593	0.0496	0.0023	0.33199	115.6	8.4	113.4	5.2	172	96	-1.94	113.4	5.2
15LJ02	0.121	0.01	0.01794	0.00086	0.178	55.74136	2.672105	0.0487	0.0029	0.25876	115.2	9.4	114.6	5.5	140	120	-0.52	114.6	5.5
15LJ02	0.1172	0.0096	0.01796	0.00085	0.220	55.67929	2.635156	0.047	0.0024	0.22406	112.3	8.7	114.7	5.4	80	100	2.09	114.7	5.4
15LJ02	0.118	0.014	0.01797	0.00098	0.205	55.6483	3.034799	0.0494	0.0049	0.10371	114	13	114.8	6.2	140	180	0.70	114.8	6.2
15LJ02	0.1203	0.0092	0.01796	0.00082	0.351	55.67929	2.54215	0.0485	0.0021	0.25007	115.2	8.3	114.8	5.2	123	91	-0.35	114.8	5.2
15LJ02	0.125	0.0099	0.01801	0.00084	0.155	55.52471	2.589714	0.0509	0.0025	0.32627	119.4	8.9	115.1	5.3	230	100	-3.74	115.1	5.3
15LJ02	0.1219	0.0097	0.01811	0.00084	0.268	55.21811	2.561193	0.0493	0.0025	0.20034	117	8.9	115.7	5.3	150	100	-1.12	115.7	5.3
15LJ02	0.1238	0.0096	0.01817	0.00083	0.402	55.03577	2.514017	0.0499	0.0022	0.19921	118.7	8.8	116.1	5.3	192	97	-2.24	116.1	5.3
15LJ02	0.1265	0.0099	0.0182	0.00084	0.384	54.94505	2.535926	0.0506	0.0023	0.12469	120.8	9	116.3	5.3	220	100	-3.87	116.3	5.3
15LJ02	0.122	0.01	0.01822	0.00087	0.253	54.88474	2.620731	0.0494	0.0027	0.20284	116.7	9.2	116.4	5.5	160	110	-0.26	116.4	5.5
15LJ02	0.124	0.01	0.01831	0.00086	0.019	54.61496	2.565203	0.0497	0.0028	0.29168	118.6	9.3	117	5.4	160	110	-1.37	117	5.4
15LJ02	0.121	0.01	0.01847	0.00086	0.203	54.14185	2.520952	0.0478	0.0028	0.27173	116.2	9.3	118	5.5	110	110	1.53	118	5.5
15LJ02	0.127	0.01	0.01858	0.00086	0.224	53.82131	2.491191	0.0501	0.0025	0.26171	121.9	9	118.6	5.4	210	110	-2.78	118.6	5.4
15LJ02	0.1231	0.0096	0.01864	0.0009	0.478	53.64807	2.590304	0.0478	0.0021	0.25262	117.7	8.6	119.1	5.7	94	91	1.18	119.1	5.7
15LJ02	0.136	0.012	0.01869	0.00088	0.121	53.50455	2.519208	0.0533	0.0033	0.28026	129	11	119.3	5.6	320	130	-8.13	119.3	5.6
15LJ02	0.131	0.012	0.01871	0.00091	0.253	53.44735	2.599524	0.0518	0.0034	0.27385	126	10	119.5	5.8	250	130	-5.44	119.5	5.8
15LJ02	0.125	0.01	0.01913	0.00089	0.406	52.27392	2.43198	0.0476	0.0025	0.14175	120.2	9.3	122.2	5.6	80	110	1.64	122.2	5.6
15LJ02	0.129	0.01	0.01914	0.0009	0.121	52.2466	2.456737	0.0492	0.0025	0.42938	122.7	9.2	122.2	5.7	160	110	-0.41	122.2	5.7
15LJ02	0.139	0.011	0.01923	0.00089	0.149	52.00208	2.406753	0.053	0.0027	0.33742	131.8	9.7	122.8	5.6	320	110	-7.33	122.8	5.6
15LJ02	0.133	0.012	0.01937	0.0009	0.170	51.62623	2.398741	0.0497	0.003	0.13655	127	10	123.6	5.7	170	120	-2.75	123.6	5.7
15LJ02	0.126	0.011	0.01942	0.00093	0.217	51.49331	2.465951	0.0489	0.0031	0.28405	120.3	9.8	124	5.9	140	120	2.98	124	5.9
15LJ02	0.13	0.01	0.01956	0.00088	0.354	51.12474	2.300091	0.0489	0.0023	0.12115	124	9.2	124.8	5.6	143	95	0.64	124.8	5.6
15LJ02	0.136	0.012	0.0199	0.00093	0.229	50.25126	2.348426	0.0504	0.0031	0.19016	129	10	127	5.9	210	120	-1.57	127	5.9
15LJ02	0.145	0.012	0.02046	0.00096	0.253	48.87586	2.293295	0.0517	0.0028	0.28535	137	10	130.6	6.1	250	110	-4.90	130.6	6.1
15LJ02	0.161	0.012	0.0227	0.001	0.459	44.05286	1.940655	0.0512	0.0022	0.051485	152	11	145	6.4	240	97	-4.83	145	6.4
15LJ02	0.18	0.82	0.0251	0.0073	0.437	39.84064	11.58712	0.051	0.05	0.011309	170	190	160	44	340	350	-6.25	160	44
15LJ02	0.18	0.014	0.0263	0.0012	0.176	38.02281	1.734881	0.0504	0.0024	0.35674	168	12	167.1	7.6	210	100	-0.54	167.1	7.6
15LJ02	0.182	0.015	0.0263	0.0012	0.118	38.02281	1.734881	0.0503	0.0029	0.34775	170	13	167.4	7.7	250	120	-1.55	167.4	7.7
15LJ02	0.192	0.016	0.0268	0.0012	0.309	37.31343	1.670751	0.052	0.0028	0.24353	178	13	170.4	7.8	270	110	-4.46	170.4	7.8
15LJ02	0.195	0.017	0.027	0.0013	0.274	37.03704	1.783265	0.0522	0.0034	0.2324	180	15	172	8.1	270	130	-4.65	172	8.1

TABLE 2
(continued)

Sample	Isotopic data: $^{207}Pb/^{235}U$	±2SE	$^{206}Pb/^{238}U$	±2SE	Error correlation	$^{238}U/^{206}Pb$	±2SE	$^{207}Pb/^{206}Pb$	±2SE	Error correlation	Calculated ages (Ma): $^{207}Pb/^{235}U$ age	±2SE	$^{206}Pb/^{238}U$ age	±2SE	$^{207}Pb/^{206}Pb$ age	±2SE	% discordant	Best age	±2SE
15LJ02	0.197	0.015	0.0272	0.0013	0.302	36.76471	1.757137	0.0525	0.0025	0.31082	183	13	173.2	7.9	302	99	-5.66	173.2	7.9
15LJ02	0.195	0.016	0.0274	0.0013	0.287	36.49635	1.731579	0.0515	0.0025	0.19433	180	13	174.4	7.9	260	110	-3.21	174.4	7.9
15LJ02	0.2	0.016	0.0278	0.0013	0.329	35.97122	1.682108	0.0535	0.0024	0.27144	186	13	176.5	8	330	100	-5.38	176.5	8
15LJ02	0.194	0.017	0.0279	0.0013	0.188	35.84229	1.670071	0.0512	0.0031	0.26446	179	14	177.5	8.3	240	120	-0.85	177.5	8.3
15LJ02	0.201	0.016	0.028	0.0013	0.225	35.71429	1.658163	0.0518	0.0026	0.2741	185	14	177.9	8	260	100	-3.99	177.9	8
15LJ02	0.187	0.014	0.0281	0.0013	0.659	35.58719	1.646382	0.0492	0.0021	-0.025682	174	12	178.9	8.3	156	91	2.74	178.9	8.3
15LJ02	0.189	0.015	0.0282	0.0013	0.323	35.46099	1.634727	0.0497	0.0025	0.15898	176	13	179.3	8.1	170	100	1.84	179.3	8.1
15LJ02	0.209	0.018	0.0289	0.0014	0.302	34.60208	1.676225	0.0533	0.003	0.16905	192	15	183.8	9	320	120	-4.46	183.8	9
15LJ02	0.201	0.018	0.0291	0.0013	0.371	34.36426	1.535173	0.0503	0.0029	-0.011108	185	15	184.8	8.4	210	120	-0.11	184.8	8.4
15LJ02	0.196	0.018	0.0291	0.0014	0.146	34.36426	1.653263	0.0495	0.0034	0.33417	180	15	185.1	8.7	180	130	2.76	185.1	8.7
15LJ02	0.253	0.021	0.0341	0.0016	0.256	29.32551	1.375977	0.0537	0.003	0.19474	228	17	216	10	350	120	-5.56	216	10
15LJ02	0.257	0.021	0.0357	0.0017	0.231	28.0112	1.333867	0.0523	0.003	0.33598	231	17	226	10	280	110	-2.21	226	10
15LJ02	0.271	0.021	0.0394	0.0018	0.536	25.38071	1.159525	0.0509	0.0021	0.14265	244	16	249	11	229	93	2.01	249	11
15LJ03	0.0534	0.0052	0.00786	0.00038	0.065	127.2265	6.150898	0.049	0.0038	0.33577	52.7	5	50.5	2.5	130	140	-4.36	50.5	2.5
15LJ03	0.0507	0.0077	0.00798	0.00044	0.165	125.3133	6.909504	0.0479	0.0065	0.15073	50.4	7.5	51.2	2.8	90	230	1.56	51.2	2.8
15LJ03	0.0559	0.0059	0.00864	0.00043	0.000	115.7407	5.760245	0.0456	0.0041	0.2957	55	5.7	55.5	2.7	50	160	0.90	55.5	2.7
15LJ03	0.0748	0.0062	0.01096	0.00051	0.000	91.24088	4.245698	0.0502	0.003	0.47725	73.5	5.8	70.3	3.2	180	120	-4.55	70.3	3.2
15LJ03	0.0717	0.0064	0.01119	0.00053	0.135	89.3655	4.232683	0.047	0.003	0.29792	70.9	6.2	71.7	3.4	60	120	1.12	71.7	3.4
15LJ03	0.076	0.0068	0.01128	0.00055	0.254	88.65248	4.322594	0.0474	0.0031	0.1311	74.2	6.4	72.3	3.5	90	120	-2.63	72.3	3.5
15LJ03	0.0736	0.0078	0.01128	0.00058	0.154	88.65248	4.558372	0.0481	0.0043	0.24038	71.7	7.4	72.3	3.7	90	160	0.83	72.3	3.7
15LJ03	0.0759	0.0076	0.01131	0.00057	0.001	88.41733	4.456046	0.0491	0.0041	0.29067	73.9	7.1	72.5	3.7	150	150	-1.93	72.5	3.7
15LJ03	0.0766	0.0062	0.01134	0.00052	0.106	88.18342	4.043684	0.049	0.0027	0.32283	75.1	5.8	72.7	3.3	140	110	-3.30	72.7	3.3
15LJ03	0.0752	0.0071	0.01137	0.00055	0.128	87.95075	4.254434	0.0483	0.0035	0.26535	73.4	6.7	72.9	3.5	150	140	-0.69	72.9	3.5
15LJ03	0.0728	0.0059	0.01139	0.00054	0.447	87.79631	4.162424	0.0464	0.0023	0.11156	71.3	5.6	73	3.4	56	99	2.33	73	3.4
15LJ03	0.082	0.013	0.01152	0.00075	0.041	86.80556	5.651403	0.0554	0.0085	0.37499	78	12	73.8	4.8	190	260	-5.69	73.8	4.8
15LJ03	0.0802	0.0078	0.01152	0.00059	0.250	86.80556	4.445771	0.0507	0.0038	0.16154	78	7.3	73.8	3.8	180	140	-5.69	73.8	3.8
15LJ03	0.0768	0.0066	0.01156	0.00054	0.121	86.50519	4.0409	0.0486	0.003	0.29197	75	6.2	74.1	3.4	130	120	-1.21	74.1	3.4
15LJ03	0.0722	0.0074	0.01159	0.00057	0.114	86.28128	4.243341	0.0463	0.0039	0.27817	71.5	7.1	74.3	3.6	20	150	3.77	74.3	3.6
15LJ03	0.076	0.015	0.01167	0.00076	0.067	85.6898	5.580484	0.0464	0.0092	0.15881	72	14	74.8	4.8	-80	300	3.74	74.8	4.8
15LJ03	0.0701	0.0065	0.01168	0.00057	0.242	85.61644	4.178199	0.0441	0.003	0.17777	68.6	6.1	74.9	3.6	-50	120	8.41	74.9	3.6
15LJ03	0.0738	0.006	0.0117	0.00054	0.127	85.47009	3.944773	0.046	0.0025	0.33965	72.2	5.7	75	3.5	20	100	3.73	75	3.5
15LJ03	0.076	0.0097	0.0117	0.00063	0.031	85.47009	4.602235	0.0493	0.0057	0.31327	73.6	9.1	75	4	150	200	1.87	75	4
15LJ03	0.082	0.012	0.0117	0.00071	0.000	85.47009	5.186646	0.0527	0.0074	0.43037	79	11	75	4.5	230	250	-5.33	75	4.5
15LJ03	0.084	0.01	0.01179	0.00064	0.202	84.81764	4.604181	0.0502	0.0052	0.15116	81.4	9.5	75.5	4.1	190	190	-7.81	75.5	4.1
15LJ03	0.0789	0.007	0.01177	0.00056	0.191	84.96177	4.042361	0.0488	0.0032	0.14334	77.8	6.6	75.6	3.5	140	120	-2.91	75.6	3.5
15LJ03	0.0735	0.0087	0.01181	0.0006	0.000	84.67401	4.301812	0.0465	0.005	0.24548	71.4	8.2	75.7	3.8	10	170	5.68	75.7	3.8
15LJ03	0.076	0.0066	0.01184	0.00056	0.000	84.45946	3.994704	0.0457	0.0029	0.47053	74.2	6.2	75.9	3.6	10	110	2.24	75.9	3.6
15LJ03	0.086	0.012	0.01187	0.00074	0.099	84.246	5.252067	0.0515	0.0068	0.29515	82	11	76.1	4.7	280	240	-7.75	76.1	4.7

TABLE 2
(continued)

Sample	Isotopic data: $\frac{^{207}Pb}{^{235}U}$	±2SE	$\frac{^{206}Pb}{^{238}U}$	±2SE	Error correlation	$\frac{^{238}U}{^{206}Pb}$	±2SE	$\frac{^{207}Pb}{^{206}Pb}$	±2SE	Error correlation	Calculated ages (Ma): $\frac{^{207}Pb}{^{235}U}$ age	±2SE	$\frac{^{206}Pb}{^{238}U}$ age	±2SE	$\frac{^{207}Pb}{^{206}Pb}$ age	±2SE	% discordant	Best age	±2SE
15LJ03	0.0792	0.0075	0.01193	0.00057	0.215	83.8223	4.004921	0.0476	0.0033	0.16413	77.6	6.9	76.4	3.7	120	130	-1.57	76.4	3.7
15LJ03	0.0804	0.0065	0.01193	0.00056	0.363	83.8223	3.934659	0.0479	0.0024	0.14095	78.7	6	76.5	3.5	110	100	-2.88	76.5	3.5
15LJ03	0.081	0.012	0.01191	0.0007	0.129	83.96306	4.934856	0.0497	0.0067	0.23455	78	11	76.6	4.4	180	240	-1.83	76.6	4.4
15LJ03	0.0783	0.0086	0.01199	0.0006	0.091	83.40284	4.17362	0.048	0.0045	0.17105	76.7	8.2	76.9	3.8	110	170	0.26	76.9	3.8
15LJ03	0.0819	0.0079	0.01203	0.0006	0.053	83.12552	4.145911	0.0485	0.0037	0.32849	79.6	7.4	77.1	3.8	160	140	-3.24	77.1	3.8
15LJ03	0.0799	0.0064	0.01205	0.00055	0.325	82.98755	3.787814	0.0478	0.0023	0.1804	77.9	6.1	77.2	3.5	90	100	-0.91	77.2	3.5
15LJ03	0.081	0.011	0.01211	0.00069	0.093	82.57638	4.705013	0.0496	0.0063	0.33386	78	10	77.6	4.4	110	220	-0.52	77.6	4.4
15LJ03	0.081	0.0097	0.01213	0.00063	0.104	82.44023	4.281727	0.0477	0.0049	0.27609	78.4	9.1	77.7	4	120	180	-0.90	77.7	4
15LJ03	0.0795	0.0084	0.01212	0.00062	0.006	82.50825	4.220719	0.0482	0.0042	0.40707	77.9	7.8	77.9	4	150	160	0.00	77.9	4
15LJ03	0.084	0.011	0.01218	0.00072	0.133	82.10181	4.853309	0.0503	0.0057	0.26146	81	10	78	4.6	170	200	-3.85	78	4.6
15LJ03	0.0813	0.0068	0.01219	0.00059	0.101	82.03445	3.970495	0.0493	0.0029	0.35077	79.2	6.4	78.1	3.7	160	120	-1.41	78.1	3.7
15LJ03	0.078	0.0067	0.01219	0.00057	0.265	82.03445	3.835901	0.0464	0.0027	0.18111	76.1	6.3	78.1	3.6	40	110	2.56	78.1	3.6
15LJ03	0.0817	0.0094	0.01221	0.00065	0.122	81.90008	4.359955	0.0466	0.0045	0.20451	79.1	8.8	78.2	4.2	70	170	-1.15	78.2	4.2
15LJ03	0.0791	0.0078	0.01221	0.0006	0.085	81.90008	4.024574	0.0462	0.0035	0.30497	77	7.3	78.3	3.8	60	140	1.66	78.3	3.8
15LJ03	0.085	0.013	0.01222	0.00069	0.222	81.83306	4.620688	0.0506	0.0066	0.076511	82	12	78.3	4.4	120	220	-4.73	78.3	4.4
15LJ03	0.0808	0.0089	0.01222	0.00064	0.174	81.83306	4.285856	0.0478	0.0042	0.21556	78.4	8.3	78.3	4.1	130	160	-0.13	78.3	4.1
15LJ03	0.075	0.0076	0.01222	0.00061	0.251	81.83306	4.084956	0.0452	0.0036	0.092242	73.6	7.1	78.3	3.9	10	140	6.00	78.3	3.9
15LJ03	0.0843	0.0086	0.01223	0.00062	0.089	81.76615	4.145136	0.0499	0.0041	0.32368	81.8	8	78.4	3.9	190	160	-4.34	78.4	3.9
15LJ03	0.0849	0.007	0.01224	0.00057	0.116	81.69935	3.804626	0.0493	0.0028	0.30077	82.6	6.5	78.4	3.6	200	120	-5.36	78.4	3.6
15LJ03	0.0823	0.0093	0.01227	0.00066	0.010	81.49959	4.383841	0.0489	0.0051	0.37754	81.3	9	78.6	4.2	180	180	-3.44	78.6	4.2
15LJ03	0.084	0.013	0.01228	0.00073	0.124	81.43322	4.8409	0.052	0.007	0.30917	80	12	78.7	4.7	190	240	-1.65	78.7	4.7
15LJ03	0.0812	0.0087	0.01231	0.00064	0.098	81.23477	4.223416	0.0486	0.0045	0.25918	78.8	8.2	78.9	4.1	100	160	0.13	78.9	4.1
15LJ03	0.0866	0.0086	0.01234	0.00059	0.094	81.03728	3.874554	0.0515	0.0041	0.22069	84.6	8.1	79.2	3.8	240	150	-6.82	79.2	3.8
15LJ03	0.083	0.01	0.0124	0.00064	0.000	80.64516	4.162331	0.0491	0.0053	0.28581	80.2	9.4	79.4	4.1	140	190	-1.01	79.4	4.1
15LJ03	0.081	0.0067	0.01242	0.00058	0.141	80.5153	3.759974	0.0478	0.0027	0.28854	79.3	6.4	79.5	3.7	100	110	0.25	79.5	3.7
15LJ03	0.0843	0.0095	0.01242	0.00062	0.150	80.5153	4.019282	0.0495	0.0046	0.21364	82.3	8.7	79.6	4	160	170	-3.39	79.6	4
15LJ03	0.0853	0.0082	0.01245	0.00061	0.059	80.32129	3.93542	0.0471	0.0036	0.23223	82.8	7.7	79.8	3.9	130	140	-3.76	79.8	3.9
15LJ03	0.087	0.012	0.01252	0.00071	0.000	79.8722	4.529494	0.0531	0.0071	0.33924	83	11	80.2	4.5	200	230	-3.49	80.2	4.5
15LJ03	0.0859	0.0072	0.01256	0.00059	0.412	79.61783	3.74001	0.0497	0.0027	0.017678	83.5	6.8	80.5	3.7	170	110	-3.73	80.5	3.7
15LJ03	0.0823	0.0076	0.0126	0.00062	0.151	79.36508	3.905266	0.0481	0.0034	0.27188	80	7.2	80.7	4	120	130	0.87	80.7	4
15LJ03	0.0799	0.0092	0.01262	0.00071	0.023	79.2393	4.457996	0.0448	0.0047	0.34173	78.1	8.7	80.9	4.5	-20	170	3.46	80.9	4.5
15LJ03	0.0843	0.0091	0.01262	0.00063	0.355	79.2393	3.955686	0.0496	0.0041	0.00059969	82.3	8.4	80.9	4	180	150	-1.73	80.9	4
15LJ03	0.078	0.012	0.01265	0.00072	0.000	79.05138	4.499367	0.0449	0.0065	0.22366	75	11	81	4.6	-90	220	7.41	81	4.6
15LJ03	0.083	0.011	0.01277	0.00075	0.161	78.30854	4.59917	0.0479	0.0058	0.2841	80	10	81.8	4.8	90	210	2.20	81.8	4.8
15LJ03	0.093	0.011	0.01299	0.00075	0.000	76.98229	4.444705	0.053	0.0061	0.43723	89	11	83.2	4.8	310	210	-6.97	83.2	4.8
15LJ03	0.1076	0.0099	0.0166	0.00082	0.000	60.24096	2.975758	0.0481	0.0035	0.44025	103.3	9.1	106.1	5.2	110	140	2.64	106.1	5.2
15LJ03	0.1171	0.009	0.01719	0.00079	0.449	58.17336	2.67347	0.0501	0.0022	0.18466	112.3	8.2	109.9	5	204	96	-2.18	109.9	5
15LJ03	0.1143	0.0092	0.01733	0.00079	0.190	57.7034	2.630449	0.0481	0.0024	0.24461	109.8	8.3	110.8	5	110	100	0.90	110.8	5
15LJ03	0.112	0.01	0.01734	0.00081	0.000	57.67013	2.693933	0.0475	0.0034	0.36609	107.6	9.5	110.8	5.1	80	130	2.89	110.8	5.1

TABLE 2

(continued)

Sample	Isotopic data										Calculated ages (Ma)								
	$^{207}Pb/^{235}U$	±2SE	$^{206}Pb/^{238}U$	±2SE	Error correlation	$^{238}U/^{206}Pb$	±2SE	$^{207}Pb/^{206}Pb$	±2SE	Error correlation	$^{207}Pb/^{235}U$ age	±2SE	$^{206}Pb/^{238}U$ age	±2SE	$^{207}Pb/^{206}Pb$ age	±2SE	% discordant	Best age	±2SE
15LJ03	0.11	0.0099	0.01735	0.00083	0.241	57.63689	2.757269	0.0461	0.003	0.14427	106.8	9	110.9	5.2	40	120	3.70	110.9	5.2
15LJ03	0.1176	0.0091	0.0175	0.00081	0.348	57.14286	2.644898	0.0478	0.0022	0.24992	112.8	8.2	111.8	5.1	94	91	-0.89	111.8	5.1
15LJ03	0.1168	0.0098	0.01753	0.00083	0.432	57.04507	2.700936	0.048	0.0026	0.047687	111.9	8.9	112	5.3	100	100	0.09	112	5.3
15LJ03	0.118	0.01	0.01766	0.00082	0.248	56.62514	2.629253	0.0484	0.0029	0.14389	112.8	9.3	112.8	5.2	130	120	0.00	112.8	5.2
15LJ03	0.119	0.02	0.01771	0.00088	0.546	56.46527	2.805728	0.0501	0.0055	-0.23212	114	17	113.2	5.6	170	170	-0.71	113.2	5.6
15LJ03	0.1171	0.0097	0.01777	0.00083	0.224	56.27462	2.628471	0.0479	0.0026	0.19459	112.7	8.6	113.5	5.3	90	110	0.70	113.5	5.3
15LJ03	0.117	0.01	0.018	0.00086	0.234	55.55556	2.654321	0.0473	0.0029	0.27077	112.4	9.3	115	5.5	80	120	2.26	115	5.5
15LJ03	0.129	0.011	0.01816	0.00087	0.075	55.06608	2.638078	0.0511	0.0031	0.29871	123	10	116	5.5	240	120	-6.03	116	5.5
15LJ03	0.1106	0.0097	0.01817	0.00087	0.110	55.03577	2.635175	0.0446	0.0027	0.26733	106.2	8.8	116.1	5.5	-30	110	8.53	116.1	5.5
15LJ03	0.124	0.01	0.0183	0.00086	0.238	54.64481	2.568007	0.0488	0.0028	0.1867	118	9.5	116.9	5.5	150	120	-0.94	116.9	5.5
15LJ03	0.124	0.011	0.01846	0.00085	0.258	54.17118	2.494339	0.0486	0.0029	0.13766	118.1	9.5	117.9	5.4	120	110	-0.17	117.9	5.4
15LJ03	0.1192	0.0097	0.01846	0.00087	0.309	54.17118	2.55303	0.0472	0.0025	0.26644	114.6	9	117.9	5.5	90	100	2.80	117.9	5.5
15LJ03	0.124	0.011	0.01848	0.00087	0.157	54.11255	2.547507	0.0474	0.0033	0.23742	118	10	118	5.5	80	130	0.00	118	5.5
15LJ03	0.125	0.01	0.01851	0.00084	0.131	54.02485	2.451695	0.0481	0.0025	0.30561	119.1	9	118.2	5.3	110	100	-0.76	118.2	5.3
15LJ03	0.126	0.011	0.01872	0.00091	0.299	53.4188	2.596747	0.0486	0.003	0.15844	120.3	9.6	119.6	5.8	160	120	-0.59	119.6	5.8
15LJ03	0.129	0.011	0.01903	0.00089	0.362	52.54861	2.457607	0.0488	0.0026	0.050779	123	9.7	121.5	5.6	140	110	-1.23	121.5	5.6
15LJ03	0.132	0.011	0.01974	0.00092	0.177	50.65856	2.360987	0.0491	0.003	0.22681	126	10	126	5.8	140	120	0.00	126	5.8
15LJ03	0.129	0.011	0.01973	0.0009	0.356	50.68424	2.312003	0.0477	0.0025	0.063325	123.3	9.6	126.2	5.6	90	100	2.30	126.2	5.6
15LJ03	0.147	0.011	0.0219	0.001	0.271	45.6621	2.085027	0.0489	0.0023	0.26067	139	10	139.4	6.3	148	98	0.29	139.4	6.3
15LJ03	0.151	0.012	0.022	0.001	0.408	45.45455	2.066116	0.05	0.0025	0.14767	143	11	140.3	6.5	190	100	-1.92	140.3	6.5
15LJ03	0.197	0.015	0.027	0.0012	0.538	37.03704	1.646091	0.0527	0.0022	0.18175	182	13	171.9	7.8	308	93	-5.88	171.9	7.8
15LJ03	0.189	0.017	0.0278	0.0013	0.173	35.97122	1.682108	0.0494	0.0032	0.20752	176	14	176.9	8.3	170	120	0.51	176.9	8.3
15LJ03	0.199	0.017	0.0285	0.0013	0.050	35.08772	1.600492	0.0502	0.0031	0.25311	183	15	180.9	8.3	200	120	-1.16	180.9	8.3

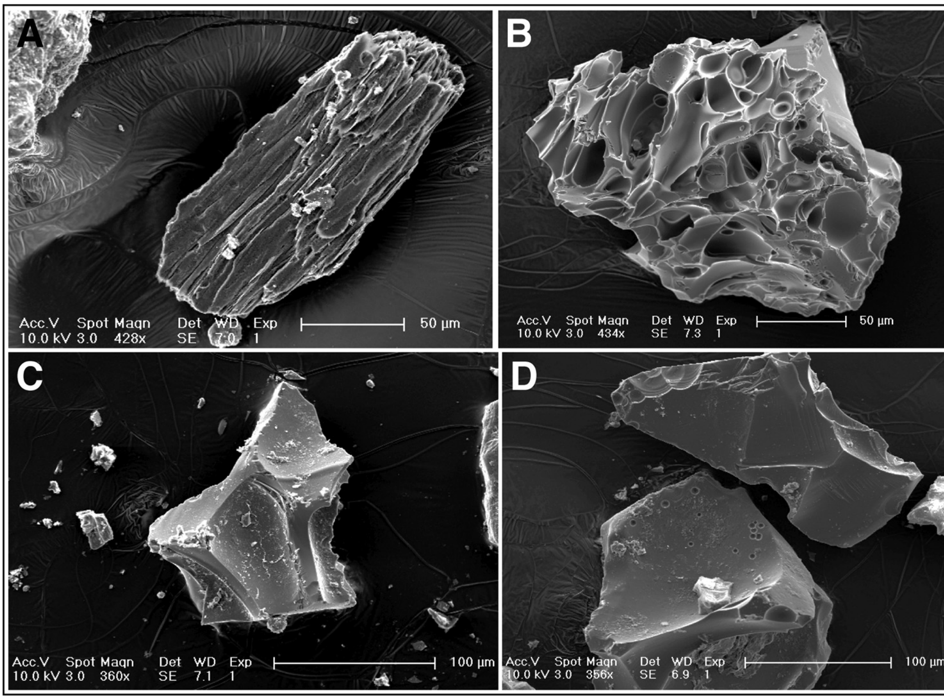

Fig. 9. Scanning electron images of glass separates. Fragments show primary volcanic textures, sharp edges indicating an airfall origin, and minimal clays adhering to grain surfaces. (A) LJ-60 Paleocene, from Lago Jeinimeni. (B) GB-09 Eocene, from Gran Barranca. (C) GB-08 Eocene, from Gran Barranca. (D) GB-97 Eocene, from Gran Barranca.

in the laboratory. The key issue is the possible diffusive isotopic exchange between environmental water and glass hydration water following initial hydration. Isotopically-enriched water exposure can change glass δD on lab time scales (*ca.* 1 year) in some experiments (Nolan and Bindeman, 2013; Cassel and Breecker, 2017), although other experiments show negligible change (Ross and others, 2015). It is difficult to relate these laboratory experiments to natural settings because the laboratory samples have been crushed, which makes them quite different from natural materials. This is analogous in some ways to the observation that glass can be devitrified on short time scales, but pristine glass is found in rocks that are tens to hundreds of Myr old (for example, Hamilton, 1992). This discrepancy between natural and laboratory rates of glass alteration has long been recognized (Colman, 1981). If natural samples were as reactive and isotopically diffusive as some lab studies suggest, then all natural glasses should be altered and isotopically reset in a few years of exposure.

Cassel and Breecker (2017) have expressed concern about isotopic resetting by younger waters and have argued that it is important to "clean" the samples using an HF acid wash. Our assessment is that this approach is burdened by two unaddressed problems: (1) HF contains a large amount of hydrogen of unknown isotopic composition and (2) the hydrogen isotope fractionation between HF and water is very large ($\alpha_{H2O\text{-}HF} = \sim 1.2$) (estimated from Harris, 1995). Cassel and Breecker (2017) did not report the isotopic composition of the HF used in their study. Industrial HF is produced by dissolving fluorite by sulfuric acid, a process which is incomplete and is likely accompanied by large and unpredictable isotopic fractionation. Some studies (Fan and others, 2014; Cassel and Breecker, 2017) have found that HF treatment produces a coherent shift in δD value, while others (Dettinger and Quade, 2015; Seligman and others, 2016) have found that it instead produces changes in δD that vary in both magnitude and direction. Differences in the source and isotopic composition of lab HF and water may explain why HF cleaning by different labs produces variable shifts in magnitude and sign of the isotopic composition. In addition, it is not clear if HF treatment is removing isotopically-reset rims or altering the δD of the glass by adding or exchanging H, or both. We considered these effects by rinsing four samples with 5 percent HF for 30 seconds. Treated samples showed variable changes in δD relative to untreated samples (three samples did not change within error, one decreased by 11‰). SEM images of glass samples treated with sonication but not HF (fig. 9) show pristine fragments, with minimal or no precipitates coating glass surfaces. Given the good quality of our samples and the theoretical and observed cautions about the effect of HF, we chose not to use HF cleaning, in keeping with the recommendations of Seligman and others (2016) and Dettinger and Quade (2015). This is also consistent with field-based tests (see Results), which argue against alteration.

METHODS

Fresh samples were collected from fluvial and aeolian mudstones in measured sedimentary sections (fig. 8). Lacustrine sediments were not sampled to avoid the issues with evaporation (for example, DeCelles and others, 2007; Cassel and Breecker, 2017). Established procedures were used to separate glass from bulk samples (for example, Cassel and others, 2009; Dettinger and Quade, 2015). Sediments were dry-sieved to isolate the 180 to 63 μm fraction, and clay and carbonate were removed by a series of rinses of deionized water, sodium pyrophosphate deflocculant solution, and 10 percent HCl. A Frantz Isodynamic magnetic separator was used to remove magnetic grains, particularly hydrogen-containing biotite. Glass was then separated in a lithium polytungstate solution with a density of 2.48 g/cm^3. Resulting splits were inspected using a microscope to select pure separates of glass. SEM images of selected samples show fresh, vesicular, angular texture indicative of airfall deposition, rather than reworking by fluvial transport, and do not show significant secondary material on the surface of glass fragments (see fig. 9). Samples were stored in a glass desiccator for one week prior to analysis. High purity separates were weighed into silver capsules, dried in a vacuum oven for ~24 hours at 80 °C, and flushed with He gas. Tests of replicates with longer drying times showed no effect on sample δD (Colwyn and Hren, 2019). The δD of the hydrated glass was measured using a thermal conversion elemental analyzer (TC/EA) attached to a Thermo MAT 253 IRMS at the University of Connecticut. Isotopic values were determined relative to repeated runs of standard materials PEF-1 (foil), NBS-22 (oil), and KGa-1 (kaolinite). Measured δD of glass was transformed to the δD of meteoric water (table 3) using the fractionation factor of Friedman and others (1993a) ($\alpha = 0.9668$), which has been validated experimentally by Seligman and others (2016) and observationally by Porter and others (2016). Water contents were determined by TC/EA (for example, Martin and others, 2017) and are ~5 weight percent (table 3), which is typical for environmentally hydrated glasses.

Modern water samples were collected in vials and sealed with Parafilm. Water isotopes were measured in triplicate using a Los Gatos Research LWIA Cavity Ring Down Spectrometer with an autosampler in the Stable Isotope Facility at the University of Wyoming. Results (table 1) were normalized to repeated runs of internal and external reference materials.

RESULTS

Volcanic glass δD data for all sites range from −108 permil to −142 permil (table 3). Conversion of these values using the fractionation factor of Friedman (1993a) gives mean values of −85 permil at Lago Jeinimeni, −98 permil at Gran Barranca, and −103

Table 3

Hydrogen isotope data from volcanic glasses

Sample	Stratigraphic height (m)	Age (Ma)	δD_{glass} (VSMOW)	StdDev	n	H_2O (wt. %)	δD_{water} (VSMOW)
Lago Jeinimeni (base of section at -46.76958, -71.82899)							
15LJ50	1.5	61.8	-118	2.1	3	2.6%	-88
15LJ51	3.4	61.4	-114	1.0	3	2.8%	-84
15LJ52	6.5	60.8	-116	1.4	3	2.4%	-86
15LJ53	14.5	59.3	-114	2.6	3	2.8%	-84
15LJ54	17.3	58.8	-110	1.8	3	5.8%	-80
15LJ58	24.4	57.5	-110	0.9	3	4.3%	-81
15LJ60	28.4	56.7	-108	1.6	3	4.4%	-78
15LJ61	32.2	56.0	-112	1.2	3	2.4%	-82
M15LJ-1.0m	34.5	55.6	-110	1.6	3	3.1%	-80
15LJ62	35.2	55.4	-112	2.4	3	3.3%	-82
PB15LJ02	44.3	53.9	-127	0.5	3	4.4%	-98
M15LJ-17.0m	50.5	52.6	-115	1.9	3	3.4%	-86
M15LJ-21.6m	55.1	51.8	-113	1.8	3	2.8%	-83
M15LJ23.65m	57.2	51.4	-113	2.0	3	2.0%	-83
Gran Barranca (multiple sections (letters) in area of -45.70998 -68.73487; see Ré and others (2010) for coordinates)							
13GB08 (MMZ)	46	39.9	-133	5.3	2	5.8%	-104
13GB09	58	38.0	-127	3.7	5	1.2%	-97
13GB90 (A)	57	37.1	-122	3.7	2	6.9%	-92
13GB12 (K)	7	34.3	-125	5.4	3	0.7%	-95
13GB13	10	34.3	-122	5.4	2	4.3%	-92
13GB14	13	34.2	-128	4.2	3	0.6%	-98
13GB23	40	33.8	-128	1.4	3	0.7%	-98
13GB25	43	33.7	-130	5.2	3	0.6%	-101
13GB26	46	33.7	-129	0.6	3	0.7%	-99
13GB28	49	33.6	-129	2.6	3	0.7%	-99
13GB32	55	33.6	-124	3.9	2	4.9%	-94
13GB33	58	33.6	-128	4.3	3	0.8%	-99
13GB34	61	33.6	-126	5.6	3	0.7%	-96
13GB35	64	33.5	-126	1.9	2	2.6%	-96
13GB36	67	33.5	-127	6.3	3	0.5%	-97
13GB37	70	33.5	-130	3.8	3	0.5%	-100
13GB38	73	33.5	-125	6.3	3	0.5%	-95
13GB39	76	33.5	-130	8.9	2	0.4%	-100
13GB104 (A)	81	30.7	-120	3.3	5	1.6%	-90
13GB41 (MMZ)	152	21.3	-128	2.8		1.4%	-98
13GB43	158	20.9	-142	4.7	2	5.4%	-113
13GB44	159	20.9	-136	2.3		1.9%	-107
13GB48	167	20.3	-132	3.0		2.2%	-102
13GB49	170	20.1	-141	2.8		2.3%	-112
13GB51	176	19.8	-131	5.5	2	6.7%	-102
13GB52	179	19.7	-142	5.1		4.1%	-113
13GB53	182	19.7	-141	3.4		2.6%	-112
13GB55	188	19.5	-142	0.9		1.1%	-113
13GB56	191	19.5	-135	0.5		0.9%	-105
13GB57	194	19.4	-140	3.4		2.8%	-111
13GB61	211	18.4	-130	0.9		1.0%	-100
Cerro Observatorio (section at -50.56478, -69.15127)							
ARG 2 MD ASH E	6	17.0	-130	0.7	2	4.7%	-100
ARG 2 MD ASH A	6.5	17.0	-124	5.2	4	5.0%	-94
ARG 2 MD ASH B	8	16.9	-138	0.7	2	4.8%	-108
ARG 2 MD ASH C	12.5	16.7	-135	0.0	2	2.6%	-105
ARG 2 MD ASH D/1	15.5	16.6	-138	1.7	4	4.1%	-109
CM ARG ASH 5A	15.5	16.6	-138	0.7	2	4.6%	-108
CMARG ASH 2	32.2	16.1	-138	0.7	2	4.4%	-108
CMARG ASH 3	72.1	15.4	-135	1.9	1	3.4%	-105
CMARG ASH 3A	72.1	15.4	-123	1.4	2	1.2%	-93
CMARG ASH 4/4A	73.1	15.4	-133	2.9	3	4.0%	-104

permil at Cerro Observatorio (table 3). The ancient precipitation δD values recorded in our glass samples (fig. 8), which are entirely from the leeward side of the range, show a similar amount of fractionation to modern water samples across the Andes (fig. 5). These relatively low δD values suggest that the Patagonian Andes have likely existed in some form since at least the Paleocene.

We have already discussed the issue of potential isotopic resetting by young waters. At this point, we add the additional observation that volcanic glass shows stratigraphic variations in isotopic composition that are comparable to those expected for climate variations (fig. 8). If the samples had been isotopically reset, we would expect the samples to be reduced towards a common value.

THE INFLUENCE OF CLIMATE

Interpretation of water isotopes requires an understanding of the initial composition of water in the atmosphere and the amount of fractionation per kilometer of orographic lifting ("isotopic lapse rate"). Temperature has a strong effect on both of these, and this is particularly important for our study because of the significant amount of global cooling during the Cenozoic. Here, we evaluate these effects by: (1) estimating surface air temperature in Patagonia upwind of the range, (2) estimating the δD of upwind precipitation, and (3) estimating the δD of downwind precipitation after orographic fractionation, assuming modern-size topography.

To estimate surface air temperature (SAT) over the ocean adjacent to western Patagonia, we start with an ice volume-corrected benthic foraminiferal $\delta^{18}O$ time series (Zachos and others, 2008; de Boer and others, 2010; de Boer and others, 2012), which provides a Cenozoic record of SST at the latitude of deep-water formation (Gordon, 2001). In the Southern Ocean, this occurs at ~70°S latitude. We then use the meridional energy-balance equation of North and others (1981, see eq. 32) and a steady equatorial temperature of ~30 °C (Rose and Ferreira, 2013) to calculate an interpolated temperature at 46°S. While there has been a debate about the Cenozoic temperature history of the tropics (for example, Huber and Caballero, 2011), modeling (Abbot and Tziperman, 2008; Rose and Ferreira, 2013; Sagoo and others, 2013) and paleotemperature measurements (Pearson and others, 2001; Norris and others, 2002; Roche and others, 2006) indicate that tropical temperatures remained steady ($27 < T < 34$ °C) during global warming and cooling. Variation within this range has little influence on our interpolation. We then account for the difference between SST and SAT by shifting our interpolated SST curve to match the local modern mean annual SAT (12 °C) (fig. 10A).

The resulting SAT curve (fig. 10A) shows long-term cooling in Patagonia of ~5 °C during the Cenozoic, punctuated by familiar thermal events such as the PETM (~56 Ma) and the MECO (~40 Ma). The transformed data retain the same age values as Zachos and others (2008). The blue and red points correspond to their raw data (typical time step ~10 kyr) and their five-point moving average (typical integration time of ~50 kyr), respectively. We use these two different renderings of the data to help evaluate how climate variability has affected the δD signature preserved in our glasses.

The second step is to estimate the δD of first precipitation in Patagonia through the Cenozoic. We use the relative relationship defined by local station records between precipitation δD and temperature in Patagonia to convert the estimated temperature curve from the first step into first precipitation δD. Using this empirical relationship to reconstruct water isotopes from temperature is essentially the reverse of commonly used isotope paleothermometers.

To make this conversion, we use a linear approximation,

$$\delta(t) = \delta(0) + b[T_s(t) - T_s(0)], \quad (1)$$

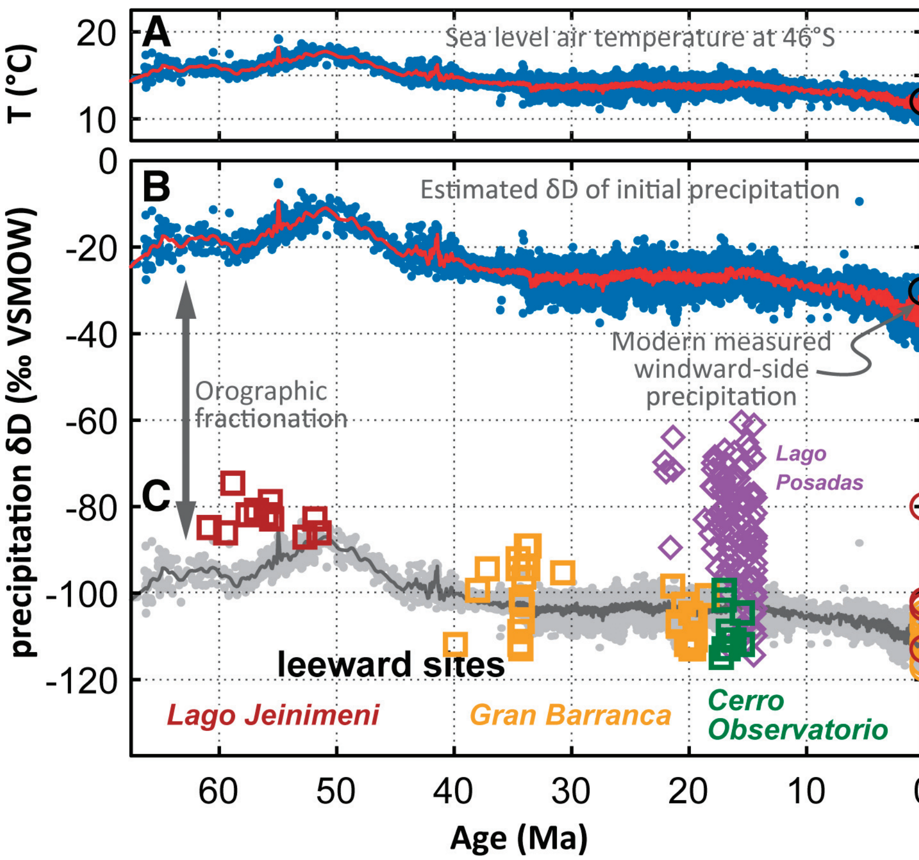

Fig. 10. Comparison of modeled and reconstructed precipitation δD in order to separate the effects of climate and tectonics on the δD signal. (A) Reconstructed SAT for western coastal Patagonia (46°S) based on marine δ^{18}O records. (B) Upwind precipitation ("first precipitation") δD modeled using reconstructed SAT from (A), modern upwind precipitation δD, and the regional T-δ relationship. (C) Modeled downwind precipitation δD assuming constant modern–size topography (gray curve) and reconstructed downwind precipitation δD from volcanic glasses (colored boxes). The heavy gray line shows the modeled δD given changing temperature with fixed modern topography; gray points reflect the scale of variability. Red/yellow/green symbols show precipitation δD reconstructed from glass, with color corresponding to section. Purple symbols show the range of soil carbonate δ^{18}O data from Lago Posadas of Blisniuk and others (2005), which are projected into precipitation δD space using a local meteoric water line from the water data of Stern and Blisniuk (2002) (including those affected by evaporation) and assuming a soil temperature of 10 °C. Analytical error (table 3) is smaller than the size of the symbols.

which is based on the well-known empirical correlation between surface temperature T_s and water isotopes δ (Dansgaard, 1964; Rozanski and others, 1993). In (1), t is time ($t = 0$ is present) and b is the slope of the T_s−δ relationship. In this case, we have empirically determined that $\delta D(0) = -30‰$ (mean of 5 highest observed δD values in low-elevation coastal Chile, from table 1) and the mean annual value for $T_s(0) = 12$ °C. To calibrate b, we use the seasonal variation in temperature and water isotopes (fig. 11). Seasons are much longer than the response time of the atmosphere, and therefore seasonal variations capture the T−δ relationship.

Seasonal variations are also representative of the full range of conditions that occurred in the past. Specifically, the intra-annual variation in temperature in western coastal Patagonia is large (~15 °C), greater than that predicted over the Cenozoic (fig.

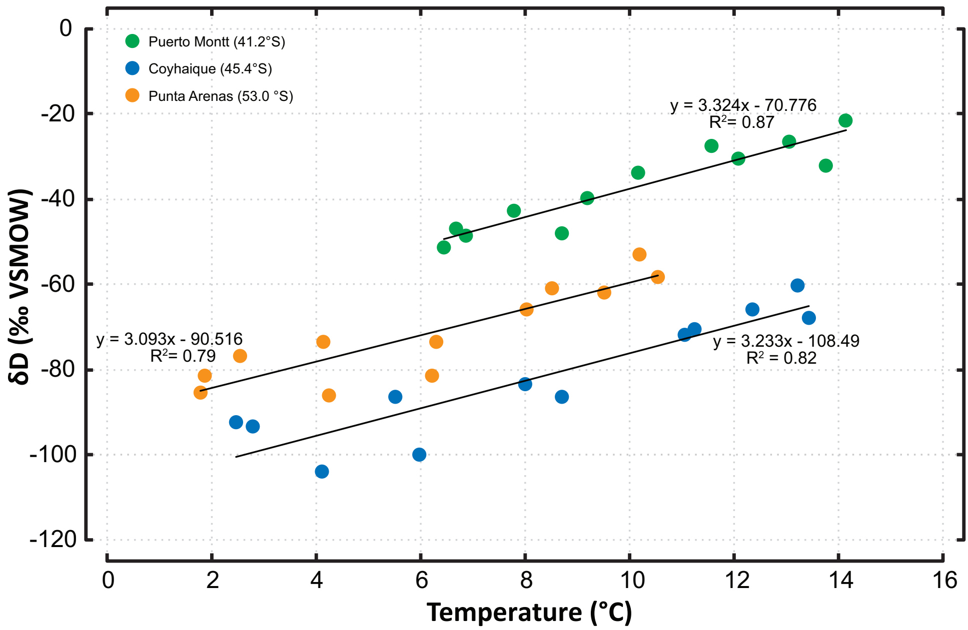

Fig. 11. Temperature–δD relationships for three IAEA-GNIP stations in Patagonia.

10A), and there are many individual precipitation events in each year. IAEA-GNIP stations at Coyhaique (45.4°S), Puerto Montt (41.2°S), and Punta Arenas (53.0°S) show a robust, consistent correlation between temperature and isotopic composition of precipitation (δD µ 3.2 T(°C)) (fig. 11). Modeled T_s−δD relationships show similar scaling for mid-latitude sites on geologically long time scales (Boyle, 1997; Hendricks and others, 2000), and isotope-enabled climate modeling indicates the slope of the late Eocene relationship is similar to the present in the region (Feakins and others, 2014).

Using (1), we transform the SAT curve (fig. 10A) into δD of precipitation, and then pin the resulting δD curve (fig. 10B) to the modern upwind precipitation δD(0) (see above). This reconstruction of Cenozoic first precipitation shows modest changes in δD (<30‰) as a result of long-term Cenozoic cooling and source δD (that is, ice volume).

The third and final step in determining the effect of Cenozoic climate change is to estimate the isotopic fractionation associated with orographic lifting. This estimate is made using a simple one-dimensional adiabatic lifting model, which accounts for uniform lifting of the overlying atmosphere (compare, Dansgaard, 1964; Smith and Barstad, 2004). (Note this is different from the parcel-based model of Rowley and others, 2001.) We assume a fully saturated atmosphere and a moist stability $N_m \approx 0.001$ rad/s. Coupled GCM results (Frierson, 2006) indicate that N_m remained fairly constant in the mid-latitudes across climate states, so we use this modern value for the entire Cenozoic. The 1-D column has an initial surface temperature at sea level given by the estimated SAT curve (fig. 10), from which we calculate the associated moist adiabat. The initial thermal gradient (environmental lapse rate) is determined from the governing relationship for N_m (Smith and Barstad, 2004). The saturated water vapor decays exponentially with height as governed by the environmental lapse rate and SAT. Lifting and precipitation follow the moist adiabat. We calculate the incremental fractionation of water vapor in the column at each position along its path by vertically

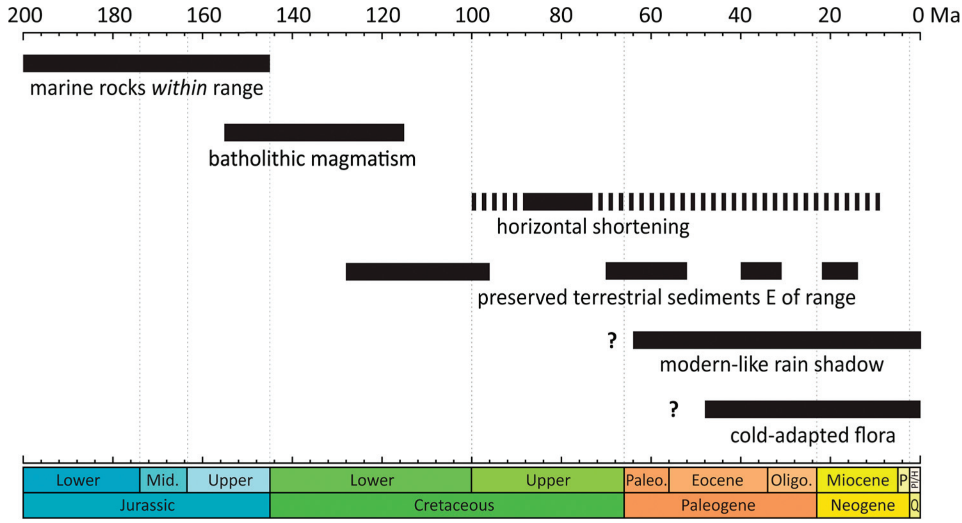

Fig. 12. Timing of events relating to and constraining the uplift of the Patagonian Andes, including the presence of marine sediments in the area of the range (Giacosa and Heredia, 2004; Hanson and Wilson, 1991), batholithic magmatism (Pankhurst and others, 1999; Seifert and others, 2005; Hervé and others, 2007), horizontal shortening in the backarc (Fosdick and others, 2011), terrestrial deposits in the backarc (Suárez and others, 2000; Blisniuk and others, 2005; Charrier and others, 2007; Metzger, ms, 2013; Navarrete and others, 2018), and the presence of cold-adapted *Nothofagus pumilio* (lenga beech) in the Andes (Mathiasen and Premoli, 2010). Although horizontal shortening occurred over nearly 100 Myr, the bulk (27 km) occurred during the interval indicated by the solid bar.

integrating the amount of condensation, the associated temperature, and the phases (solid, liquid) being formed. This integration is carried down wind, and the complement is the isotopic composition of the resulting precipitation (Ciais and Jouzel, 1994).

We finally use the model to calculate a reference curve for leeward precipitation δD, accounting for climate change (that is, surface temperature and lapse rate) but holding the amount of lifting constant. This 1-D lifting model provides an estimate of the leeward δD record *if topography had remained constant through the Cenozoic*. We note that the predicted leeward precipitation δD matches the observed modern values and their range well (fig. 10), indicating that our estimate of the effect of climate is a useful approximation.

Our focus in using this approach is not to determine a quantitative height of ancient topography. Because large-scale mountain ranges can vary in shape, maximum height, and relief, we instead ask the question: was the size of ancient topography significantly larger or smaller than the present?

DISCUSSION AND CONCLUSIONS

The match between the observed water isotope data and the predicted leeward precipitation δD based on a modern-size Andes (fig. 10) is striking. That leads to the most robust conclusion of this study: a significant isotopic rain shadow—of a magnitude similar to the modern—has existed in Patagonia since at least the Paleocene. This conclusion fits well with the abundant sedimentological evidence for the presence of the Patagonian Andes as an important, elevated sediment source since the Late Cretaceous. The timing of significant uplift in the Patagonian Andes is constrained by geologic data to between ~135 Ma and ~70 Ma (fig. 12).

In estimating the past size of the Patagonian Andes (or any mountain range), it is important to acknowledge the substantial uncertainties, particularly related to age control and the modeled leeward δD. This is why we have chosen to estimate paleotopography qualitatively and in reference to the modern state. As an example, one might think that the difference between the older samples at Lago Jenimeni and the modeled curve is significant, which would imply a small amount of uplift. However, there is enough uncertainty in the older parts of the Lago Jeinimeni age model (fig. 8) that the samples could easily be clustered toward the Early Eocene (the upper age is tightly constrained), where the samples fall on the modeled curve. Conversely, we think that we have minimized the errors associated with the model because of the good match with observed modern water δD, and because of the behavior of the model, which shows the expected slight convergence of initial and leeward precipitation δD under the warmer conditions of the Paleogene. However, without a high-resolution suite of terrestrial data across the Cenozoic to compare with, it is not possible to fully test the accuracy of the modeled estimate. Thus our model is appropriate for the back-of-the-envelope approach we have chosen, but not for identifying small changes in topography. The difference between model and data for the older samples at Lago Jenimeni is beyond the resolution of this approach, as it would represent a change in topography of $<$15 percent of the current size.

It is important to note that leeward water isotope records capture an integrated height of the orographic barrier. We observe that precipitation falls at all elevations, suggesting that moist air travels over both high and low topography, and downwind mixing of moist air and precipitation integrates this signal. The large reconstructed depletion between windward and leeward water isotopes ($\sim$80‰) requires substantial lifting, indicating that the high summits are probably important in lifting (Smith and Evans, 2007). Our water isotope-based reconstruction of past topography estimates the integrated height, not the maximum height of the topography. Thus it is possible that the maximum summit height could have been higher if the valleys were larger. For example, prior to the Late Miocene onset of glaciation in Patagonia (Wenzens, 2006; Christeleit and others, 2017), the Andes were likely lower relief, although our data indicate that the integrated height was similar to modern as late as the Middle Miocene.

Based on our results and the geological data discussed previously, we see the history of the Patagonian Andes as one of Cretaceous uplift followed by relative stability of high topography through the Cenozoic. This conclusion is consistent with geological data discussed previously (see also fig. 12), including (1) patterns of foreland basin development and sedimentation, (2) the presence of cold-tolerant flora in the Paleogene (Mathiasen and Premoli, 2010), and (3) the timing of major magmatism and deformation. The temporal constraints on the timing of the formation of high topography in the Patagonian Andes from this study and others (fig. 12) suggest that intrusion of the Patagonian batholith and/or crustal shortening likely were responsible for uplift (for example, Gianni and others, 2018).

Though our Cenozoic record (fig. 10) has coarse temporal resolution, the data do not reflect a punctuated history during that time, instead suggesting that the height of the Patagonian Andes may have been in an approximately steady state during the Cenozoic. The intrusive rocks of the Patagonian batholith require on the order of 10 km of erosion to reach their current position at the surface (fig. 3D). If there was no long-term change in the height of the orographic barrier posed by the Andes, as our record suggests, then that erosion must have been balanced by the slow uplift, as shown by thermochronological data (Thomson and others, 2010; Herman and Brandon, 2015). While the idea of a mountain belt in long-term steady state may seem at odds with some field observations, other Cordilleran orogens (for example, the Sierra Nevada) show similar histories of uplift followed by long-term persistence of high topography (House and others, 1998; Cassel and others, 2009;

McPhillips and Brandon, 2012). The gradual, protracted exhumation of Cordilleran orogens has implications for the timing and rate of silicate weathering (for example, Kump and others, 2000; McKenzie and others, 2016) related to this style of mountain building.

The work of Blisniuk and others (2005) is often cited as evidence for Miocene formation of the Patagonian Andes. However, as they note, their soil carbonate $\delta^{18}O$ data show a high degree of scatter due to evaporation, with the lowest values (least affected by evaporation) equivalent to the hydrated glass δD values we observe. The observed variation in contemporaneous volcanic glass data from both Cerro Observatorio and Gran Barranca is smaller, but comparable with the variation in the estimate based on the marine record and modern precipitation (fig. 10). We interpret this difference to be the result of the formation modes of soil carbonates, which precipitate in response to evaporation (Cerling and Quade, 1993), and volcanic glasses, which are hydrated by shallow groundwater that is largely insensitive to evaporation (Criss, 1999). Importantly, both our observations and those of Blisniuk and others (2005) indicate an arid, evaporative environment in the back-arc during this time. This result is consistent not with formation of the Andes at that time but with an isotopic rain shadow that persisted before and during the Early-Middle Miocene.

The existence of this rain shadow through the Cenozoic is attested to by the existence of the glasses we studied. At surface temperatures, glass—particularly if hydrated—can be replaced or dissolved relatively quickly if water is abundant (Friedman and Long, 1984). The Paleocene and Eocene samples we analyzed are among the oldest hydrated glass samples ever analyzed for δD. We speculate that the preservation of these glasses is due to the presence of the rain shadow in Patagonia since the time of deposition. In short, the existence of relatively old, well-preserved glass probably requires a dry climate. However, it is important to note that the persistence of an isotopic rain shadow does not imply a modern rainfall amount in eastern Patagonia through the entire Cenozoic. The isotopic rain shadow is a function of the difference between initial and final atmospheric temperature and the amount of lifting over topography. In greenhouse climates, the precipitation amount on the leeward side of the Andes would have likely been higher (although still much drier than the windward side), if the reconstructed isotopic gradient was maintained.

The idea of Cretaceous uplift is easily tested by future studies that extend the record of Patagonian paleotopography back into the Cretaceous. This will be important in determining whether an association between voluminous granitic magmatism and construction of high topography is a common feature of Cordilleran orogenic systems. These findings also bring forward the question of whether the Cretaceous formation of the Patagonian Andes was an important factor in the diversification of numerous plant and animal taxa (Wilf and others, 2013), which led to the high diversity that was well established in Patagonia by the early Paleogene (Reguero and others, 2002; Wilf and others, 2003; Wilf and others, 2005; Iglesias and others, 2007; Tejedor and others, 2009).

The new record we present here tracks changes in the amount of orographic lifting in Patagonia through the Cenozoic. After accounting for the effect of global climate change on precipitation δD, we find that the Andes have been a high topographic feature since at least the Paleocene. This unexpectedly long history of high topography, similar to the Sierra Nevada (for example, Mulch and others, 2006; Cassel and others, 2009; Hren and others, 2010), suggests that we need to revisit our ideas about the way(s) high topography is created and maintained in Cordilleran settings. We also highlight the importance in accounting for the effects of climate change on precipitation δD when using stable isotope-based approaches to reconstruct paleotopography.

ACKNOWLEDGMENTS

DAC, MTB, and MTH conceived this project; DAC, CM, AP, MGC, MM, and MTB did the field work; MTH, DAC, AP, and MGC made the stable isotope measurements; JH, DAC, and MM did the zircon U/Pb work; RDG, MTB, and DAC developed the synthesis of the regional climatology; and DAC and MTB wrote the paper with input from all co-authors. This work was improved by discussions with Marcelo Farias, Alfonso Encinas, Lucas Martin Fennell, Ari Iglesias, David Rowley, and Keith Ma. Reviews of a previous version of this manuscript by Elizabeth Cassel and an anonymous reviewer were constructive. We are extremely grateful for local assistance with access from Antonia Beatrice Gilabert of the Sarmiento region and Cesar Andrade of Reserva Nacional Lago Jeinimeni. Planning assistance from Andrea Piñones was invaluable. We acknowledge assistance in the field from Chelsea Colwyn and members of the 2014–2015 Patagonia Integrative Field Research program. Support for this work was provided by grants to Colwyn from the Geological Society of America, AAPG, SEPM, Yale Institute for Biospheric Studies, the Greenberg Fund, and the John F. Enders Fellowship as well as NSF EAR-1650313 and EAR-1650396 to Brandon and Hren, respectively.

REFERENCES

Abbot, D. S., and Tziperman, E., 2008, A high-latitude convective cloud feedback and equable climates: Quarterly Journal of the Royal Meteorological Society, v. 134, n. 630, p. 165–185, https://doi.org/10.1002/qj.211

Agosta, E., Compagnucci, R., and Ariztegui, D., 2015, Precipitation linked to Atlantic moisture transport: Clues to interpret Patagonian palaeoclimate: Climate Research, v. 62, n. 3, p. 219–240, https://doi.org/10.3354/cr01272

Ague, J. J., and Brimhall, G. H., 1988, Magmatic arc asymmetry and distribution of anomalous plutonic belts in the batholiths of California: Effects of assimilation, crustal thickness, and depth of crystallization: GSA Bulletin, v. 100, n. 6, p. 912–927, https://doi.org/10.1130/0016-7606(1988)100<0912:MAAADO>2.3.CO;2

Ameghino, F., 1906, Les formations sédimentaires du Crétacé supérieur et du Tertiaire de Patagonie entre les faunes mammalogiques et celles ed l'ancien continent: Anales del Museo Nacional de Buenos Aires, Series 3, v. 15, n. 8, p. 1–568.

Anovitz, L. M., Cole, D. R., and Riciputi, L. R., 2009, Low-temperature isotopic exchange in obsidian: Implications for diffusive mechanisms: Geochimica et Cosmochimica Acta, v. 73, n. 13, p. 3795–3806, https://doi.org/10.1016/j.gca.2009.02.035

Bechis, F., Encinas, A., Concheyro, A., Litvak, V. D., Aguirre-Urreta, B., and Ramos, V. A., 2014, New age constraints for the Cenozoic marine transgressions of northwestern Patagonia, Argentina (41°–43° S): Paleogeographic and tectonic implications: Journal of South American Earth Sciences, v. 52, p. 72–93, https://doi.org/10.1016/j.jsames.2014.02.003

Bellosi, E. S., 2010a, Loessic and fluvial sedimentation in Sarmiento Formation pyroclastics, middle Cenozoic of central Patagonia, *in* Madden, R. H., Carlini, A. A., Vucetich, M. G., and Kay, R. F., editors, The Paleontology of Gran Barranca: Evolution and Environmental Change through the Middle Cenozoic of Patagonia: New York, Cambridge University Press, p. 278–292.

——— 2010b, Physical stratigraphy of the Sarmiento formation (middle Eocene-lower Miocene) at Gran Barranca, central Patagonia, *in* Madden, R. H., Carlini, A. A., Vucetich, M. G., and Kay, R. F., editors, The paleontology of Gran Barranca: Evolution and environmental change through the middle Cenozoic of Patagonia: New York, Cambridge University Press, p. 19–31.

Blisniuk, P. M., Stern, L. A., Chamberlain, C. P., Idleman, B., and Zeitler, P. K., 2005, Climatic and ecologic changes during Miocene surface uplift in the Southern Patagonian Andes: Earth and Planetary Science Letters, v. 230, n. 1–2, p. 125–142, https://doi.org/10.1016/j.epsl.2004.11.015

Boyle, E. A., 1997, Cool tropical temperatures shift the global δ^{18}O-T relationship: An explanation for the ice core δ^{18}O-borehole thermometry conflict?: Geophysical Research Letters, v. 24, n. 3, p. 273–276, https://doi.org/10.1029/97GL00081

Breecker, D. O., Sharp, Z. D., and McFadden, L. D., 2009, Seasonal bias in the formation and stable isotopic composition of pedogenic carbonate in modern soils from central New Mexico, USA: GSA Bulletin, v. 121, n. 3–4, p. 630–640, https://doi.org/10.1130/B26413.1

Breitsprecher, K., and Thorkelson, D. J., 2009, Neogene kinematic history of Nazca–Antarctic–Phoenix slab windows beneath Patagonia and the Antarctic Peninsula: Tectonophysics, v. 464, n. 1–4, p. 10–20, https://doi.org/10.1016/j.tecto.2008.02.013

Canavan, R. R., Carrapa, B., Clementz, M. T., Quade, J., DeCelles, P. G., and Schoenbohm, L. M., 2014, Early Cenozoic uplift of the Puna Plateau, Central Andes, based on stable isotope paleoaltimetry of hydrated volcanic glass: Geology, v. 42, n. 5, p. 447–450, https://doi.org/10.1130/G35239.1

Cassel, E. J., and Breecker, D. O., 2017, Long-term stability of hydrogen isotope ratios in hydrated volcanic glass: Geochimica et Cosmochimica Acta, v. 200, p. 67–86, https://doi.org/10.1016/j.gca.2016.12.001

Cassel, E. J., Graham, S. A., and Chamberlain, C. P., 2009, Cenozoic tectonic and topographic evolution of the northern Sierra Nevada, California, through stable isotope paleoaltimetry in volcanic glass: Geology, v. 37, n. 6, p. 547–550, https://doi.org/10.1130/G25572A.1

Cerling, T. E., and Quade, J., 1993, Stable carbon and oxygen isotopes in soil carbonates, *in* Swart, P. K., Lohmann, K. C., McKenzie, J. A., and Savin, S. M., editors, Climate Change in Continental Isotopic Records: Geophyscial Monograph Series, v. 78, p. 217–231, https://doi.org/10.1029/GM078p0217

Cerling, T. E., Brown, F. H., and Bowman, J. R., 1985, Low-temperature alteration of volcanic glass: Hydration, Na, K, ^{18}O and Ar mobility: Chemical Geology: Isotope Geoscience Section, v. 52, n. 3–4, p. 281–293, https://doi.org/10.1016/0168-9622(85)90040-5

Charrier, R., Pinto, L., and Rodríguez, M. P., 2007, Tectonostratigraphic evolution of the Andean Orogen in Chile, *in* Moreno, T., and Gibbons, W., editors, The Geology of Chile: The Geological Society, London, p. 21–114, https://doi.org/10.1144/GOCH.3

Chou, C., and Neelin, J. D., 2001, Mechanisms limiting the southward extent of the South American summer monsoon: Geophysical Research Letters, v. 28, n. 12, p. 2433–2436, https://doi.org/10.1029/2000GL012138

Christeleit, E. C., Brandon, M. T., and Shuster, D. L., 2017, Miocene development of alpine glacial relief in the Patagonian Andes, as revealed by low-temperature thermochronometry: Earth and Planetary Science Letters, v. 460, p. 152–163, https://doi.org/10.1016/j.epsl.2016.12.019

Ciais, P., and Jouzel, J., 1994, Deuterium and oxygen 18 in precipitation: Isotopic model, including mixed cloud processes: Journal of Geophysical Research-Atmospheres, v. 99, n. D8, p. 16793–16803, https://doi.org/10.1029/94JD00412

Colman, S. M., 1981, Rock-weathering rates as functions of time: Quaternary Research, v. 15, n. 3, p. 250–264, https://doi.org/10.1016/0033-5894(81)90029-6

Colwyn, D. A., and Hren, M. T., 2019, An abrupt decrease in Southern Hemisphere terrestrial temperature during the Eocene-Oligocene transition: Earth and Planetary Science Letters, v. 512, p. 227–235, https://doi.org/10.1016/j.epsl.2019.01.052

Coplen, T. B., 1993, Uses of environmental isotopes, *in* Alley, W. M., editor, Regional Ground-Water Quality: New York, Van Nostrand Reinhold, p. 227–254.

Crane, W. H., ms, 2004, Depositional History of the Upper Cretaceous Cerro Toro Formation, Silla Syncline Magallanes Basin, Chile: Stanford, California, Stanford University, Ph. D. Thesis, 275 p.

Criss, R. E., 1999, Principles of stable isotope distribution: New York, Oxford, Oxford University Press, 264 p.

Dansgaard, W., 1964, Stable isotopes in precipitation: Tellus, v. 16, n. 4, p. 436–468, https://doi.org/10.3402/tellusa.v16i4.8993

de Boer, B., van de Wal, R. S. W., Bintanja, R., Lourens, L., and Tuenter, E., 2010, Cenozoic global ice-volume and temperature simulations with 1-D ice-sheet models forced by benthic δ^{18}O records: Annals of Glaciology, v. 51, n. 55, p. 23–33, https://doi.org/10.3189/172756410791392736

de Boer, B., van de Wal, R. S. W., Lourens, L. J., and Bintanja, R., 2012, Transient nature of the Earth's climate and the implications for the interpretation of benthic δ^{18}O records: Palaeogeography, Palaeoclimatology, Palaeoecology, v. 335–336, p. 4–11, https://doi.org/10.1016/j.palaeo.2011.02.001

DeCelles, P. G., Quade, J., Kapp, P., Fan, M., Dettman, D. L., and Ding, L., 2007, High and dry in central Tibet during the late Oligocene: Earth and Planetary Science Letters, v. 253, n. 3–4, p. 389–401, https://doi.org/10.1016/j.epsl.2006.11.001

DeCelles, P. G., Ducea, M. N., Kapp, P., and Zandt, G., 2009, Cyclicity in Cordilleran orogenic systems: Nature Geoscience, v. 2, n. 4, p. 251–257, https://doi.org/10.1038/ngeo469

Dettinger, M. P., and Quade, J., 2015, Testing the analytical protocols and calibration of volcanic glass for the reconstruction of hydrogen isotopes in paleoprecipitation, *in* DeCelles, P. G., Ducea, M. N., Carrapa, B., and Kapp, P A., editors, Geodynamics of a Cordilleran Orogenic Systme: Geological Society of America Memoirs, v. 212, p. 261–276, https://doi.org/10.1130/2015.1212(14)

Dickinson, W. R., 2004, Evolution of the North American cordillera: Annual Review of Earth Planetary Science, v. 32, p. 13–45, https://doi.org/10.1146/annurev.earth.32.101802.120257

Dingwell, D. B., 1996, Volcanic dilemma–flow or blow?: Science, v. 273, n. 5278, p. 1054, https://doi.org/10.1126/science.273.5278.1054

Dott Jr., R. H., Winn Jr., R. D., and Smith, C. H. L., 1982, Relationship of Late Mesozoic and Early Cenozoic sedimentation to the tectonic evolution of the southernmost Andes and Scotia Arc, *in* Craddock, C., editor, Antarctic Geoscience: Madison, Wisconsin, Univeristy of Wisconsin Press, p. 193–202.

Draxler, R. R., and Rolph, G. D., 2013, HYSPLIT (HYbrid Single-Particle Lagrangian Integrated Trajectory). Model access via NOAA ARL READY Website (http://www.arl.noaa.gov/HYSPLIT.php). College Park, Maryland, NOAA Air Resources Laboratory.

Ducea, M., 2001, The California arc: Thick granitic batholiths, eclogitic residues, lithospheric-scale thrusting, and magmatic flare-ups: GSA Today, v. 11, n. 11, p. 4–10, https://doi.org/10.1130/1052-5173(2001)011<0004:TCATGB>2.0.CO;2

Dunn, R. E., Madden, R. H., Kohn, M. J., Schmitz, M. D., Strömberg, C. A., Carlini, A. A., Ré, G. H., and Crowley, J., 2013, A new chronology for middle Eocene–early Miocene South American Land Mammal Ages: GSA, v. 125, n. 3–4, p. 539–555, https://doi.org/10.1130/B30660.1

Encinas, A., Folguera, A., Oliveros, V., Del Mauro, L. D. G., Tapia, F., Riffo, R., Hervé, F., Finger, K. L., Valencia, V. A., Gianni, G., and Alvarez, O., 2016, Late Oligocene–early Miocene submarine volcanism and deep-marine sedimentation in an extensional basin of southern Chile: Implications for the tectonic development of the North Patagonian Andes: GSA Bulletin, v. 128, n. 5–6, p. 807–823, https://doi.org/10.1130/B31303.1

Encinas, A., Folguera, A., Bechis, F., Finger, K. L., Zambrano, P., Pérez, F., Bernabé, P., Tapia, F., Riffo, R., Buatois, L., Orts, D., Nielsen, S. N., Valencia, V. V., Cuitiño, Oliveros, V., De Girolamo del Mauro, L., 2018, The Late Oligocene–Early Miocene Marine Transgression of Patagonia, The Evolution of the Chilean-Argentinean Andes: Springer Earth System Sciences, p. 443–474, https://doi.org/10.1007/978-3-319-67774-3_18

Encinas, A., Folguera, A., Riffo, R., Molina, P., Fernández Paz, L., Litvak, V. D., Colwyn, D. A., Valencia, V. A., and Carrasco, M., 2019, Cenozoic basin evolution of the Central Patagonian Andes: Evidence from geochronology, stratigraphy, and geochemistry: Geoscience Frontiers, v. 10, n. 3, p. 1139–1165, https://doi.org/10.1016/j.gsf.2018.07.004

Fan, M., Heller, P., Allen, S. D., and Hough, B. G., 2014, Middle Cenozoic uplift and concomitant drying in the central Rocky Mountains and adjacent Great Plains: Geology, v. 42, n. 6, p. 547–550, https://doi.org/10.1130/G35444.1

Feakins, S. J., Warny, S., and DeConto, R. M., 2014, Snapshot of cooling and drying before onset of Antarctic Glaciation: Earth and Planetary Science Letters, v. 404, p. 154–166, https://doi.org/10.1016/j.epsl.2014.07.032

Fildani, A., and Hessler, A. M., 2005, Stratigraphic record across a retroarc basin inversion: Rocas Verdes–Magallanes basin, Patagonian Andes, Chile: GSA Bulletin, v. 117, n. 11–12, p. 1596–1614, https://doi.org/10.1130/B25708.1

Fildani, A., Cope, T. D., Graham, S. A., and Wooden, J. L., 2003, Initiation of the Magallanes foreland basin: Timing of the southernmost Patagonian Andes orogeny revised by detrital zircon provenance analysis: Geology, v. 31, n. 12, p. 1081–1084, https://doi.org/10.1130/G20016.1

Flint, S. S., Prior, D. J., Agar, S. M., and Turner, P., 1994, Stratigraphic and structural evolution of the Tertiary Cosmelli Basin and its relationship to the Chile triple junction: Journal of the Geological Society, v. 151, n. 2, p. 251–268, https://doi.org/10.1144/gsjgs.151.2.0251

Folguera, A., and Ramos, V. A., 2011, Repeated eastward shifts of arc magmatism in the Southern Andes: A revision to the long-term pattern of Andean uplift and magmatism: Journal of South American Earth Sciences, v. 32, n. 4, p. 531–546, https://doi.org/10.1016/j.jsames.2011.04.003

Fosdick, J. C., Romans, B. W., Fildani, A., Bernhardt, A., Calderón, M., and Graham, S. A., 2011, Kinematic evolution of the Patagonian retroarc fold-and-thrust belt and Magallanes foreland basin, Chile and Argentina, 51°30' S: GSA Bulletin, v. 123, n. 9–10, p. 1679–1698, https://doi.org/10.1130/B30242.1

Fosdick, J. C., Grove, M., Graham, S. A., Hourigan, J. K., Lovera, O., and Romans, B. W., 2015, Detrital thermochronologic record of burial heating and sediment recycling in the Magallanes foreland basin, Patagonian Andes: Basin Research, v. 27, n. 4, p. 546–572, https://doi.org/10.1111/bre.12088

Friedman, I., and Smith, R. L., 1958, The deuterium content of water in some volcanic glasses: Geochimica et Cosmochimica Acta, v. 15, n. 3, p. 218–228, https://doi.org/10.1016/0016-7037(58)90059-0

——— 1960, A new dating method using obsidian—Part I, The development of the method: American Antiquity, v. 25, n. 4, p. 476–493, https://doi.org/10.2307/276634

Friedman, I., Gleason, J., Sheppard, R. A., and Gude, A. J., 1993a, Deuterium fractionation as water diffuses into silicic volcanic ash: Geophysical Monograph Series, v. 78, p. 321–323, https://doi.org/10.1029/GM078p0321

Friedman, I., Gleason, J., and Warden, A., 1993b, Ancient climate from deuterium content of water in volcanic glass: Geophysical Monograph Series, v. 78, p. 309–319, https://doi.org/10.1029/GM078p0309

Frierson, D. M. W., 2006, Robust increases in midlatitude static stability in simulations of global warming: Geophysical Research Letters, v. 33, n. 24, https://doi.org/10.1029/2006GL027504

Galewsky, J., 2009, Rain shadow development during the growth of mountain ranges: An atmospheric dynamics perspective: Journal of Geophysical Research-Earth Surface, v. 114, p. F01018, https://doi.org/10.1029/2008JF001085

Garreaud, R., Lopez, P., Minvielle, M., and Rojas, M., 2013, Large scale control on the Patagonian Climate: Journal of Climate, n. 2012, https://doi.org/10.1175/JCLI-D-12-00001.1

Garreaud, R. D., Gabriela Nicora, M., Bürgesser, R. E., and Ávila, E. E., 2014, Lightning in western Patagonia: Journal of Geophysical Research-Atmospheres, v. 119, n. 8, p. 4471–4485, https://doi.org/10.1002/2013JD021160

Garzione, C. N., Quade, J., DeCelles, P. G., and English, N. B., 2000, Predicting paleoelevation of Tibet and the Himalaya from $\delta^{18}O$ vs. altitude gradients in meteoric water across the Nepal Himalaya: Earth and Planetary Science Letters, v. 183, n. 1–2, p. 215–229, https://doi.org/10.1016/S0012-821X(00)00252-1

Gat, J. R., 1996, Oxygen and hydrogen isotopes in the hydrologic cycle: Annual Review of Earth and Planetary Sciences, v. 24, n. 1, p. 225–262, https://doi.org/10.1146/annurev.earth.24.1.225

Georgieva, V., Melnick, D., Schildgen, T. F., Ehlers, T. A., Lagabrielle, Y., Enkelmann, E., and Strecker, M. R., 2016, Tectonic control on rock uplift, exhumation, and topography above an oceanic ridge collision: Southern Patagonian Andes (47° S), Chile: Tectonics, v. 35, n. 6, p. 1317–1341, https://doi.org/10.1002/2016TC004120

Ghiglione, M. C., Ramos, V. A., Cuitiño, J., and Barberón, V., 2016, Growth of the Southern Patagonian Andes (46–53°S) and Their Relation to Subduction Processes, *in* Folguera, A., Naipauer, M., Sagripanti, L., Ghiglione, M. C., Orts, D., Giambiagi, L., editors, Growth of the Southern Andes: Cham, Switzerland, Springer, Springer Earth System Sciences, p. 201–240, https://doi.org/10.1007/978-3-319-23060-3_10

Giacosa, R., and Heredia, N., 2004, Structure of the North Patagonian thick-skinned fold-and-thrust belt, southern central Andes, Argentina (41°–42°S): Journal of South American Earth Sciences, v. 18, n. 1, p. 61–72, https://doi.org/10.1016/j.jsames.2004.08.006

Gianni, G. M., Dávila, F. M., Echaurren, A., Fennell, L., Tobal, J., Navarrete, C. R., Quezada, P., Folguera, A., and Giménez, M., 2018, A geodynamic model linking Cretaceous orogeny, arc migration, foreland

dynamic subsidence and marine ingression in southern South America: Earth-Science Reviews, v. 185, p. 437–462, https://doi.org/10.1016/j.earscirev.2018.06.016
Gordon, A. L., 2001, Bottom water formation: Elsevier, Encyclopedia of Ocean Sciences, p. 334–340, https://doi.org/10.1006/rwos.2001.0006
Gorring, M. L., Kay, S. M., Zeitler, P. K., Ramos, V. A., Rubiolo, D., Fernandez, M. I., and Panza, J. L., 1997, Neogene Patagonian plateau lavas: Continental magmas associated with ridge collision at the Chile Triple Junction: Tectonics, v. 16, n. 1, p. 1–17, https://doi.org/10.1029/96TC03368
Grambow, B., 2006, Nuclear waste glasses-How durable?: Elements, v. 2, n. 6, p. 357–364, https://doi.org/10.2113/gselements.2.6.357
Gutiérrez, N. M., Le Roux, J. P., Vásquez, A., Carreño, C., Pedroza, V., Araos, J., Oyarzun, J. L., Pino, J. P., Rivera, H. A., and Hinojosa, L. F., 2017, Tectonic events reflected by palaeocurrents, zircon geochronology, and palaeobotany in the Sierra Baguales of Chilean Patagonia: Tectonophysics, v. 695, p. 76–99, https://doi.org/10.1016/j.tecto.2016.12.014
Hamilton, L. H., 1992, The oldest abundant volcanic glass on Earth: Australian Journal of Earth Sciences, v. 39, n. 1, p. 55–59, https://doi.org/10.1080/08120099208728000
Hanson, R. E., and Wilson, T. J., 1991, Submarine rhyolitic volcanism in a Jurassic proto-marginal basin; southern Andes, Chile and Argentina: Geological Society of America Special Papers, v. 265, p. 13–28, https://doi.org/10.1130/SPE265-p13
Harris, N. J., 1995, A systematic theoretical study of harmonic vibrational frequencies and deuterium isotope fractionation factors for small molecules: The Journal of Physical Chemistry, v. 99, n. 40, p. 14689–14699, https://doi.org/10.1021/j100040a017
Held, I. M., and Hou, A. Y., 1980, Nonlinear axially symmetric circulations in a nearly inviscid atmosphere: Journal of the Atmospheric Sciences, v. 37, n. 3, p. 515–533, https://doi.org/10.1175/1520-0469(1980)037<0515:NASCIA>2.0.CO;2
Hendricks, M. B., DePaolo, D. J., and Cohen, R. C., 2000, Space and time variation of $\delta^{18}O$ and δD in precipitation: Can paleotemperature be estimated from ice cores?: Global Biogeochemical Cycles, v. 14, n. 3, p. 851–861, https://doi.org/10.1029/1999GB001198
Herman, F., and Brandon, M., 2015, Mid-latitude glacial erosion hotspot related to equatorial shifts in southern Westerlies: Geology, v. 43, n. 11, p. 987–990, https://doi.org/10.1130/G37008.1
Hervé, F., Pankhurst, R. J., Fanning, C. M., Calderón, M., and Yaxley, G. M., 2007, The South Patagonian batholith: 150 my of granite magmatism on a plate margin: Lithos, v. 97, n. 3–4, p. 373–394, https://doi.org/10.1016/j.lithos.2007.01.007
House, M. A., Wernicke, B. P., and Farley, K. A., 1998, Dating topography of the Sierra Nevada, California, using apatite (U–Th)/He ages: Nature, v. 396, n. 6706, p. 66–69, https://doi.org/10.1038/23926
Hren, M. T., Pagani, M., Erwin, D. M., and Brandon, M., 2010, Biomarker reconstruction of the early Eocene paleotopography and paleoclimate of the northern Sierra Nevada: Geology, v. 38, n. 1, p. 7–10, https://doi.org/10.1130/G30215.1
Huber, M., and Caballero, R., 2011, The early Eocene equable climate problem revisited: Climate of the Past, v. 7, n. 2, p. 603–633, https://doi.org/10.5194/cp-7-603-2011
Iglesias, A., Wilf, P., Johnson, K. R., Zamuner, A. B., Cúneo, N. R., Matheos, S. D., and Singer, B. S., 2007, A Paleocene lowland macroflora from Patagonia reveals significantly greater richness than North American analogs: Geology, v. 35, n. 10, p. 947–950, https://doi.org/10.1130/G23889A.1
Insel, N., Poulsen, C. J., Ehlers, T. A., and Sturm, C., 2012, Response of meteoric $\delta^{18}O$ to surface uplift – Implications for Cenozoic Andean Plateau growth: Earth and Planetary Science Letters, v. 317–318, p. 262–272, https://doi.org/10.1016/j.epsl.2011.11.039
Jackson, L. J., Beate, B. O., Horton, B. K., and Mothes, P. A., 2017, Investigating the relationship between δD in hydrated volcanic glass and meteoric water: A case study using a single late Pleistocene (~200 ka) rhyolitic deposite exposed along a 4000 meter elevation transect, *in* Cabero, A., Zúñiga, M. A., Le Pennec, J.-L., Narvaez, D., Hernández, M. J., Nocquet, J. M., and Gomez, F. V., editors, Memorias VIII Jornadas en Ciencias de la Tierra: Quito, Ecuador, EPN Editorial.
Koffman, B. G., Kreutz, K. J., Breton, D. J., Kane, E. J., Winski, D. A., Birkel, S. D., Kurbatov, A. V., and Handley, M. J., 2014, Centennial-scale variability of the Southern Hemisphere westerly wind belt in the eastern Pacific over the past millennium: Climate of the Past, v. 10, n. 3, p. 1125–1144, https://doi.org/10.5194/cp-10-1125-2014
Kump, L. R., Brantley, S. L., and Arthur, M. A., 2000, Chemical weathering, atmospheric CO_2, and climate: Annual Review of Earth and Planetary Sciences, v. 28, n. 1, p. 611–667, https://doi.org/10.1146/annurev.earth.28.1.611
Lagabrielle, Y., Suárez, M., Rossello, E. A., Hérail, G., Martinod, J., Régnier, M., and de la Cruz, R., 2004, Neogene to Quaternary tectonic evolution of the Patagonian Andes at the latitude of the Chile Triple Junction: Tectonophysics, v. 385, n. 1–4, p. 211–241, https://doi.org/10.1016/j.tecto.2004.04.023
Lamy, F., Hebbeln, D., Röhl, U., and Wefer, G., 2001, Holocene rainfall variability in southern Chile: A marine record of latitudinal shifts of the Southern Westerlies: Earth and Planetary Science Letters, v. 185, n. 3–4, p. 369–382, https://doi.org/10.1016/S0012-821X(00)00381-2
Lechler, A. R., and Galewsky, J., 2013, Refining paleoaltimetry reconstructions of the Sierra Nevada, California, using air parcel trajectories: Geology, v. 41, n. 2, p. 259–262. https://doi.org/10.1130/G33553.1
Lechler, A. R., Niemi, N. A., Hren, M. T., and Lohmann, K. C., 2013, Paleoelevation estimates for the northern and central proto–Basin and Range from carbonate clumped isotope thermometry: Tectonics, v. 32, n. 3, p. 295–316, https://doi.org/10.1002/tect.20016
Macellari, C., Barrio, C. A., and Manassero, M., 1989, Upper Cretaceous to Paleocene depositional sequences and sandstone petrography of southwestern Patagonia (Argentina and Chile): Journal of South American Earth Sciences, v. 2, n. 3, p. 223–239, https://doi.org/10.1016/0895-9811(89)90031-X

Maffione, M., 2016, Kinematic evolution of the Southern Andean orogenic arc, *in* Ghiglione, M., editor, Geodynamic Evolution of the Southernmost Andes: Cham, Switzerland, Springer, Earth System Sciences, p. 173–200, https://doi.org/10.1007/978-3-319-39727-6_7

Martin, E., Bindeman, I., Balan, E., Palandri, J., Seligman, A., and Villemant, B., 2017, Hydrogen isotope determination by TC/EA technique in application to volcanic glass as a window into secondary hydration: Journal of Volcanology and Geothermal Research, v. 348, p. 49–61, https://doi.org/10.1016/j.jvolgeores.2017.10.013

Martínez, O. A., and Coronato, A. M. J., 2008, The late Cenozoic fluvial deposits of Argentine Patagonia: Developments in Quaternary Sciences, v. 11, p. 205–226, https://doi.org/10.1016/S1571-0866(07)10009-9

Matheos, S. D., and Raigemborn, M. S., 2012, Sedimentology and paleoenvironment of the Santa Cruz Formation, *in* Vizcaíno, S. F., Kay, R. F., and Bargo, M. S., editors, Early Miocene Paleobiology in Patagonia: High-latitude Paleocommunities of the Santa Cruz Formation: Cambridge, United Kingdom, Cambridge University Press, p. 59–82, https://doi.org/10.1017/CBO9780511667381.005

Mathiasen, P., and Premoli, A. C., 2010, Out in the cold: Genetic variation of *Nothofagus pumilio* (Nothofagaceae) provides evidence for latitudinally distinct evolutionary histories in austral South America: Molecular Ecology, v. 19, n. 2, p. 371–385, https://doi.org/10.1111/j.1365-294X.2009.04456.x

McGuire, K. J., McDonnell, J. J., Weiler, M., Kendall, C., McGlynn, B. L., Welker, J. M., and Seibert, J., 2005, The role of topography on catchment−scale water residence time: Water Resources Research, v. 41, n. 5, https://doi.org/10.1029/2004WR003657

McKenzie, N. R., Horton, B. K., Loomis, S. E., Stockli, D. F., Planavsky, N. J., and Lee, C.-T. A., 2016, Continental arc volcanism as the principal driver of icehouse-greenhouse variability: Science, v. 352, n. 6284, p. 444–447, https://doi.org/10.1126/science.aad5787

McPhillips, D., and Brandon, M. T., 2012, Topographic evolution of the Sierra Nevada measured directly by inversion of low-temperature thermochronology: American Journal of Science, v. 312, n. 2, p. 90–116, https://doi.org/10.2475/02.2012.02

Metzger, C., ms, 2013, Paleosol Records of Middle Miocene Climate Change: Eugene, Oregon, University of Oregon, Ph. D. thesis, 172 p., http://hdl.handle.net/1794/13414

Miller, R. B., Gordon, S. M., Bowring, S., Doran, B., McLean, N., Michels, Z., Shea, E., and Whitney, D. L., 2016, Linking deep and shallow crustal processes during regional transtension in an exhumed continental arc, North Cascades, northwestern Cordillera (USA): Geosphere, v. 12, n. 3, p. 900–924, https://doi.org/10.1130/GES01262.1

Monger, J. W. H., Price, R. A., and Tempelman-Kluit, D. J., 1982, Tectonic accretion and the origin of the two major metamorphic and plutonic welts in the Canadian Cordillera: Geology, v. 10, n. 2, p. 70–75, https://doi.org/10.1130/0091-7613(1982)10<70:TAATOO>2.0.CO;2

Moy, C. M., Dunbar, R. B., Moreno, P. I., Francois, J.-P., Villa-Martínez, R., Mucciarone, D. M., Guilderson, T. P., and Garreaud, R. D., 2008, Isotopic evidence for hydrologic change related to the westerlies in SW Patagonia, Chile, during the last millennium: Quaternary Science Reviews, v. 27, n. 13–14, p. 1335–1349, https://doi.org/10.1016/j.quascirev.2008.03.006

Mulch, A., and Chamberlain, C. P., 2007, Stable isotope paleoaltimetry in orogenic belts — The silicate record in surface and crustal geological archives: Reviews in Mineralogy and Geochemistry, v. 66, n. 1, p. 89–118, https://doi.org/10.2138/rmg.2007.66.4

Mulch, A., Graham, S. A., and Chamberlain, C. P., 2006, Hydrogen isotopes in Eocene river gravels and paleoelevation of the Sierra Nevada: Science, v. 313, n. 5783, p. 87–89, https://doi.org/10.1126/science.1125986

Mulch, A., Sarna-Wojcicki, A. M., Perkins, M. E., and Chamberlain, C. P., 2008, A Miocene to Pleistocene climate and elevation record of the Sierra Nevada (California): Proceedings of the National Academy of Sciences of the United States of America, v. 105, n. 19, p. 6819–6824, https://doi.org/10.1073/pnas.0708811105

Navarrete, C. R., Gianni, G. M., Echaurren, A., and Folguera, A., 2018, Lower Jurassic to Early Paleogene Intraplate Contraction in Central Patagonia, *in* Folguera, A., Contreras Reyes, E., Heredia, N., Encinas, A., B. Iannelli, S., Oliveros, V., M. Dávila, F., Collo, G., Giambiagi, L., Maksymowicz, A., Iglesia Llanos, M. P., Turienzo, M., Naipauer, M., Orts, D., D. Litvak, V., Alvarez, O., and Arriagada, C., editors, The Evolution of the Chilean-Argentinean Andes: Cham, Switzerland, Springer, p. 245–271, https://doi.org/10.1007/978-3-319-67774-3_10

Nolan, G. S., and Bindeman, I. N., 2013, Experimental investigation of rates and mechanisms of isotope exchange (O, H) between volcanic ash and isotopically-labeled water: Geochimica et Cosmochimica Acta, v. 111, p. 5–27, https://doi.org/10.1016/j.gca.2013.01.020

Norris, R. D., Bice, K. L., Magno, E. A., and Wilson, P. A., 2002, Jiggling the tropical thermostat in the Cretaceous hothouse: Geology, v. 30, n. 4, p. 299–302, https://doi.org/10.1130/0091-7613(2002)030<0299:JTTTIT>2.0.CO;2

North, G. R., Cahalan, R. F., and Coakley Jr., J. A., 1981, Energy balance climate models: Reviews of Geophysics, v. 19, n. 1, p. 91–121, https://doi.org/10.1029/RG019i001p00091

Pankhurst, R. J., Weaver, S. D., Hervé, F., and Larrondo, P., 1999, Mesozoic-Cenozoic evolution of the North Patagonian batholith in Aysen, southern Chile: Journal of the Geological Society, v. 156, n. 4, p. 673–694, https://doi.org/10.1144/gsjgs.156.4.0673

Parrish, J. T., Ziegler, A. M., and Scotese, C. R., 1982, Rainfall patterns and the distribution of coals and evaporites in the Mesozoic and Cenozoic: Palaeogeography, Palaeoclimatology, Palaeoecology, v. 40, n. 1–3, p. 67–101, https://doi.org/10.1016/0031-0182(82)90085-2

Pearson, P. N., Ditchfield, P. W., Singano, J., Harcourt-Brown, K. G., Nicholas, C. J., Olsson, R. K., Shackleton, N. J., and Hall, M. A., 2001, Warm tropical sea surface temperatures in the Late Cretaceous and Eocene epochs: Nature, v. 413, n. 6855, p. 481–487, https://doi.org/10.1038/35097000

Pindell, J. L., and Tabbutt, K. D., 1995, Mesozoic-Cenozoic Andean paleogeography and regional controls on hydrocarbon systems, *in* Tankard, A. J., Suárez, S., and Welsink, H. J., editors, Petroleum basins of South America: AAPG Memoir, v. 62, p. 101–128.

Pingel, H., Alonso, R. N., Mulch, A., Rohrmann, A., Sudo, M., and Strecker, M. R., 2014, Pliocene orographic barrier uplift in the southern Central Andes: Geology, v. 42, n. 8, p. 691–694, https://doi.org/10.1130/G35538.1

Poage, M. A., and Chamberlain, C. P., 2001, Empirical relationships between elevation and the stable isotope composition of precipitation and surface waters: Considerations for studies of paleoelevation change: American Journal of Science, v. 301, n. 1, p. 1–15, https://doi.org/10.2475/ajs.301.1.1

Porter, T. J., Froese, D. G., Feakins, S. J., Bindeman, I. N., Mahony, M. E., Pautler, B. G., Reichart, G.-J., Sanborn, P. T., Simpson, M. J., and Weijers, J. W., 2016, Multiple water isotope proxy reconstruction of extremely low last glacial temperatures in Eastern Beringia (Western Arctic): Quaternary Science Reviews, v. 137, p. 113–125, https://doi.org/10.1016/j.quascirev.2016.02.006

Poulsen, C. J., Ehlers, T. A., and Insel, N., 2010, Onset of convective rainfall during gradual late Miocene rise of the central Andes: Science, v. 328, p. 490–493.

Quade, J., Garzione, C. N., and Eiler, J. M., 2007, Paleoelevation reconstruction using pedogenic carbonates: Reviews in Mineralogy and Geochemistry, v. 66, n. 1, p. 53–87, https://doi.org/10.2138/rmg.2007.66.3

Ramos, V. A., 2005, Seismic ridge subduction and topography: Foreland deformation in the Patagonian Andes: Tectonophysics, v. 399, n. 1–4, p. 73–86, https://doi.org/10.1016/j.tecto.2004.12.016

Ramos, V. A., and Ghiglione, M. C., 2008, Tectonic evolution of the Patagonian Andes: Developments in Quaternary Sciences, v. 11, p. 57–71, https://doi.org/10.1016/S1571-0866(07)10004-X

Ramos, V. A., and Kay, S. M., 1992, Southern Patagonian plateau basalts and deformation: Backarc testimony of ridge collisions: Tectonophysics, v. 205, n. 1–3, p. 261–282, https://doi.org/10.1016/0040-1951(92)90430-E

Rapela, C. W., Spalletti, L. A., Merodio, J. C., and Aragón, E., 1988, Temporal evolution and spatial variation of early Tertiary volcanism in the Patagonian Andes (40°S–42°30′ S): Journal of South American Earth Sciences, v. 1, n. 1, p. 75–88, https://doi.org/10.1016/0895-9811(88)90017-X

Ré, G. H., Bellosi, E. S., Heizler, M., Vilas, J. F., Madden, R. H., Carlini, A. A., Kay, R. F., and Vucetich, M. G., 2010, A geochronology for the Sarmiento Formation at Gran Barranca, *in* Madden, R. H., Carlini, A. A., Vucetich, M. G., and Kay, R. F., editors, The Paleontology of Gran Barranca: Evolution and Environmental Change through the Middle Cenozoic of Patagonia: New York, Cambridge University Press, p. 46–58.

Reguero, M. A., Marenssi, S. A., and Santillana, S. N., 2002, Antarctic Peninsula and South America (Patagonia) Paleogene terrestrial faunas and environments: Biogeographic relationships: Palaeogeography, Palaeoclimatology, Palaeoecology, v. 179, n. 3–4, p. 189–210, https://doi.org/10.1016/S0031-0182(01)00417-5

Ringham, M. C., Hoke, G. D., Huntington, K. W., and Aranibar, J. N., 2016, Influence of vegetation type and site-to-site variability on soil carbonate clumped isotope records, Andean piedmont of Central Argentina (32–34°S): Earth and Planetary Science Letters, v. 440, p. 1–11, https://doi.org/10.1016/j.epsl.2016.02.003

Roche, D. M., Donnadieu, Y., Pucéat, E., and Paillard, D., 2006, Effect of changes in $\delta^{18}O$ content of the surface ocean on estimated sea surface temperatures in past warm climate: Paleoceanography, v. 21, n. 2, https://doi.org/10.1029/2005PA001220

Rohrmann, A., Strecker, M. R., Bookhagen, B., Mulch, A., Sachse, D., Pingel, H., Alonso, R. N., Schildgen, T. F., and Montero, C., 2014, Can stable isotopes ride out the storms? The role of convection for water isotopes in models, records, and paleoaltimetry studies in the central Andes: Earth and Planetary Science Letters, v. 407, p. 187–195, https://doi.org/10.1016/j.epsl.2014.09.021

Romans, B. W., Fildani, A., Hubbard, S. M., Covault, J. A., Fosdick, J. C., and Graham, S. A., 2011, Evolution of deep-water stratigraphic architecture, Magallanes Basin, Chile: Marine and Petroleum Geology, v. 28, n. 3, p. 612–628, https://doi.org/10.1016/j.marpetgeo.2010.05.002

Rose, B. E. J., and Ferreira, D., 2013, Ocean heat transport and water vapor greenhouse in a warm equable climate: A new look at the low gradient paradox: Journal of Climate, v. 26, n. 6, p. 2117–2136, https://doi.org/10.1175/JCLI-D-11-00547.1

Ross, A. M., Seligman, A. N., Bindeman, I. N., and Nolan, G., 2015, Analysis of hydrogen isotopic exchange: Lava Creek Tuff ash and isotopically labeled water: AGU Fall Meeting Abstracts, abstract id. PP11B-2221

Ross, C. S., and Smith, R. L., 1955, Water and other volatiles in volcanic glasses: American Mineralogist, v. 40, n. 11–12, p. 1071–1089.

Rowley, D. B., and Garzione, C. N., 2007, Stable isotope-based paleoaltimetry: Annual Review of Earth and Planetary Sciences, v. 35, p. 463–508, https://doi.org/10.1146/annurev.earth.35.031306.140155

Rowley, D. B., Pierrehumbert, R. T., and Currie, B. S., 2001, A new approach to stable isotope-based paleoaltimetry: Implications for paleoaltimetry and paleohypsometry of the High Himalaya since the Late Miocene: Earth and Planetary Science Letters, v. 188, n. 1–2, p. 253–268, https://doi.org/10.1016/S0012-821X(01)00324-7

Rozanski, K., Araguás-Araguás, L., and Gonfiantini, R., 1993, Isotopic patterns in modern global precipitation, *in* Swart, P. K., Lohmann, K. C., McKenzie, J. A., and Savin, S. M., editors, Climate Change in Continental Isotopic Records: American Geophysical Union, Geophysical Monograph Series, v. 78, p. 1–36, https://doi.org/10.1029/GM078p0001

Sachse, D., Billault, I., Bowen, G. J., Chikaraishi, Y., Dawson, T. E., Feakins, S. J., Freeman, K. H., Magill, C. R., McInerney, F. A., Van der Meer, M. T., Polissar, P., Robins, R. J., Sachs, J. P., Schmidt, H-L., Sessions, A. L., White, J. W. C., West, J. B., and Kahmen, A., 2012, Molecular paleohydrology: Interpreting the hydrogen-isotopic composition of lipid biomarkers from photosynthesizing organisms: Annual Review of Earth and Planetary Sciences, v. 40, p. 221–249, https://doi.org/10.1146/annurev-earth-042711-105535

Sagoo, N., Valdes, P., Flecker, R., and Gregoire, L. J., 2013, The Early Eocene equable climate problem: Can perturbations of climate model parameters identify possible solutions?: Philosophical Transactions of the Royal Society A, v. 371, n. 2001, p. 20130123, https://doi.org/10.1098/rsta.2013.0123

Saylor, J. E., and Horton, B. K., 2014, Nonuniform surface uplift of the Andean plateau revealed by deuterium isotopes in Miocene volcanic glass from southern Peru: Earth and Planetary Science Letters, v. 387, p. 120–131, https://doi.org/10.1016/j.epsl.2013.11.015

Schneider, T., 2006, The general circulation of the atmosphere: Annual Review of Earth and Planetary Scences, v. 34, p. 655–688, https://doi.org/10.1146/annurev.earth.34.031405.125144

Seifert, W., Rosenau, M., and Echtler, H., 2005, Crystallization depths of granitoids of South Central Chile estimated by Al-in-hornblende geobarometry: Implications for mass transfer processes along the active continental margin: Neues Jahrbuch fur Geologie und Palaontologie-Abhandlungen, v. 236, n. 1–2, p. 115–128, https://doi.org/10.1127/njgpa/236/2005/115

Seligman, A. N., Bindeman, I. N., Watkins, J. M., and Ross, A. M., 2016, Water in volcanic glass: From volcanic degassing to secondary hydration: Geochimica et Cosmochimica Acta, v. 191, p. 216–238, https://doi.org/10.1016/j.gca.2016.07.010

Seton, M., Müller, R. D., Zahirovic, S., Gaina, C., Torsvik, T., Shephard, G., Talsma, A., Gurnis, M., Turner, M., Maus, S., and Chandler, M., 2012, Global continental and ocean basin reconstructions since 200 Ma: Earth-Science Reviews, v. 113, n. 3–4, p. 212–270, https://doi.org/10.1016/j.earscirev.2012.03.002

Sharman, G. R., Graham, S. A., Grove, M., and Hourigan, J. K., 2013, A reappraisal of the early slip history of the San Andreas fault, central California, USA: Geology, v. 41, n. 7, p. 727–730, https://doi.org/10.1130/G34214.1

Simpson, G. G., 1930, Scarritt-Patagonian Expedition Field Notes: New York, American Museum of Natural History, p. Available at http://paleo.amnh.org/notebooks/index.html

——— 1933, Stratigraphic nomenclature of the early Tertiary of central Patagonia: New York, American Museum of Natural History.

Smith, R. B., 1979, The influence of mountains on the atmosphere: Advances in Geophysics, v. 21, p. 87–230, https://doi.org/10.1016/S0065-2687(08)60262-9

Smith, R. B., and Barstad, I., 2004, A linear theory of orographic precipitation: Journal of the Atmospheric Sciences, v. 61, n. 12, p. 1377–1391, https://doi.org/10.1175/1520-0469(2004)061<1377:ALTOOP>2.0.CO;2

Smith, R. B., and Evans, J. P., 2007, Orographic precipitation and water vapor fractionation over the southern Andes: Journal of Hydrometeorology, v. 8, n. 1, p. 3–19, https://doi.org/10.1175/JHM555.1

Stern, L. A., and Blisniuk, P. M., 2002, Stable isotope composition of precipitation across the southern Patagonian Andes: Journal of Geophysical Research-Atmospheres, v. 107, n. D23, p. 4667, https://doi.org/10.1029/2002JD002509

Suárez, M., De la Cruz, R., and Troncoso, A., 2000, Tropical/subtropical upper Paleocene–lower Eocene fluvial deposits in eastern central Patagonia, Chile (46°45′ S): Journal of South American Earth Sciences, v. 13, n. 6, p. 527–536, https://doi.org/10.1016/S0895-9811(00)00042-0

Tejedor, M. F., Goin, F. J., Gelfo, J. N., López, G., Bond, M., Carlini, A. A., Scillato-Yané, G. J., Woodburne, M. O., Chornogubsky, L., Aragón, E., Reguero, M. A., Czaplewski, N. J., Vincon, S., Martin, G. M., and Ciancio, M. R., 2009, New early Eocene mammalian fauna from western Patagonia, Argentina: American Museum Novitates, p. 1–43, https://doi.org/10.1206/577.1

Thomson, S. N., Brandon, M. T., Tomkin, J. H., Reiners, P. W., Vásquez, C., and Wilson, N. J., 2010, Glaciation as a destructive and constructive control on mountain building: Nature, v. 467, n. 7313, p. 313–317, https://doi.org/10.1038/nature09365

Tuthorn, M., Zech, R., Ruppenthal, M., Oelmann, Y., Kahmen, A., del Valle, H. F., Eglinton, T., Rozanski, K., and Zech, M., 2015, Coupling δ^2H and $\delta^{18}O$ biomarker results yields information on relative humidity and isotopic composition of precipitation - A climate transect validation study: Biogeosciences, v. 12, n. 12, p. 3913–3924, https://doi.org/10.5194/bg-12-3913-2015

Vera, C., Higgins, W., Amador, J., Ambrizzi, T., Garreaud, R., Gochis, D., Gutzler, D., Lettenmaier, D., Marengo, J., Mechoso, C. R., Nogues-Paegle, J., Silva Dias, P. L., and Zhang, C., 2006, Toward a unified view of the American monsoon systems: Journal of Climate, v. 19, n. 20, p. 4977–5000, https://doi.org/10.1175/JCLI3896.1

Wenzens, G., 2006, Terminal Moraines, Outwash Plains, and Lake Terraces in the Vicinity of Lago Cardiel (49°S; Patagonia, Argentina)-Evidence for Miocene Andean Foreland Glaciations: Arctic, Antarctic, and Alpine Research, v. 38, n. 2, p. 276–291, https://doi.org/10.1657/1523-0430(2006)38[276:TMOPAL]2.0.CO;2

Wheeler, L. B., and Galewsky, J., 2017, Atmospheric flow patterns around the Southern Alps of New Zealand and implications for paleoaltimetry: Geophysical Research Letters, v. 44, n. 22, https://doi.org/10.1002/2017GL074753

Whitney, D., Miller, R., and Paterson, S., 1999, *P-T-t* evidence for mechanisms of vertical tectonic motion in a contractional orogen: North-western US and Canadian Cordillera: Journal of Metamorphic Geology, v. 17, n. 1, p. 75–90, https://doi.org/10.1046/j.1525-1314.1999.00181.x

Wilf, P., Cúneo, N. R., Johnson, K. R., Hicks, J. F., Wing, S. L., and Obradovich, J. D., 2003, High plant diversity in Eocene South America: Evidence from Patagonia: Science, v. 300, n. 5616, p. 122–125, https://doi.org/10.1126/science.1080475

Wilf, P., Johnson, K. R., Cúneo, N. R., Smith, M. E., Singer, B. S., and Gandolfo, M. A., 2005, Eocene plant diversity at Laguna del Hunco and Río Pichileufú, Patagonia, Argentina: The American Naturalist, v. 165, n. 6, p. 634–650, https://doi.org/10.1086/430055

Wilf, P., Cúneo, N. R., Escapa, I. H., Pol, D., and Woodburne, M. O., 2013, Splendid and seldom isolated:

The paleobiogeography of Patagonia: Annual Review of Earth and Planetary Sciences, v. 41, n. 1, p. 561, https://doi.org/10.1146/annurev-earth-050212-124217
Williams, G. P., 1988, The dynamical range of global circulations—I: Climate Dynamics, v. 2, n. 4, p. 205–260, https://doi.org/10.1007/BF01371320
Wilson, T. J., 1991, Transition from back-arc to foreland basin development in the southernmost Andes: Stratigraphic record from the Ultima Esperanza District, Chile: GSA Bulletin, v. 103, n. 1, p. 98–111, https://doi.org/10.1130/0016-7606(1991)103<0098:TFBATF>2.3.CO;2
Zachos, J. C., Dickens, G. R., and Zeebe, R. E., 2008, An early Cenozoic perspective on greenhouse warming and carbon-cycle dynamics: Nature, v. 451, n. 7176, p. 279–283, https://doi.org/10.1038/nature06588